



Norwegian University of  
Science and Technology

## Drillstring Dynamics

Comparative analysis between a lumped element model's ability to recreate axial vibrations observed from measurements of dynamic strain using small-scale drillstring model

**Thomas Løklingholm**

Petroleum Geoscience and Engineering

Submission date: June 2016

Supervisor: Sigve Hovda, IPT

Norwegian University of Science and Technology  
Department of Petroleum Engineering and Applied Geophysics





**NTNU – Trondheim**  
Norwegian University of  
Science and Technology

# Drillstring dynamics

Comparative analysis between a lumped element model's ability to recreate axial vibrations observed from measurements of dynamic strain using small-scale drillstring model

Thomas Løklingholm

Spring 2016

TPG4910 Master thesis

Department of Petroleum Engineering and Applied Geophysics

Norwegian University of Science and Technology

Supervisor: Associate Professor Sigve Hovda

## **Sammendrag**

Masse-fjær modell er ønskelige for deres matematiske enkelhet og deres praktiske anvendelse for simulering av aksiale vibrasjoner, men disse modellene bare approksimerer de dynamiske egenskapene, og det er derfor nødvendig å ta målinger for å validere disse analytiske modellene. Det er derfor tatt i bruk en liten fysisk modell av en borestreng for å validere de aksiale vibrasjoner simulert av analytiske modellen. I resultatene fra den målte er det klare forskjeller mellom teoretiske og målte data. Denne oppgaven viser resultatene oppdaget og sammenligninger dem med de simulerte vibrasjoner fra den sammensatte masse-fjær modellen. Hvor disse forskjellene diskuteres og evalueres, og argumenter er foreslått for å forklare årsaken bak de observerte forskjellene.

## **Abstract**

Lumped element models are desirable for their mathematical simplicity and their practical application for simulating axial vibrations. These models however only approximate the dynamic behavior, and is why real time measurements are essential for validating these analytical models. This is why a small-scale physical model of a drillstring was used for validating the axial vibrations simulated by the analytical model. These axial vibrations from the model were measured using strain gauges, where the vibrations where indicated by dynamic strain measurements. These measured results of axial vibrations showed that there were clear differences between theoretical and measured data. This thesis presents the results discovered and the comparison between the simulated vibrations from the lumped element model, and the measured axial vibrations produced from the small-scale drillstring model. These existing differences are discussed and evaluated, and suggestions and arguments are proposed to explain the causality behind the difference observed between analytical model and the measured axial vibrations.

# Contents

- List of Figures ..... iv
- List of Tables..... vii
- Abbreviations ..... viii
- 1 Introduction ..... 1
- 2 Background theory ..... 3
  - 2.1 Drillstring dynamics ..... 3
  - 2.2 Equipment and software ..... 5
    - 2.2.1 Strain gauge..... 5
    - 2.2.2 Signal amplifier ..... 10
    - 2.2.3 Analog-to-Digital converter ..... 11
    - 2.2.4 LabVIEW ..... 12
- 3 Lumped element model of drillstring..... 13
  - 3.1 Underdamped..... 19
  - 3.2 Critically damped ..... 20
  - 3.3 Overdamped..... 21
- 4 Physical drillstring model..... 21
- 5 Measurement of axial vibrations with strain gauges using physical drillstring model .... 24
  - 5.1 Experimental setup with physical drillstring model ..... 24
    - 5.1.1 Lab stand setup..... 25
    - 5.1.2 Ceiling hook setup..... 25
  - 5.2 Experimental process and data Acquisition..... 27
  - 5.3 Dynamic strain measured data..... 30
    - 5.3.1 Lab stand setup: 4.3 kg mass release without BHA ..... 31
    - 5.3.2 Lab stand setup: 4.3 kg mass release with BHA section..... 31
    - 5.3.3 Lab stand setup: 10kg mass release with BHA ..... 32
    - 5.3.4 Ceiling hook setup: 10kg mass release for 0.975m drillstring model ..... 33
    - 5.3.5 Ceiling hook setup: 10kg mass release for 2.865m drillstring model ..... 34
- 6 Analytical model approximation and comparison with dynamic strain measurements... 35
  - 6.1 How the analytical model is used to represent the DS model as lumped element model 35
    - 6.1.1 Displacement  $y_j(t)$  to strain  $\epsilon_j(t)$  ..... 42

6.1.2	Analytical model damping approximation .....	45
6.2	Comparison between simulation from the analytical model and the measured dynamic strain .....	47
6.2.1	Analytical model and dynamic strain measurement for 4.3 kg mass release with BHA(lab stand setup) .....	47
6.2.2	Analytical model for 4.3 kg mass release with BHA(lab stand setup).....	48
6.2.3	Analytical model for 10kg mass release with 0.975m drillstring(ceiling hook setup) .....	51
6.2.4	Analytical model for 10kg mass release with 2.865m drillstring(ceiling hook setup) .....	53
6.3	Fourier analysis.....	55
7	Discussion: Causes for variation between measured strain and the analytical model .....	56
7.1	Damping mechanisms and approximating measured data .....	56
7.1.1	Viscous Damping .....	57
7.1.2	Hysteretic/Structural damping.....	61
7.1.3	Coloumb friction,kinematic momentum loss and non-axial movement as cause for damping .....	68
7.1.4	Damping caused by energy transmission through the creation of external vibrations .....	70
7.2	Analytical model limitations and difficult experimental process .....	75
7.2.1	Modeling viscoelasticity .....	75
7.2.2	Accurately comparing analytical model to the measured data originating from the strain gauges .....	79
7.2.3	Difficulty approximating the analytical model as underdamped,critically damped and overdamped.....	81
7.2.4	Lingering weight during mass release.....	82
7.2.5	The difficulty of determining the true time stamp for mass release during dynamic strain measurements .....	83
7.3	Uncertainty when measuring the axial vibrations produced in the drillstring model .....	84
7.3.1	Strain gauge as a source of error in strain measurements .....	84
7.3.2	SNR/Background noise .....	90
7.3.3	Signal Amplifier and ADC.....	93
7.3.4	Sampling rate/frequency .....	94
8	Conclusion and Future work .....	97
8.1	Conclusion .....	97
8.2	Future work.....	98

9 Bibliography..... 99

**Appendix A: Non-conventional recovery method using axial vibrations**

# List of Figures

<i>Figure 2.1 Vibration types originating from drillstring (Schlumberger, 2010)</i> .....	3
<i>Figure 2.2 Whirl types for BHA (Schlumberger, 2010)</i> .....	4
<i>Figure 2.3 Bonded metallic single element strain gauge (National Instruments, 2016)</i> .....	6
<i>Figure 2.4 Wheatstone bridge (National Instruments, 2016)</i> .....	7
<i>Figure 2.5 Full-Bridge Type III measuring axial strength and reject bending strain (National Instruments, 2016)</i> .	7
<i>Figure 2.6 Full-Bridge Type III Circuit Diagram (National Instruments, 2016)</i> .....	8
<i>Figure 2.7 Overview of different rosette types (tradeKorea, 2016)</i> .....	9
<i>Figure 2.8 Wheatstone bridge circuit configured with a signal amplifier (Electronic Tutorials, 2016)</i> .....	10
<i>Figure 2.9 USB-8451 ADC-DAC used in the measurements( National Instruments, 2009)</i> .....	11
<i>Figure 2.10 comparison between signal quality with regards to 3-bit and 16-bit converters (Engineering 360, 2011)</i> .....	11
<i>Figure 2.11 LabVIEW flowchart for sampling data from 4 different sensory points used in dynamic strain measurements</i> .....	12
<i>Figure 3.1 Illustration of <math>n=3</math> mass and spring elements in a mass-spring-damped system</i> .....	13
<i>Figure 3.2 Diagram illustrating the how the initial conditions abide by hooks law regardless of number of <math>n</math> segments for the lumped element model</i> .....	18
<i>Figure 4.1 Layout of the drillstring model illustrating dimensions of DP and BHA sections</i> .....	22
<i>Figure 5.1 Diagram illustrating the experimental setup for measuring axial vibrations using strain gauges(with and without BHA)</i> .....	25
<i>Figure 5.2 the 0.975m drillstring model attached to a ceiling hook with steel wire for altered experimental setup</i> .....	26
<i>Figure 5.3 increased length drillstring model showing positions of strain gauges(sensory points)</i> .....	27
<i>Figure 5.4 Illustration of the mass release method used to incite the transient response for the dynamic strain measurements</i> .....	28
<i>Figure 5.5 Diagram highlighting the transmission of data from the strain gauges to Labview on the PC</i> .....	29
<i>Figure 5.6 shows the entire process of nulling offset and loading/releasing 4.3 kg mass “only drillpipe section”</i> 29	
<i>Figure 5.7 Dynamic strain measured after releasing 4.3kg mass for drillstring without BHA section shown for sensory points 1-3 over a 0.4 sec interval</i> .....	31
<i>Figure 5.8 Dynamic strain measured after releasing 4.3kg mass for drillstring with BHA section shown for sensory points 1-3 over a 0.4 sec interval</i> .....	32
<i>Figure 5.9 Dynamic strain measured after releasing 10 kg mass for drillstring with BHA section shown over a 0.4 sec interval</i> .....	33
<i>Figure 5.10 Dynamic strain for all sensory points for 10kg mass release with 0.975m drillstring model over a 0.4 sec interval</i> .....	33
<i>Figure 5.11 Dynamic strain for all sensory points for 10kg mass release for 2.865m drillstring model</i> .....	34
<i>Figure 6.1 Diagram of DP-section of the physical model showing how it is constructed.</i> .....	36
<i>Figure 6.2 DP-section represented using the effective lengths of plexiglas and steel, which are values used for the analytical model</i> .....	39
<i>Figure 6.3 Analytical view of the drillstring model represented by the “smallest” number of elements.</i> .....	41
<i>Figure 6.4 Diagram illustrating the basic principles of strain (NPTEL, 2011)</i> .....	42
<i>Figure 6.5 Initial condition for 10kg static strain from the analytical model(equation 20) modelled as a 0.975m drillstring</i> .....	43
<i>Figure 6.6 Measured static strain for all four sensory when subjected to 10kg end mass</i> .....	44
<i>Figure 6.7 The variation of damping constant expressed by using constant damping coefficient for all elements(2<sup>nd</sup> method)</i> .....	46
<i>Figure 6.8 Difference between the two methods of approximating damping for the analytical model shown for the top element <math>j=1</math></i> .....	46

Figure 6.9 comparison between measured data (sensory point 3) and analytical model for a 4.3kg mass release of the drillstring without BHA section over a 0.4 second interval .....	48
Figure 6.10 underdamped behavior comparison between measured data (sensory point 3) and analytical model for a 4.3kg mass release of the drillstring with BHA section over a 0.4 second interval.....	49
<b>Figure 6.11</b> Variation between BHA and no BHA for a 4.3kg mass release from the analytical model evaluated at $j=7$ .....	50
Figure 6.12 Comparison between measured data (sensory point 3) compared to analytical model transient response for 10kg mass release by varying values of damping constant .....	51
Figure 6.13 Comparison of how strain rate is the same for 10kg and 4.3kg mass release, from -30 microstrain to zero.....	52
Figure 6.14 Comparison between measured data (sensory point 3) compared to analytical model transient response for 10kg mass release by varying values of damping constant .....	53
Figure 6.15 frequency comparison as shown from the bottom elements of a 0.975m and 2.875m long drillstring .....	54
Figure 6.16 Fourier analysis comparison between analytical and measured data .....	55
Figure 7.1 Surge and Swab due to pipe movement that shows the velocity profile in the well (Skalle, 2014).....	57
Figure 7.2 Damping of element $j=1$ in drillstring without BHA with $\alpha = 0.99$ shows visible damping in interval of 0.4 seconds.....	59
Figure 7.3 Variation in damping ratios from top element $j=1$ to bottom $j=10$ for $n=10$ element drillstring model without BHA when $\alpha = 0.99$ .....	60
Figure 7.4 stress-strain curve for linear-viscoelastic material (J. ZHANG, 1993).....	61
Figure 7.5 Graph showing relationship between creep compliance and relaxation modulus and time for different materials (Princeton, 2010).....	62
Figure 7.6 Stress strain curve for a viscoelastic material subjected to hysteresis (University of Cambridge, 2016) .....	63
Figure 7.7 Relationship between the loss coefficient and Young's modulus for a large array of different materials (Ashby, 2005) .....	66
Figure 7.8 damping using equivalent hysteretic damping coefficient showing the results of element $j=1$ .....	67
Figure 7.9 Damping ratio for each element using equivalent damping coefficient from hysteretic/structural damping .....	68
Figure 7.10 Diagram highlighting the difference between long and short arm lengths for the clamps arms .....	71
Figure 7.11 Graph illustrating the results when a 10kg mass is used on the drillstring model(BHA inc) with adjusted arm length for each clamp 0.4 sec interval .....	72
Figure 7.12 comparison between 10kg mass release with BHA-section for adjusted clamp arm length and ceiling hook with sensory point 3 as reference point .....	74
Figure 7.13 (A) pure linear elastic behavior (spring element), (B) non-linear viscoelastic behavior (Polymod, 2015) .....	76
Figure 7.14 Difference between linear elastic and viscoelastic materials (Misra, Ramesh, & Okamura, 2008) ...	76
Figure 7.15 Different modeling approaches used for viscoelastic materials (Princeton, 2010) .....	77
Figure 7.16 Alternative lumped element model in order to encapsulate viscoelastic behavior using Voigt/Kelvin	78
Figure 7.17 Evaluating the DP as $n=100$ elements showing the first 10 elements in the top plexiglas segment..	80
Figure 7.18 Evaluating the DP as $n=10$ elements showing the first 1 elements in the top plexiglas segment.....	80
Figure 7.19 phase shift between two sinusoidal waves (Australian Government: Bureau of Metrology, 2016) ...	83
Figure 7.20 illustrates combination of mounting variations possible with strain gauges on one side of a plexiglas segment (angles are exaggerated for illustration purposes) .....	86
Figure 7.21 strain as function of time for a viscoelastic material subjected to constant stress (French, 1991)....	87
Figure 7.22 Strain reduction with time when subjected to static load of 10kg .....	88
Figure 7.23 Background noise recorded during static measurement, where no load is applied .....	91

*Figure 7.24 Comparison between different degrees of filters using simple moving average with different sample sizes ranging from 10-1000..... 92*

*Figure 7.25 Natural frequency of elements from the analytical model evaluated as n=14 elements with BHA(DP-section with n=10)..... 95*

*Figure 7.26 Natural frequency of elements from the analytical model evaluated as n=10 elements without BHA ..... 96*

## List of Tables

<i>Table 4.1 Dimensions and physical parameters for individual segment type .....</i>	<i>22</i>
<i>Table 6.1 Dimensions for DP section of the physical drillstring model highlighting difference between total and effective lengths for plexiglas and steel segments.....</i>	<i>36</i>
<i>Table 7.1 show the respective damping parameters for top element <math>j=1</math> for different values of <math>\alpha</math>(evaluated as <math>n=10</math> and <math>n=14</math> elements) .....</i>	<i>58</i>
<i>Table 7.2 Dimensions and parameters used to estimate vibration in the clamp arms .....</i>	<i>73</i>
<i>Table 7.3 Values for which different parts of the drillstring is defined as underdamped for 0.675m and 0.975m drillstring .....</i>	<i>81</i>
<i>Table 7.4 Calibration values for measured voltage that causes measured data to coincide with Hooke's law....</i>	<i>89</i>

## Abbreviations

NPT	Non-Productive Time
DP	Drill-pipe
DS	Drill-string
BHA	Bottom Hole Assembly
SNR	Signal-to-noise-ratio
ADC	Analog-to-Digital converter
DOF	Degree of freedom
ODE	Ordinary differential equation
SMA	Simple Moving Average

# 1 Introduction

Drillstring dynamics is an important topic of study for drilling operations. The drilling process is constantly faced by the challenges accompanied by drillstring vibrations in the form of axial (bit bounce), torsional (stick-slip) and lateral (whirl) vibrations, which causes a multitude of issues such as tool degradation, reduced borehole quality, and reduced ROP. These have all a detrimental effect on drilling performance and lead to NPT (Dupriest, 2010). There is therefore great value in being able to model the vibrational behavior that a drillstring is subjected to. Modeling these vibrations have tremendous practical applications for drilling operations. A good understanding of the effects of drillstring vibrations can be used in a number of different areas to improve drilling performance. Additional benefit of such applications is the optimization of drilling assemblies that helps prevent the most crucial situations of non-productive time (Schlumberger, 2016)

In addition to drilling operations, enhanced understating of the drillstring vibrations can also be used for Recovery operations for stuck pipe/member. This non-conventional recovery method is done by creating resonant vibrations in the drill string in order to free the stuck member (Buck Bernat, 1997). This is explained in further detail in appendix A.

There are many different types of models that can be used to represent the vibrations observed in the drillstring. Two examples being lumped element model and distributed parameter model. (Benaroya, 2004). Lumped systems consist of sets of discrete points, and due to the associated simplifications means that the spatial derivatives can be neglected, and the system will only be a function of time. Overall lumped element models are less complex than distributed parameter models, and is the reason why lumped element model was selected to model axial vibrations in the drillstring.

In this thesis the lumped element model is introduced as a mass-spring system as theoretical view of a drillstring. This analytical model was derived to simulate the axial vibrations produced during the transient response of a mass-spring system (drillstring). In order to verify this analytical model, a small-scale drillstring model was used. This model was setup such a that one could measure axial vibrations with strain gauges, by measuring the dynamic strain experienced during its transient response. The experimental process involved included subjecting this small-scale model to static load, and then subsequently removing it in order to induce the systems natural vibration. The analytical model was then used to simulate the axial

vibrations from the small-scale model based on the same conditions from the strain measurements. The focus of this thesis is on the numerical accuracy of the lumped element model, and its ability to simulate the measured axial vibrations seen in the dynamic strain measurements. Where the possible factors causing the variation between the analytical model and the measured data, will be discussed and evaluated.

The necessary background information is provided in chapter 2. This includes general theory of the different types of vibrations, encompassed by drillstring dynamics. It also presents general knowledge related to equipment and software used, which enabled axial vibration(dynamic strain) to be measured. For this part theory regarding strain gauges, signal amplifiers, ADC and the LabVIEW software is covered. Chapter 3 provides the general derivation regarding the lumped element model used. In Chapter 4 the small-scale drillstring model and its dimensions are presented, and its respective distinctions from a real drillstring explained. Then the experimental process involved with measuring the axial vibrations, the experimental setup, and the results from the measured dynamic strain is shown in chapter 5. The approximation of the analytical model to that of the small-scale drillstring model is presented in chapter 6. This chapter also includes the comparison between the analytical model and the measured strain from chapter 5. The variations that was discovered are then discussed in chapter 7, which consist of three large sections 7.1,7.2 and 7.3. The first section presents the possible damping mechanism, which explains the behavior seen in chapter 6, in addition to investigating the limitations in the experimental setup from chapter 5. Then section 7.2 will propose and suggest arguments as to why the variation between measured and analytical data occurred, by investigating limitations of the analytical model and the experimental process. Then the final section 7.3 will present all the possible uncertainties that are involved in the experiment, after which the thesis will be concluded.

## 2 Background theory

In this section, background theory will be presented to provide a general understanding of the different type of vibrations and their perspective traits. In addition to the equipment and software used to measure axial vibration in the small-scale drillstring model.

### 2.1 Drillstring dynamics

Drillstring vibrations can result in decreased on-bottom drilling time, reduced ROP, failure of the equipment and poor borehole quality. There are three fundamental drillstring vibrations that is encompassed by drillstring dynamics, which are axial, torsional and lateral vibration. All of these types are originate from the drillstring, and all pose challenges for overall drilling performance.

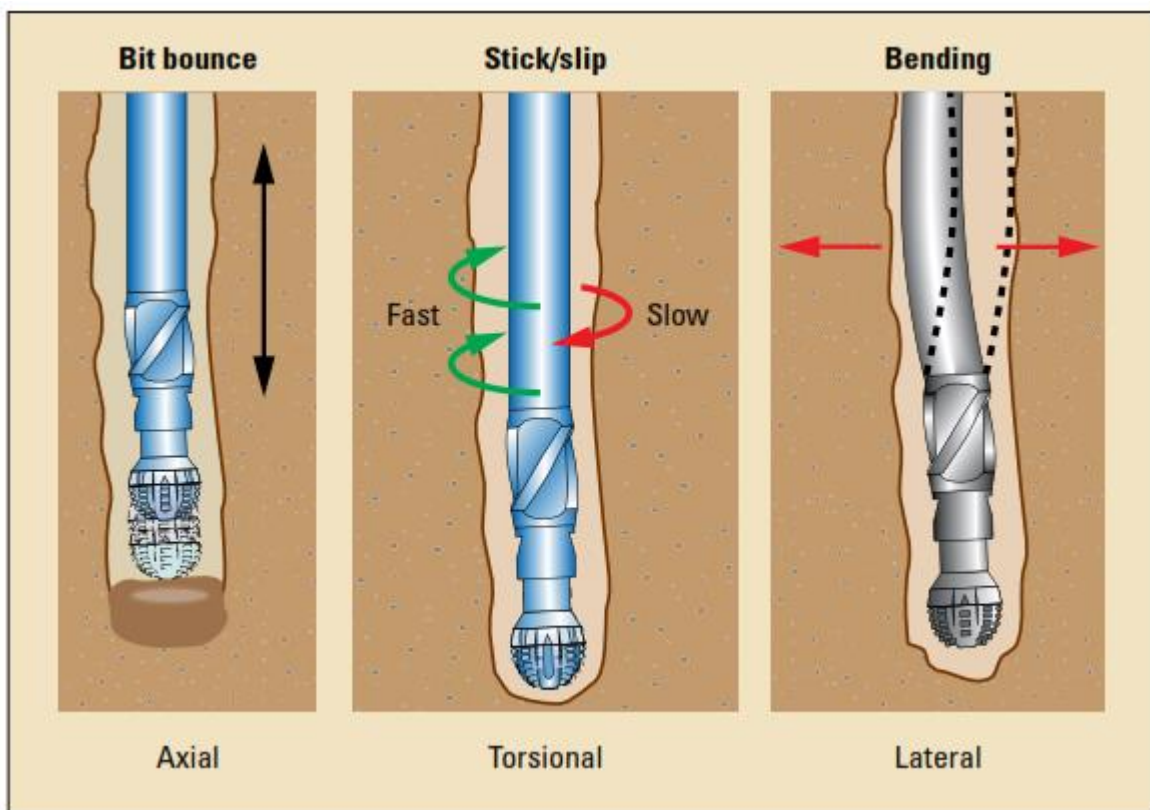


**Figure 2.1** Vibration types originating from drillstring (Schlumberger, 2010)

Axial vibration is longitudinal motion along the drillstring and is experienced in the form of bit bounce. As the drillstring bounces up and down it can cause damage to downhole equipment and subsequently result in non-productive time while tripping and replacing the tool. It also sometimes hard to detect axial vibrations, as even severe vibration may not be visible at the surface.

Torsional vibrations in the drillstring is experienced as erratic RPM with cycles of zero RPM followed with sudden increase. This type of vibration is normally referred to as stick/slip, and causes extreme fatigue to drill collars and also damages the bit.

Lateral vibration is a transverse vibration and can occur in combination with centrifugal motion of the bit, which defined as backward and forward whirl depending on the direction of the rotation. This is the most destructive type of vibration and is the primary perpetrator for BHA damage and poor borehole quality.

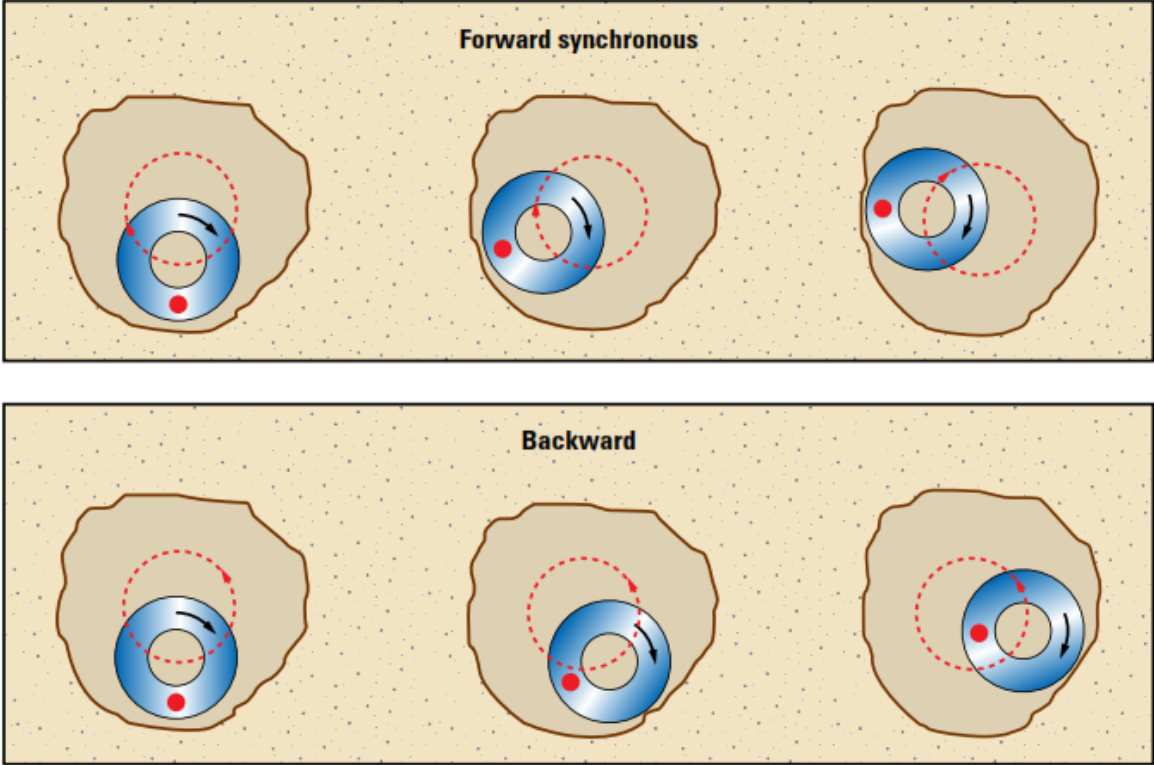


Figure 2.2 Whirl types for BHA (Schlumberger, 2010)

The three types of vibrations have different effects on drilling performance and have fundamental differences. They are most often coupled as they are not mutually exclusive events. Axial vibrations might lead to lateral vibration in the BHA, axial and torsional vibration observed at the rig during drilling might be related to lateral vibrations downhole (Schlumberger, 2010). This is why enhanced knowledge of axial vibrations also promotes further understanding on why lateral or torsional vibrations is observed, in addition to appropriate countermeasures necessary.

## **2.2 Equipment and software**

This chapter will give a general description of all the different equipment and software used for measuring the dynamic axial strain, which directly corresponds to axial vibrations

### **2.2.1 Strain gauge**

The method for measuring strain in the experiments in this thesis, were performed using strain gauges. Strain measurements represent the individual displacement of each sensory point on the model. The measured dynamic variation in displacement is therefore indicative of axial vibration in the physical drillstring model.

There are several methods of measuring the strain, but the most common one is with a strain gauges (National Instruments, 2016). Strain gauges are configured in a circuit where the amount of strain experienced by strain gauge corresponds to change in electrical resistance. This alteration in electrical in electrical resistance causes a change in voltage, which can be used to calculate strain.

The most common resistance value in a strain gauge is 120  $\Omega$ . The strain gauge consists of a metallic foil arranged in a grid pattern. The strain gauges are very small, with approximate dimensions of 20 x 20 mm. The grid pattern maximizes the amount of foil, but the grid itself is minimized to reduce the effect of shear strain and Poisson strain. The metallic foil is bonded to a thin backing, also called the carrier. This backing is attached to the specimen by special glue. The type of glue is dependent on the type of material whether it is steel or plastic, and the required lifetime of the measurement system. The surface where the strain gauges are be attached to the specimen has to be smoothed with sand paper, deoiled with solvents, and traces of the solvent has to be washed away. Immediately after this process, the strain gauges must be glued and attached to the specimen, in order to avoid oxidization or pollution of the prepared area.

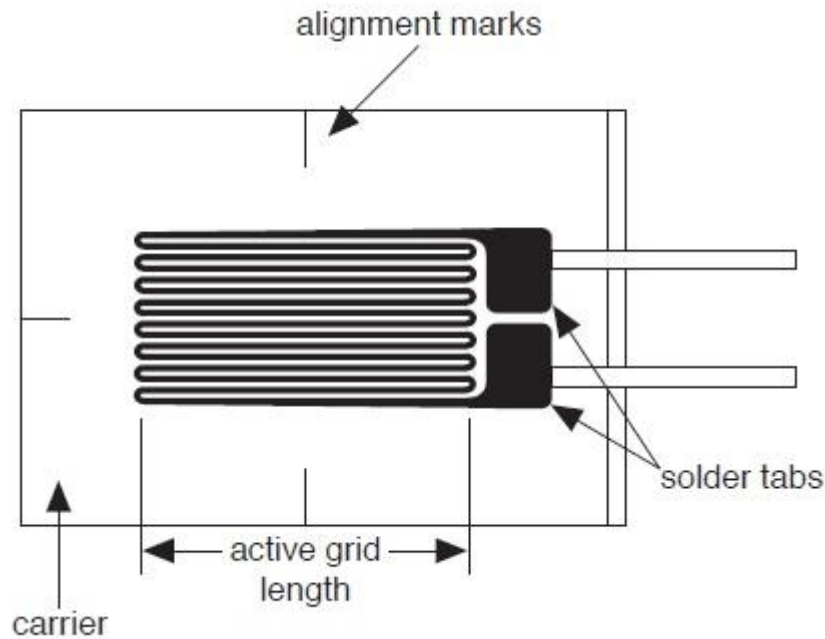


**Figure 2.3** Bonded metallic single element strain gauge (National Instruments, 2016)

Strain gauges are normally used in bridge configurations, which are unique circuit types used for strain gauge measurements. Voltage excitation from a power source is applied to input leads of the bridge circuit, and voltage readings are taken from the output leads, which are then converted to strain. This strain is typically measured in millistrain or microstrain depending on the sensitivity of the measurement. It is therefore very important that uncertainties in the measurement are controlled as much as possible in order to retain sufficient accuracy and precision.

### **2.2.1.1 Strain gauge bridge configuration used for dynamic strain measurements**

In order to measure strain the strain gauges are arranged in into a bridge circuit known as a Wheatstone bridge. Different type of bridge circuits are classified by the number of active strain gauges. These different type of bridge configurations are known as quarter-bridge, half-bridge and full-bridge, where the number of active gauges range from one to four. The Wheatstone bridge that is used in the dynamic strain measurements is a type of full-bridge.

The most common bridge circuit is the full-bridge configuration. This bridge circuit consist of four resistive arms with an excitation voltage,  $V_{EX}$ , that is applied across the bridge. Where the resistance in each four bridge arms represent a strain gauge

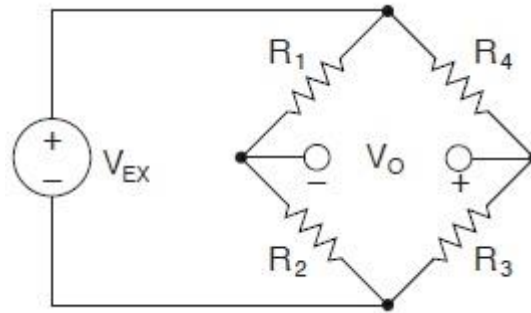


**Figure 2.4** Wheatstone bridge (National Instruments, 2016)

The full-bridge circuit can increase the sensitivity of the circuit compared to quarter-bridge circuit and half-bridge circuit. The full-bridge type III only measures axial strength. The bridge has four active strain gauge elements where two are mounted in the direction of axial strain, one at the bottom and the other at the top on the opposite side. The other two strain gauges works as Poisson gauges and are mounted perpendicular to the principle strain measurement with one on each side of the strain specimen. When the strain gauges are mounted this way they compensate for Poisson’s strain and rejects bending strain.

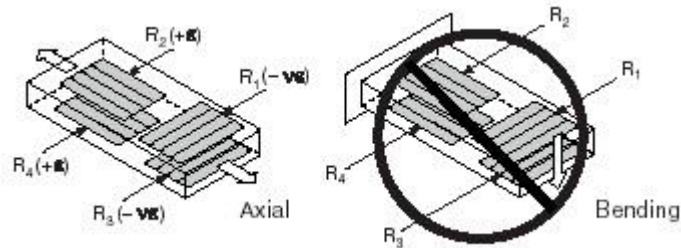


**Figure 2.5** Full-Bridge Type III measuring axial strength and reject bending strain (National Instruments, 2016)

In order to calculate strain from the voltage output, multiple parameters are required to correctly correlate the strain with change in voltage. This relationship is between voltage and strain is shown in equation below

$$\epsilon_{axial} = \frac{-2V_r}{GF((\nu + 1) - \nu_r(\nu - 1))} \quad (1)$$

Where Equation  $\epsilon_{axial}$  is axial strain, GF is the gauge factor,  $\nu$  is the Poisson ratio of the specimen and  $V_r$  is the effective voltage ratio reading caused by strain. Where the ratio for  $V_r$  can be expressed as

$$V_r = \frac{V_{strained} - V_{unstrained}}{V_{EX}} \quad (2)$$

The variable  $V_{strained}$  is the measured voltage when strained,  $V_{unstrained}$  is the initial unstrained voltage and  $V_{EX}$  is the excitation voltage. The excitation voltage is a constant value, which was set to 5V for the strain measurements. Inserting equation 2 into equation 1 the equation can be expressed as

$$\epsilon_{axial} = \frac{-2}{GF((\nu+1) - (\frac{V_{strained} - V_{unstrained}}{kV_{EX}})(\nu-1))} (\frac{V_{strained} - V_{unstrained}}{kV_{EX}}) \quad (3)$$

The value  $k$  is the voltage amplification factor from the signal amplifier, which ensures that the proper values of voltage is used

Lastly the gauge factor (GF) expresses the strain gauge's sensitivity to strain. It is defined as the ratio of the fractional change in resistance to the fractional change in length (strain).

$$GF = \frac{\Delta R / R}{\Delta L / L} = \frac{\Delta R / R}{\epsilon}$$

Where  $\Delta R$  is the change in strain gauge resistance,  $R$  is the unstrained resistance and  $\epsilon$  is strain. The GF for metallic strain gauges is typically 2.

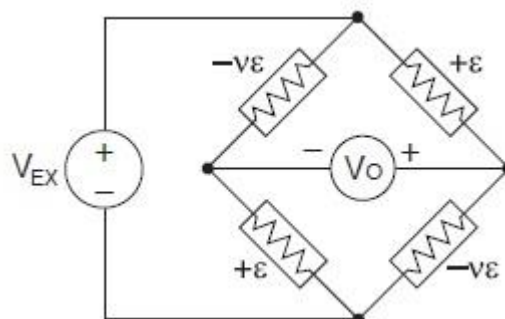
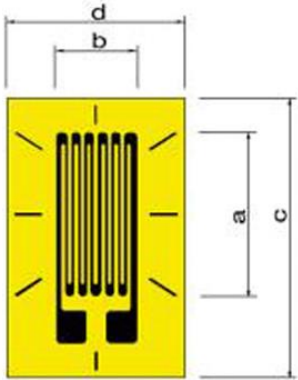


**Figure 2.6** Full-Bridge Type III Circuit Diagram (National Instruments, 2016)

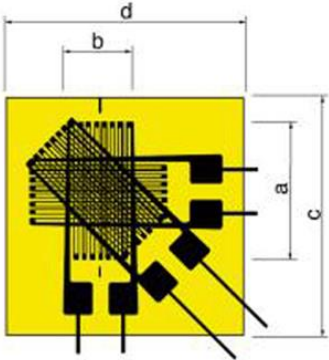
The full-bridge configuration shown with four active gauges is used to measure axial strain.

**2.2.1.2 Strain gauge rosette types**

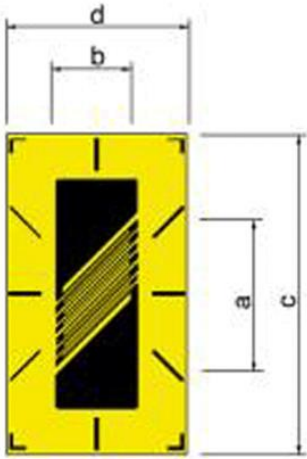
The only strain gauge type mentioned so far is the single element gauge. There are however many different types of strain gauges used for static and dynamic strain measurements. These different types range from stacked grid 90°, shear type to the two element 90° grid. The gauge type is selected based on what type of strain that is going to be measured. The stacked grid type rosette is usually chosen in order to determine the directions of the principal axes, whilst the shear rosette is used for shear strains.



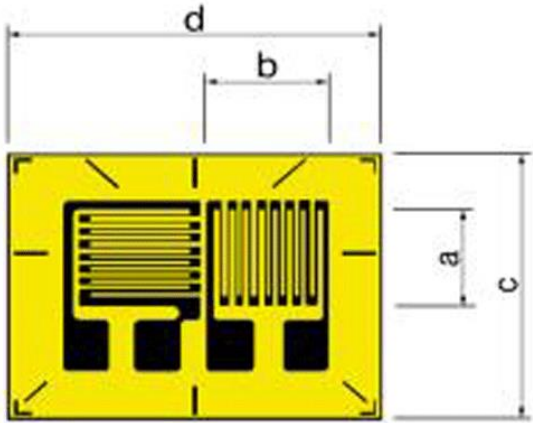
Regular single element strain gauge



Stacked grid 90°



Shear type



Two element 90° grid

**Figure 2.7** Overview of different rosette types (tradeKorea, 2016)

Dynamic strain measurements done in this thesis are conducted using so called Tee rosettes which is the two element  $90^\circ$  grid. The Tee rosette enables linear strain to be augmented by increasing the gauge factor when the two grids are connected, with an increased GF at 1.3 times the normal value with this arrangement (Vaughan, 1975). This was not done for the bridge configuration used in the measurements, which meant that GF was still equal to 2. This rosette type works well in full bridge configurations that emphasize the sensitivity for axial strain. This is because the perpendicular strain gauge setup cancels or reduces the amount of voltage measured from bending. The Tee rosette therefore synergizes well with the full-bridge type III setup.

### 2.2.2 Signal amplifier

There are many different types of signal amplifiers but the one used to measure strain in this thesis is known as a differential signal amplifier. The circuit for this amplifier is configured to amplify the difference between two input voltages (Electronic Tutorials, 2016), hence the name differential amplifier.

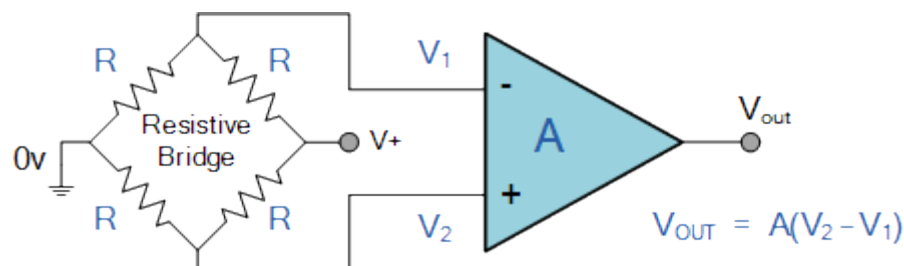


**Figure 2.8** Wheatstone bridge circuit configured with a signal amplifier (Electronic Tutorials, 2016)

The diagram above illustrates how the differential amplifier receives two voltage signals from the Wheatstone bridge, and produces an amplified voltage differential. The amplification is defined by the amplification factor  $k$ , which is often adjustable, however this depends on the signal amplifier. This factor value can range from anything from 10 to 1000. If the voltage output is measured at 1mV without a signal amplifier, then it will be 1V with a signal amplifier using an amplification factor of 1000.

The reason why signal amplifiers are useful, is that they are used to increase the sensitivity of the strain measurements. Signal amplifiers therefore often allow strain measurements to be conducted, which was previously impossible.

### 2.2.3 Analog-to-Digital converter

ADC is a device that has the ability to translate an analog electrical signal into a corresponding digital value (Analog devices, 2016). This digital value is reported by the ADC as ratiometric value, which is the ratio between a reference voltage and the measured analog voltage (Kester, 2005). The ADC used in the measurements in this thesis is an usb type shown in figure below.



Figure 2.9 USB-8451 ADC-DAC used in the measurements( (National Instruments, 2009)

It is the ADC that sets the maximum capacity for the sampling rate, which is 44 000Hz for the model used in the dynamic strain measurements. The total capacity can vary greatly depending on the individual ADC. It also determines the quality of converted analog signal. This is seen when you compare two ADCs where one has an 3-bit converter and the other a 16-bit converter.

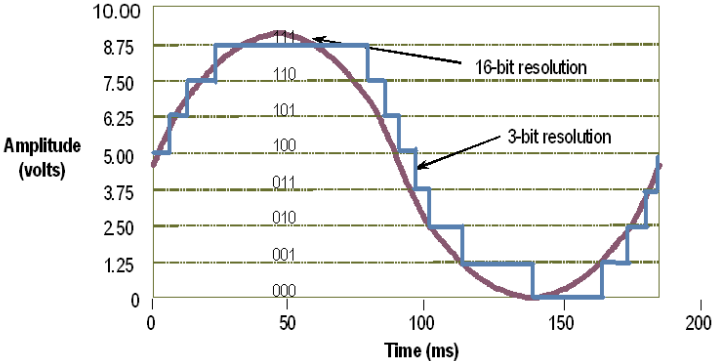


Figure 2.10 comparison between signal quality with regards to 3-bit and 16-bit converters (Engineering 360, 2011)

The precision of the ADC and the resulting strain measurement are directly related to the size of the bit converter.

## 2.2.4 LabVIEW

When using strain gauges to measure static strain it is not necessary to use software like LabVIEW as the potential difference across the bridge circuit can be measured using a multimeter/voltmeter. In order to measure dynamic axial strain, LabVIEW is required in order to record the continuous variation in strain that is caused by the axial vibrations.

LabVIEW is software that uses G programming language which enables quick data acquisition, logical operation and analysis. This graphical data flow language distinguishes it from other programming languages, which has more administrative complexity with memory allocation and syntax (National Instruments, 2016). The result is an intuitive graphical approach that puts emphasis on data and data operations instead

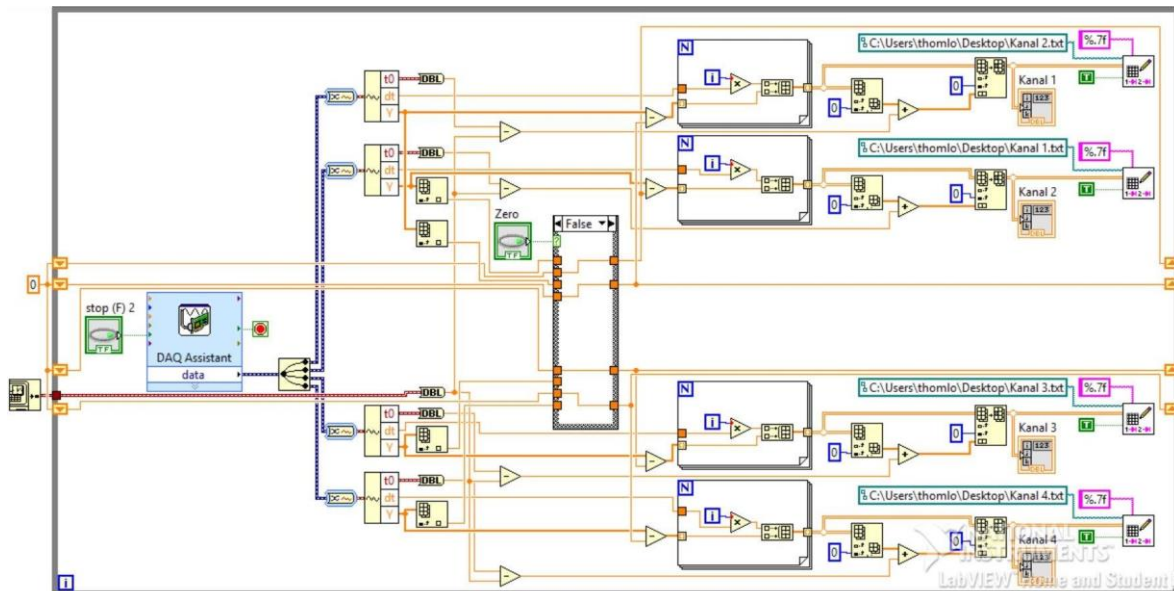


**Figure 2.11** LabVIEW flowchart for sampling data from 4 different sensory points used in dynamic strain measurements

LabVIEW supports integration of a large amount hardware, large variety of data acquisition devices and sensors. The main strength of LabVIEW is its ability to integrate these different hardware devices in order to automate the measurement (National Instruments, 2016) This is what makes it possible to use strain gauges to measure variation in axial strain with sampling rates up to 44 000 Hz from the ADC, which is impossible for manual individual measurements.

### 3 Lumped element model of drillstring

Mechanical vibrations from the small-scale drillstring model in this thesis is modelled as a lumped element system with  $n$ -degrees of freedom. Where the only motion expressed by the model is the displacement in the axial direction. The system being expressed as mass-spring-damper in association with  $n$ -degrees of freedom simplifies the model enough for an analytical expression to be used. These assumptions made with regards to axial vibration is what makes it possible to attain the closed form solution for this analytical model. The lumped element model is derived using notes from (Benaroya, 2004) and (S.Hovda, 2015)

The analytical model starts by modelling the drillstring as a set of  $n$ -blocks that are connected by  $n$ -springs. The one dimensional coordinate system is set such that positive is in the downward direction.

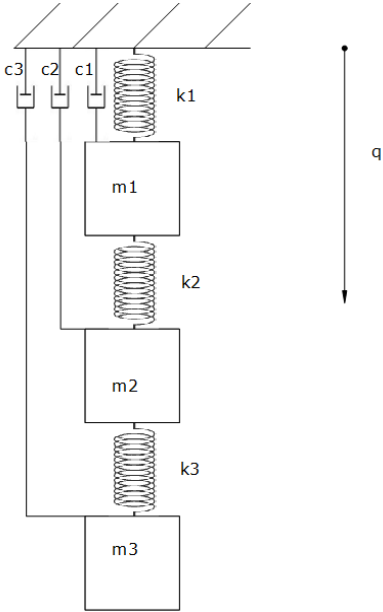


Figure 3.1 Illustration of  $n=3$  mass and spring elements in a mass-spring-damped system

The mass and spring constants are represented by variables  $m_i$  and  $k_i$  respectively, whilst the damping effect in the system is illustrated as a dashpot with damping coefficient  $c_i$ . The variable  $q_i$  represents the position of the blocks with the top position starting at zero. Using Newton's second law of motion this system of mass springs can be represented as

$$0 = \begin{cases} -m_i \ddot{q}_i + m_i g - k_1 q_1 + k_2 (q_2 - q_1) - c_i \dot{q}_i & \text{for } i = 1 \\ -m_i \ddot{q}_i + m_i g - k_i (q_i - q_{i-1}) + k_2 (q_{i+1} - q_i) - c_i \dot{q}_i & \text{for } 2 \leq i \leq n-1 \\ -m_n \ddot{q}_n + m_n g - k_n (q_n - q_{n-1}) - c_n \dot{q}_n & \text{for } i = n \end{cases} \quad (4)$$

The assumption made is that the buoyancy term can be neglected from the force of gravity, This is because the model is not going to be submerged in liquid, and buoyancy due to air at 25° Celsius is completely negligible. It is important to note that each mass is treated as dimensionless, where the mass is concentrated at an infinitesimally small point. The springs are assumed be massless, but has spatial dimensions. This is because the drillstring is modelled as a lumped system. Where the drillstring is divided into discrete points where the mass points are rigid bodies and the only interaction between occurs through kinematic pairs, in the form of springs (Hartenberg & Denavit, 1964).

Equation 4 describing the forces in the mass-spring-damped system can be viewed as a system of n coupled second order linear differential equations. This can be written in matrix form as

$$\mathbf{M}\ddot{\mathbf{q}} + \mathbf{C}\dot{\mathbf{q}} + \mathbf{K}\mathbf{q} = \mathbf{g} \quad (5)$$

Where  $\mathbf{M}$  is a diagonal matrix with masses  $m_i$  on the diagonal and diagonal matrix  $\mathbf{C}$  with values of  $c_i$  on the diagonal.  $\mathbf{K}$  is a tridiagonal matrix with values along its main diagonal and its adjacent diagonals as shown below. It is important to note that matrices  $\mathbf{M}$ ,  $\mathbf{C}$  and  $\mathbf{K}$  have dimensions n x n

$$\mathbf{K} = \begin{bmatrix} k_1 + k_2 & -k_2 & 0 & \cdots & 0 & 0 & 0 \\ -k_2 & k_2 + k_3 & -k_3 & \cdots & 0 & 0 & 0 \\ 0 & -k_3 & k_3 + k_4 & \cdots & 0 & 0 & 0 \\ \vdots & \vdots & \vdots & \ddots & \vdots & \vdots & \vdots \\ 0 & 0 & 0 & \cdots & k_{n-2} + k_{n-1} & -k_{n-1} & 0 \\ 0 & 0 & 0 & \cdots & -k_{n-1} & k_{n-1} + k_n & -k_n \\ 0 & 0 & 0 & \cdots & 0 & -k_n & k_n \end{bmatrix}$$

The next step is to remove the gravity term so that the equilibrium position  $y_i = 0$  represents the systems natural resting position, instead of the rare case with zero axial strain as with a massless spring when  $q_i = 0$ . In order to achieve this the coordinate transformation  $y = q - \mathbf{K}^{-1} \mathbf{g}$  needs to be applied to equation 5, which then becomes

$$\mathbf{M}\ddot{\mathbf{y}} + \mathbf{C}\dot{\mathbf{y}} + \mathbf{K}\mathbf{y} = 0 \quad (6)$$

The only issue remaining is that matrix  $\mathbf{K}$  is not a diagonal matrix, which means that the existing system is coupled. The system must therefore be decoupled, and this is done by solving the generalized eigenvalue problem for  $\mathbf{M}$  and  $\mathbf{K}$  where

$$\mathbf{M}\mathbf{v} = \lambda\mathbf{K}\mathbf{v}$$

Solving this problem results in a diagonal matrix  $\mathbf{D}$  with eigenvalues and matrix  $\mathbf{V}$  with eigenvectors, with both having dimension  $n \times n$ . The relationship between these four matrices can be describes as

$$\mathbf{V}^T \mathbf{M} \mathbf{V} = \mathbf{I}$$

$$\mathbf{V}^T \mathbf{K} \mathbf{V} = \mathbf{D}$$

Lastly by doing one more coordinate transformation where  $\mathbf{y} = \mathbf{V}\mathbf{x}$  and multiplying equation 6 with  $\mathbf{V}^T$  results in

$$\ddot{\mathbf{x}} + \mathbf{V}^T \mathbf{C} \mathbf{V} \dot{\mathbf{x}} + \mathbf{D} \mathbf{x} = 0 \quad (7)$$

Using the approximation for relationship  $\mathbf{C} = c\mathbf{M}$  where  $c$  is a constant value, which can be approximated as the largest value of  $c_i/m_i$ , where  $c_i$  is the damping coefficient per element.

The value  $c$  will be referred to as the damping constant in this thesis, which is used to define the damping of all the individual segments. Inserting  $\mathbf{C} = c\mathbf{M}$  into equation 7 results in

$$\ddot{\mathbf{x}} + c\dot{\mathbf{x}} + \mathbf{D}\mathbf{x} = 0 \quad (8)$$

Now that the system has been decoupled it is possible to solve for  $\mathbf{x}$ , but  $c$  and  $\mathbf{D}$  will first be substituted out with more recognizable coefficients. These substitutions are  $\zeta_i = c/2\omega_i$  and  $D_{ii} = \omega_i^2$ , and this then results in the familiar 2<sup>nd</sup> order ODE with linearly expressed damping

$$\ddot{x}_i + 2\zeta_i \omega_i \dot{x}_i + \omega_i^2 x_i = 0 \quad (9)$$

The analytical model allows the oscillations from the system to be determined based on mechanical properties of the model. The measurements conducted in this thesis deal with changing the initial condition for  $x_i(0)$  by applying an end mass, and by subsequently releasing it in order to incite vibrations in the system. This means that the type of vibration as well as type of damping needs to be accurately determined. This is to ensure that the best possible comparison is made with the dynamic strain measurements.

The damping scenario is determined by the roots of the characteristic equation of the ODE, and provide three general solutions for the analytical model. These three different scenarios possible depends on the value of the damping ratio  $\zeta_i$ , which will result in the system being critically damped, over damped and under damped. The roots of the characteristic equation shown below.

$$\begin{aligned}\gamma_{i,1} &= -\zeta_i \omega_i + \omega_i \sqrt{\zeta_i^2 - 1} \\ \gamma_{i,2} &= -\zeta_i \omega_i - \omega_i \sqrt{\zeta_i^2 - 1}\end{aligned}\tag{10}$$

This in turn means that the solution to the differential equation will be in the form

$$x_i(t) = A_i e^{\gamma_{i,1}t} + B_i e^{\gamma_{i,2}t}\tag{11}$$

The superposition of modal solutions solution for  $x_i(t)$  must then be applied, which corresponds to the coordinate transformation  $\mathbf{y} = \mathbf{V}\mathbf{x}$ . Using equation 10 and equation 11 one can obtain final solution for the lumped element model as shown below

$$y_j(t) = \sum_{i=1}^n V_{ji} x_i(t)\tag{12}$$

In equation 12 elements j is equal to the total number of n elements. This means that when one evaluates a model as n=10 elements, the total number of j elements is also 10.

The final step would then be to determine the values of A and B based on the initial conditions of the system from  $x_i(0)$  and  $\dot{x}_i(0)$ . The initial conditions are perhaps the most important set of information that allows the analytical model to numerically the transient response of a physical drillstring model when subjected to a mass-release reaction. The main criterion for this is that analytical model has to abide by Hooke's law. Displacement due to the force of the mass applied needs to be correct for all values of n elements. This means that the displacement due to additional weight is independent of the number n elements that the system is evaluated as. This is shown in figure 3.2 where the final element in the drillstring has the same initial displacement from its natural equilibrium, regardless if this is the final element of total n=4 elements or n=1. Given that the system is exposed to the same amount of weight.

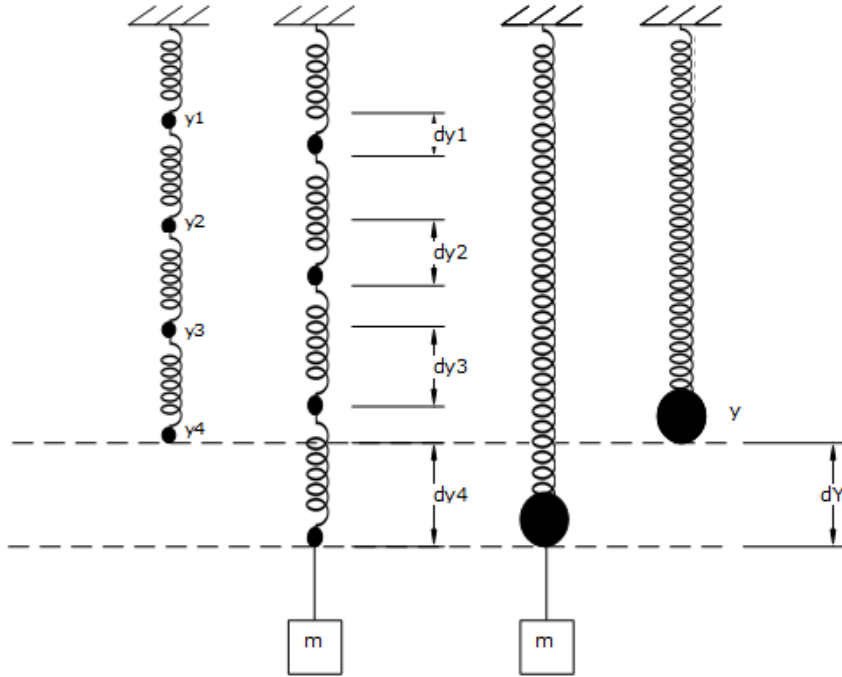


**Figure 3.2** Diagram illustrating the how the initial conditions abide by hooks law regardless of number of n segments for the lumped element model

In order for this to be the case for the analytical model, then the initial condition must be  $\mathbf{x}(0) = (\mathbf{K}^{-1}\mathbf{w})$ . Where  $\mathbf{w}$  is a vector with zero values except at the element where the additional weight is added

$$\mathbf{w} = \begin{bmatrix} 0 \\ 0 \\ \vdots \\ \text{weight} \end{bmatrix}$$

This causes all the n elements of  $x_i$  to be displaced in accordance with Hooke's law as displayed in figure 3.2. Due to the nature of the coordinate transformation when expressing displacement in terms of  $y_j(t)$ , the coordinate transform  $\mathbf{V}^{-1}\mathbf{y} = \mathbf{x}$  means that initial condition for  $y_j(0)$  is

$$y_j(0) = \sum_{i=1}^n V_{ji} (\mathbf{V}^{-1}\mathbf{x}(0))_i$$

The other important part for each solution is that the column vector  $A_i$  and  $B_i$  will be expressed in terms of  $\mathbf{V}^{-1}$ ,  $\mathbf{K}$  and  $\mathbf{w}$ . This sets the initial condition to be equal to displacement caused because displacement in addition to gravity.

### 3.1 Underdamped

The first damped scenario is when the system is underdamped, which occurs when  $0 < \zeta_i < 1$  for which the characteristic equation has two complex roots. In this case, the damping in the system is not enough to prevent the system from oscillating and axial vibrations becomes distinguishable. If one recognizes that the roots of the characteristic equation can be written  $\gamma_i = -\zeta_i \omega_i \pm \omega_i \sqrt{1 - \zeta_i^2} i$ , then solution to under damped scenario can be written in the form

$$x_i(t) = e^{-\zeta_i \omega_i \pm i \omega_i \sqrt{1 - \zeta_i^2} t}$$

Then by applying Euler's formulae  $e^{it} = \cos(t) + i \sin(t)$  the equation can be written as

$$x_i(t) = e^{-\zeta_i \omega_i t} (\cos(\omega_i \sqrt{1 - \zeta_i^2} t) \pm i \sin(\omega_i \sqrt{1 - \zeta_i^2} t))$$

The problem with the current equation is that it has an imaginary term and the interest lies only with real solutions. The solutions in a linear homogenous ODE are made up of sums of linearly independent solutions, where the imaginary part of the solution separately satisfy the ODE. The constant in front of the sine can then be considered arbitrary then the equation can be rewritten as

$$x_i(t) = e^{-\zeta_i \omega_i t} (A_i \cos(\omega_i \sqrt{1 - \zeta_i^2} t) + B_i \sin(\omega_i \sqrt{1 - \zeta_i^2} t))$$

Then the process to attain the solution becomes straightforward where the initial conditions become  $x_i(0) = A_i$  and  $\dot{x}_i(0) = B_i \omega_{d,i} - A_i \zeta_i \omega_i$ , and using the expression for damped natural frequency  $\omega_{d,i} = \omega_i \sqrt{1 - \zeta_i^2}$ . Inserting these values  $x_i(t)$  can be written as

$$x_i(t) = \left( A_i \cos(\omega_{d,i} t) + \frac{\zeta_i \omega_i}{\omega_{d,i}} A_i \sin(\omega_{d,i} t) \right) e^{-\zeta_i \omega_i t}$$

Then by applying the by the superposition of modal solutions and inserting  $A_i = (\mathbf{V}^{-1}\mathbf{K}^{-1}\mathbf{w})_i$ , as well as using  $\zeta_i = c / 2\omega_i$ . The final solution for the underdamped system becomes

$$y_j(t) = \sum_{i=1}^n V_{ji} (\mathbf{V}^{-1}\mathbf{K}^{-1}\mathbf{w})_i \left( \cos(\omega_{d,i}t) + \frac{c}{2\omega_{d,i}} \sin(\omega_{d,i}t) \right) e^{-\frac{c}{2}t} \quad (13)$$

This represents underdamped behavior of the analytical model.

### 3.2 Critically damped

The second scenario is for critically damped vibration, which is the fastest displacement the system can experience without oscillating. This occurs when  $\zeta_i = 1$  which causes the characteristic equation to have double roots. The solution for this instance becomes due to repeating roots

$$x_i(t) = A_i e^{-\omega_i t} + B_i t e^{-\omega_i t}$$

Using the intital conditions  $x_i(0) = (\mathbf{K}^{-1}\mathbf{w})_i$  and  $\dot{x}_i(0) = 0$ , results in  $x_i(0) = A_i$  and  $\dot{x}_i(0) = B_i - \omega_i A_i$ . The equation can be rewritten as

$$x_i(t) = A_i (1 + \omega_i t) e^{-\omega_i t}$$

Then the applying the coordinate transformation  $\mathbf{y} = \mathbf{V}\mathbf{x}$  you get

$$y_j(t) = \sum_{i=1}^n V_{ji} A_i (1 + \omega_i t) e^{-\omega_i t}$$

The initial condition needs to satisfy Hooke's law, which occurs when  $A_i = (\mathbf{V}^{-1}\mathbf{K}^{-1}\mathbf{w})_i$  this means that final solution for the critically damped scenario becomes.

$$y_j(t) = \sum_{i=1}^n V_{ji} (\mathbf{V}^{-1}\mathbf{K}^{-1}\mathbf{w})_i (1 + \omega_i t) e^{-\omega_i t} \quad (14)$$

Equation 14 is the critically damped solution for analytical model used to compare to the experimental data.

### 3.3 Overdamped

Over damped is similar to critically damped but here the damping ratio is  $\zeta_i > 1$  for which the characteristic equation has two real roots. The solution of this is in the form

$$x_i(t) = A_i e^{\gamma_{i,1}t} + B_i e^{\gamma_{i,2}t}$$

With the over damped scenario the initial conditions are a bit different compared to the critically damped solution. In this case values for  $A_i$  and  $B_i$  cannot be simplified more than as shown

$$A_i = \left( 1 + \frac{\gamma_{i,1}}{\gamma_{i,2} - \gamma_{i,1}} \right) x_i(0)$$

$$B_i = -\frac{\gamma_{i,1}}{\gamma_{i,2} - \gamma_{i,1}} x_i(0)$$

Then by applying the superposition of modal solutions, substituting in values of  $A_i$  and  $B_i$  with  $\mathbf{x}(0) = \mathbf{K}^{-1}\mathbf{w}$  one gets the solution in the form

$$y_j(t) = \sum_{i=1}^n \mathbf{V}_{ji} (\mathbf{V}^{-1}\mathbf{K}^{-1}\mathbf{w})_i \left( \left( 1 + \frac{\gamma_{i,1}}{\gamma_{i,2} - \gamma_{i,1}} \right) e^{\gamma_{i,1}t} - \frac{\gamma_{i,1}}{\gamma_{i,2} - \gamma_{i,1}} e^{\gamma_{i,2}t} \right) \quad (15)$$

Equation 15 is the final solution for the analytical model, which is used to describe the over damped behavior.

## 4 Physical drillstring model

The small-scale physical drillstring model that is used to conduct the dynamic strain measurements is made from plexiglas segments and steel joint segments, where plexiglas is the trademark name for a type of thermoplastic. The entirety of the model can be viewed as chain where all the segments are bolted together. This allows the strain gauges that are attached to the individual segments to be relocated without a having to remove and attach new strain gauges each time.

The model was also designed so that it would follow complex 2D wellpaths for which the effects of coloumb friction and transmission loss could be investigated in detail. This however

is not investigated in this thesis. The purpose behind the individual design choice for the model is discussed in further detail in “TPG4520 Drilling technology specialization project”

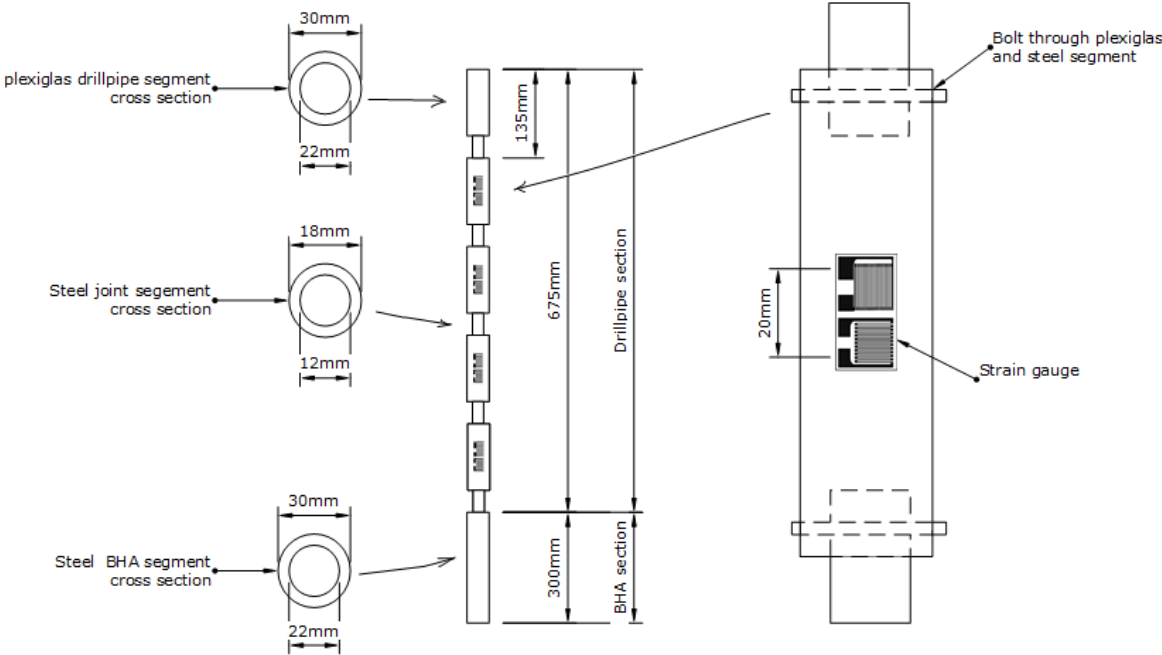


**Figure 4.1** Layout of the drillstring model illustrating dimensions of DP and BHA sections

Figure 4.1 illustrates the general layout of the model and how it is divided into a DP section which is the part consisting of interlocking plexiglas and steel. The BHA section that is made out of a single segment. The diagram illustrates how the strain gauges are mounted on the model. These strain gauge make up bridge circuits which what enables strain to be measured. These bridge circuit is referred to as sensory points in this thesis. The placement of these sensory points are sequential from top to bottom. Where sensory point 1 is at the top and sensory point 4 is at the bottom.

The dimensions and parameters for the chain model are presented in the table below

Segment	Outer diameter[mm]	Inner diameter[mm]	Total Length[mm]	Mass[g]	Young’s modulus[GPa]
Plexiglas	30	22	95	34	3.1
Steel joint	18	12	100	110	200
BHA	30	22-0	300	1534	200

**Table 4.1** Dimensions and physical paramaters for individual segment type

The model as shown in the figure 4.1 is displayed consisting of 5 plexiglas, 5 steel joint and 1 BHA segments at a total length of 0.975m and a total mass of 2.3kg. This was one of the primary configurations used for in measurements. Dynamic strain measurements were also done with the model adjusted to 19 plexiglas,19 steel joint,1 BHA segment with a total length of 2.875m and total mass of 4.3kg.

Being a model however means that it differs a great deal from an actual drillstring .The first two aspects are the mass distribution and length distribution between the drillpipe section and the BHA. The BHA section is approximately 10% of the total length and 20% of the total mass of the drillstring (University of Aberdeen, 2014), as an average indicator of length/mass relationship. The distribution for drillstring model with n=10 segments(5 plexiglas an steel segments) is that the BHA accounts for 30% of the length and 68% of the total mass. The actual difference between real drillstring parameters are not limiting factors for measuring axial vibrations. The analytical model can be made to represent any number of parameters and distributions of mass and length, and the objective is to match these results with measured data. As long as the lumped element model is correctly approximated to the drillstring model, using correct parameters. This however means that the measured results from using this model does translate to the axial vibrations that observed in a real drillstring.

The other important difference is that the drillstring model is made out intervals of plastic and steel. In addition to the fact that the BHA is a partially milled out cylinder. The overall effect is that the distribution of mass in the DP section and BHA section are also much different in addition to variation in mechanical properties between steel and thermoplastic.

## **5 Measurement of axial vibrations with strain gauges using physical drillstring model**

The focus of this chapter is based around the experimental setup using the physical drillstring model from chapter 4. In addition to describing the entire process of measuring axial vibrations through dynamic strain measurements. Then to present the results from the dynamic strain measurements.

### **5.1 Experimental setup with physical drillstring model**

The dynamic strain measurements that was conducted with the physical drillstring model were done using two different experimental setups, a lab stand and ceiling hook setup. These measurements were done by altering length, internal mass and size of the end mass comparing the effect it had on the systems transient response. The lab stand setup had the focus of highlighting the difference in axial vibrations measured from the model with and without BHA. The ceiling hook setup had the focus on highlighting the effect of variation in length. This is why the measurements with the ceiling hook setup have no result for drillstring without BHA.

### 5.1.1 Lab stand setup

The setup for the first number of experiments that was conducted were done by having the entire model be fastened at the top plexiglas segment using a combination two lab stands. The top plexiglas segment was fastened with interlocking clamp arms to support the weight. This was done in order to increase the stability of the entire structure to improve measurement accuracy.

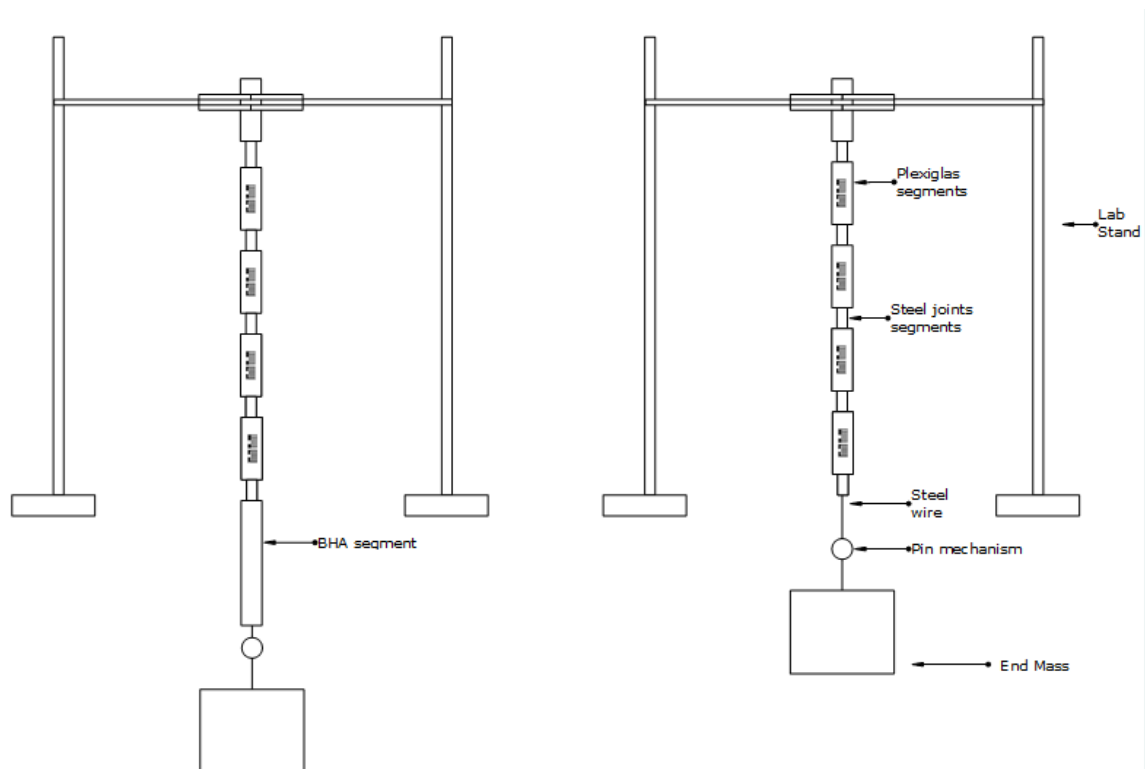


**Figure 5.1** Diagram illustrating the experimental setup for measuring axial vibrations using strain gauges (with and without BHA)

The two variations of this setup shown in figure 5.1 were done to measure the difference in transient response for the drillstring model with and without BHA.

### 5.1.2 Ceiling hook setup

The second experimental setup was done by attaching the drillstring model to a hook in the ceiling. This allowed the drillstring model to be modified for much larger lengths than with the previous setup. The reason behind this change was that the lab stand was unable to support the increased weight accompanied by increasing the length. The second reason was that the ceiling hook ensured that the vertically suspended drillstring was more firmly attached than previously. This was done in hopes to further reduce the uncertainty in the measurement.

This setup allowed the drillstring standard model with 10 drillpipe segments to be increased to 38, which meant that the total length of the drillstring model was increased to 2.865m. This was in order to see what variation the drillstring length would have on the measured data, and if this change was noticeable compared to measurements done with the 0.975m drillstring.

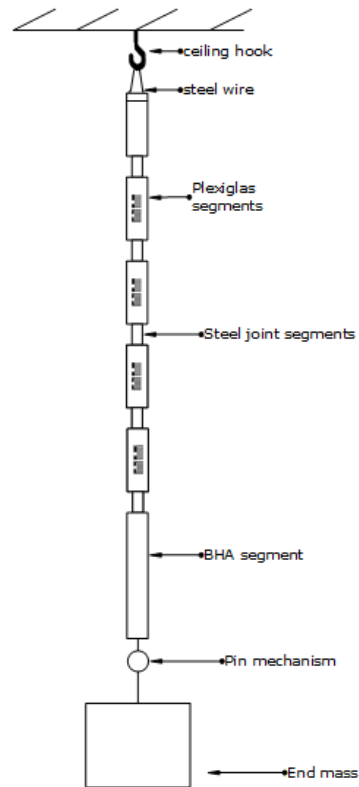


**Figure 5.2** the 0.975m drillstring model attached to a ceiling hook with steel wire for altered experimental setup

The setup is illustrated in figure 5.2, which shows how the 0.975m (n=10 DP segments) drillstring model is vertically suspended by the ceiling hook.

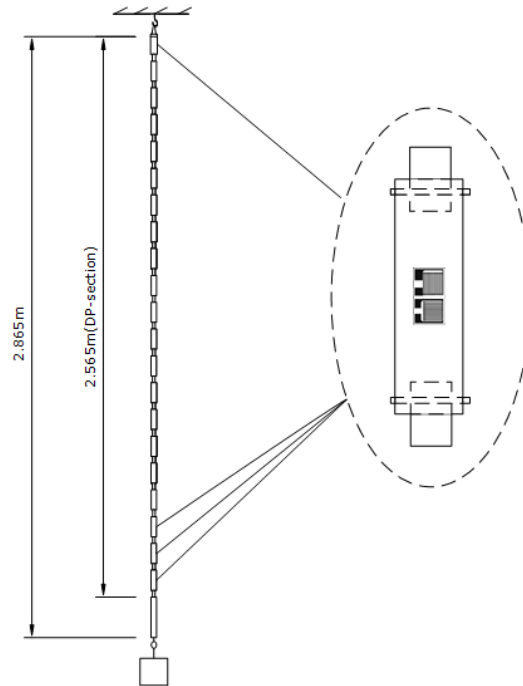


**Figure 5.3** increased length drillstring model showing positions of strain gauges(sensory points)

Figure 5.3 shows the 2.865m ( $n=38$  DP segments) and the placement of the individual strain gauges. The sequential order for each sensory point was retained, meaning that number 1 was still at the top segment and 4 at the bottom, where 2 and 3 were placed at the 3<sup>rd</sup> and 2<sup>nd</sup> final segment.

## 5.2 Experimental process and data Acquisition

The process by which the axial vibrations are created in the measurements was by exposing the system to an initial condition, for which the drillstring is subjected to strain in addition to gravity. There is no driving force causing the system to oscillate. This means that the axial vibrations created oscillate at the natural frequencies for the system, which is the systems transient/natural response.

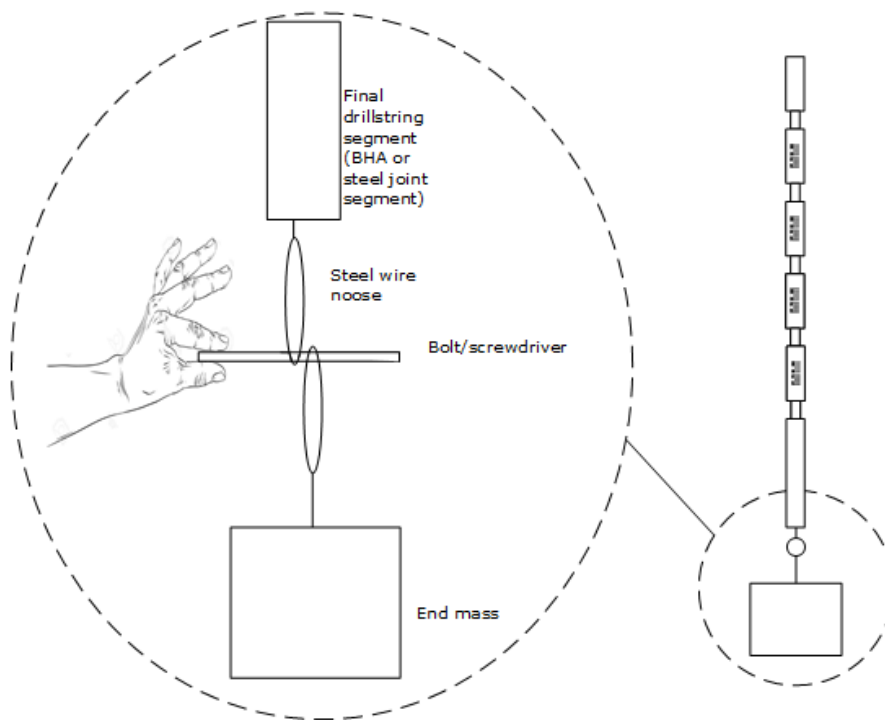


**Figure 5.4** Illustration of the mass release method used to incite the transient response for the dynamic strain measurements

In these measurements this was done by using an end mass that was attached to a pin mechanism. The end of the drillstring and the mass was attached to a steel wire, where the ends were tied as a noose. The pin that went between the two nooses is what serves as the pin mechanism. This pin mechanism worked as illustrated in figure 5.4, where a bolt/screwdriver was inserted between the nooses to prevent the end mass from falling. This bolt/screwdriver when released had no force supporting it on the left side, and subsequently rotates and allows the end mass to fall. The process was easy to repeat and allowed the measurements to be conducted and as many times necessary in order to get a good amount of data.

When the system undergoes a transient response, the measured data is transferred from the strain gauges to the signal amplifier, ADC and then the PC. These components were connected in the sequence showed below, which also shows the flow of data in the signal chain.

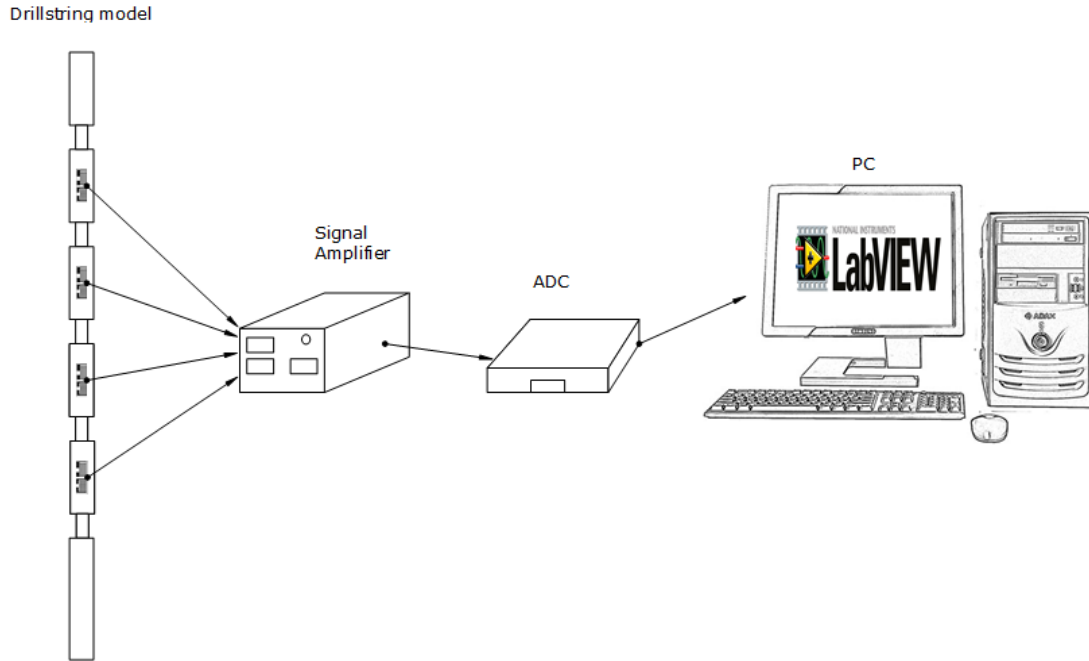


**Figure 5.5** Diagram highlighting the transmission of data from the strain gauges to Labview on the PC

The diagram illustrates how the four strain gauge sensors are connected to a differential amplifier, which is connected to the ADC. Data collected and converted by the ADC is then processed using LabVIEW software on the computer.

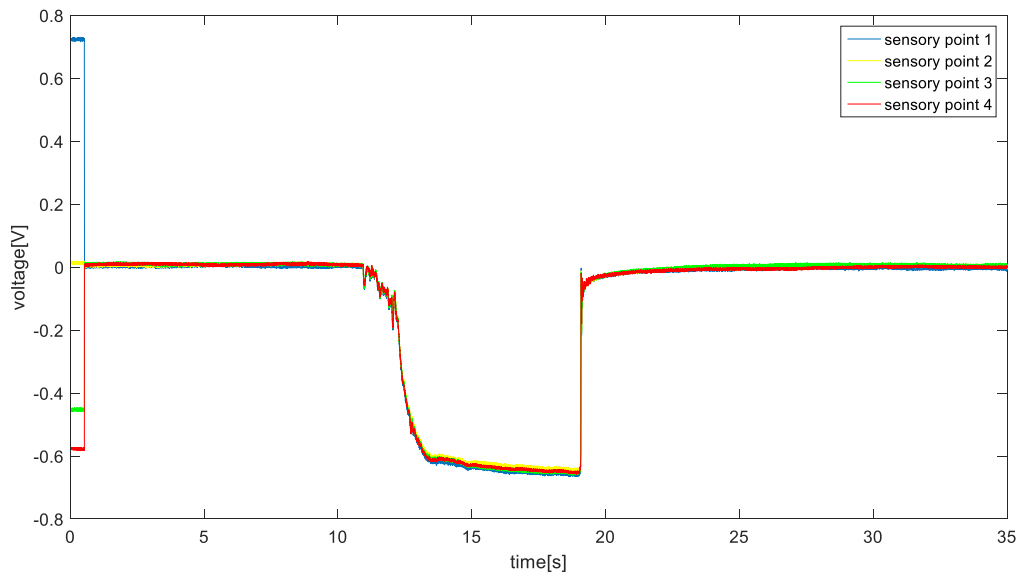


**Figure 5.6** shows the entire process of nulling offset and loading/releasing 4.3 kg mass “only drillpipe section”

The data obtained from labVIEW from each sensory point show the entire process of the measurement, where the voltage readings are first nullified using built in offset nulling calibration in Labview. This process also sets the equilibrium state for the model to exclude the strain caused by gravity, which is necessary when correlating the results with the analytical model. The final part of each test is that the model is loaded with the mass, which is not released until a stable voltage reading is achieved. The mass release method is then done as fast as possible in order to keep the approximation for the initial conditions as accurate as possible.

The voltage measured is not automatically converted into strain, which instead are computed after each measurement. The raw voltage readings from the strain gauges are converted into strain using equation 3 in combination with computational software to handle the quantity of data measured.

### **5.3 Dynamic strain measured data**

This section will present the dynamic strain results from the both of experimental setups. The strain measured were conducted using the 0.975m and 0.675m drillstring, with respective mass of 2.3kg and 0.7kg. In addition to the 2.875m drillstring configuration which had a total mass of 4.3kg. All the measurements conducted are also shown for the same interval of time selected as 0.4 seconds, to ensure that similarities and variations could be easily highlighted. The sensitivity involved with dynamic strain measurement meant that many of the measurements could not be used, and is why only the best results are presented.

In addition, technical difficulties meant that the measurements conducted with the lab stand setup only had 3 functional sensory points. This was because the bottom sensory point had to be replaced (sensory point 4). However, this had no compromising effects on the measurements overall. It just meant that the measurements with the ceiling hook, had more measurement per data set compared to the ones with the lab stand.

The final part is that for the dynamic strain measurements, tensile strain is displayed as negative whilst compressive strain is positive. Axial strain that is caused by tension is normally represented as positive, but in this thesis is shown as negative in order to have the strain correspond with the actual displacement, where positive is the opposite direction of gravity.

### 5.3.1 Lab stand setup: 4.3 kg mass release without BHA

This measurement was conducted with the 675 mm long DP section of the drillstring weighing roughly 740g. The measurement using only drillpipe section of the model without using BHA for additional mass had the results as shown in figure 5.7.

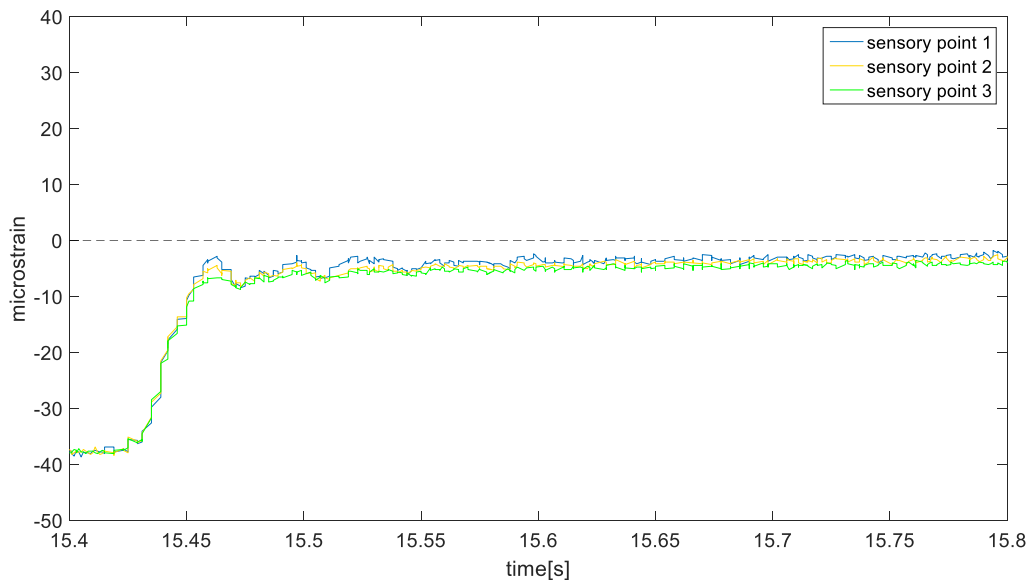


**Figure 5.7** Dynamic strain measured after releasing 4.3kg mass for drillstring without BHA section shown for sensory points 1-3 over a 0.4 sec interval

The results from releasing the weight produced a graph that illustrates the rapid change from its initial position toward the equilibrium position until the strain reached approximately -7 microstrain, where the strain asymptotically returns to zero strain. These results seem to might indicate overdamped, because there were no visible vibration. This however depends on how you evaluate the results, although poorly defined it is still possible to discern small vibrations(oscillations) in the data.

### 5.3.2 Lab stand setup: 4.3 kg mass release with BHA section

The measurement conducted using the entire 975mm drillstring model with the BHA section, where the BHA section itself has weighed approximately 1574g. This increased the inherent mass of the system from 0.7kg to 2.3kg. This test were done with the mass still attached to the end of DP section and not the BHA section, so that the same  $w$  could be used when comparing the results to the analytical data.

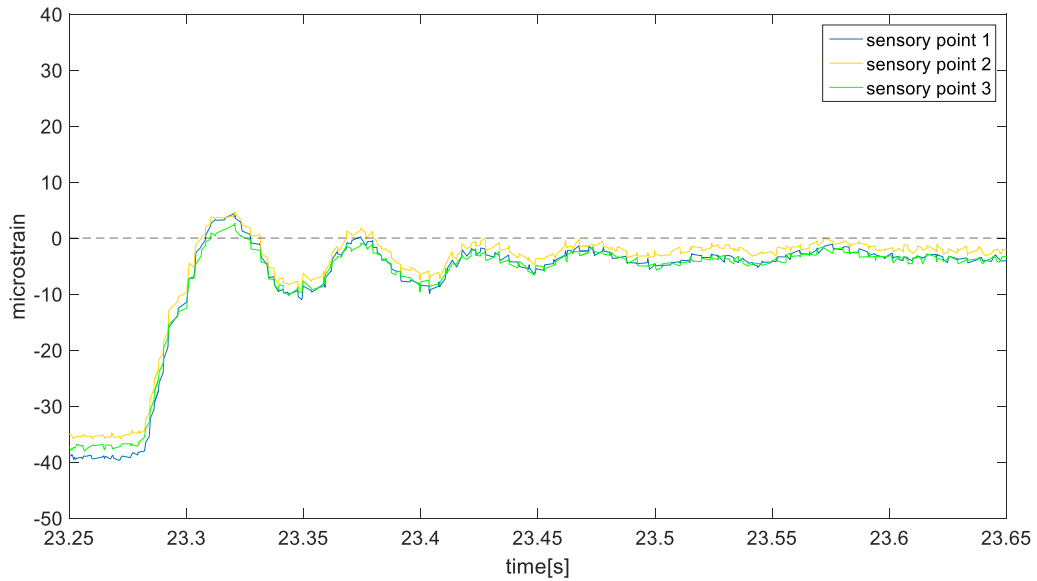


**Figure 5.8** Dynamic strain measured after releasing 4.3kg mass for drillstring with BHA section shown for sensory points 1-3 over a 0.4 sec interval

The results in figure 5.8 show a clear indication of axial vibration. This also showed that the inherent mass from the BHA had visible effects on the systems transient response. The system is also clearly underdamped, with the distinction being that the vibration does not occur about zero.

### 5.3.3 Lab stand setup: 10kg mass release with BHA

Measurement were also done to see if there would be any noticeable change when changing the weight of the end mass. The results gave similar response to 4.3kg mass release albeit more poorly defined oscillations/vibrations.

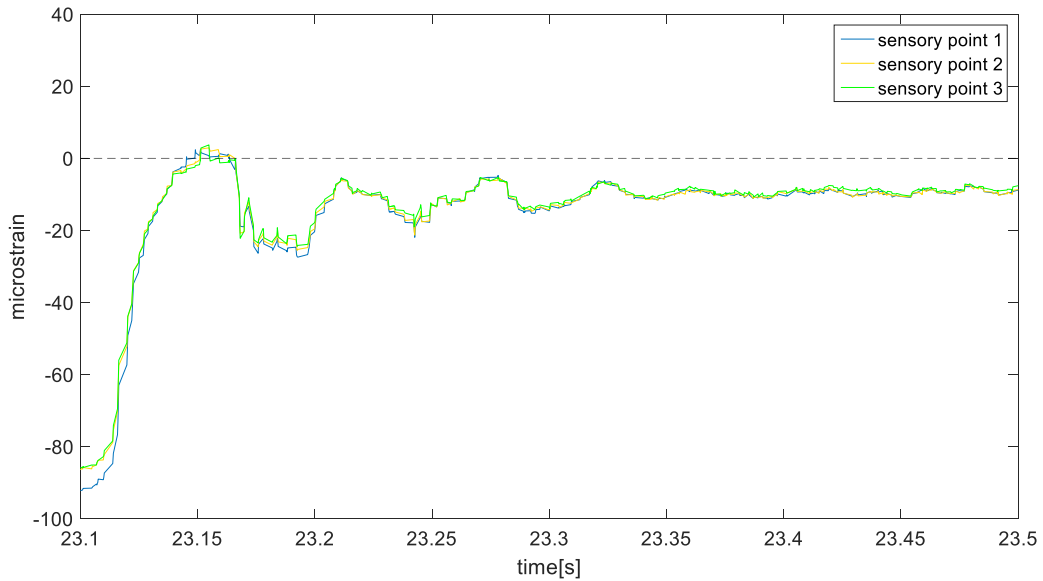


**Figure 5.9** Dynamic strain measured after releasing 10 kg mass for drillstring with BHA section shown over a 0.4 sec interval

The main discernable variations is that the intital condition roughly doubled. It is possible to also see the changes with regards to the amplitude , which increased accordingly.

### 5.3.4 Ceiling hook setup: 10kg mass release for 0.975m drillstring model

In addition to measure the effect length had on measured dynamic strain, the ceiling hook setup served to highlight the effect the variation the experimental setup had on measurement.

The result from a 10kg mass release with a 0.975m drillstring model is the figure below

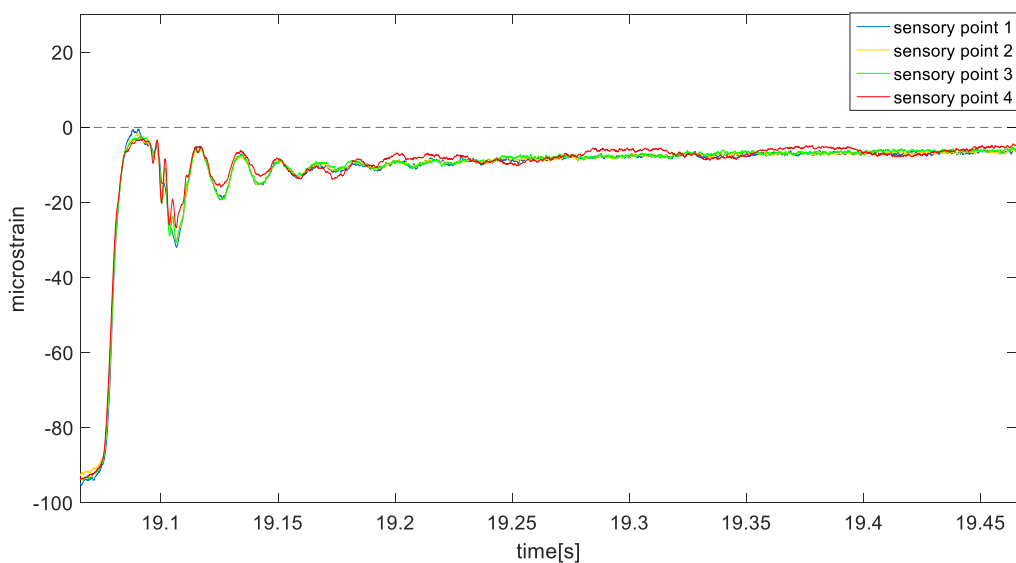


**Figure 5.10** Dynamic strain for all sensory points for 10kg mass release with 0.975m drillstring model over a 0.4 sec interval

Similar to the measured data shown in figure 5.9, there is clear indication of axial vibration in the results, corresponding to an underdamped behavior. It is however also very apparent that the measured data are much more defined than seen with the lab stand setup. There is also an apparent increase in frequency, which should not be occurring.

### 5.3.5 Ceiling hook setup: 10kg mass release for 2.865m drillstring model

The results from 10kg mass release from 2.865m long drillstring is as shown in the figure below

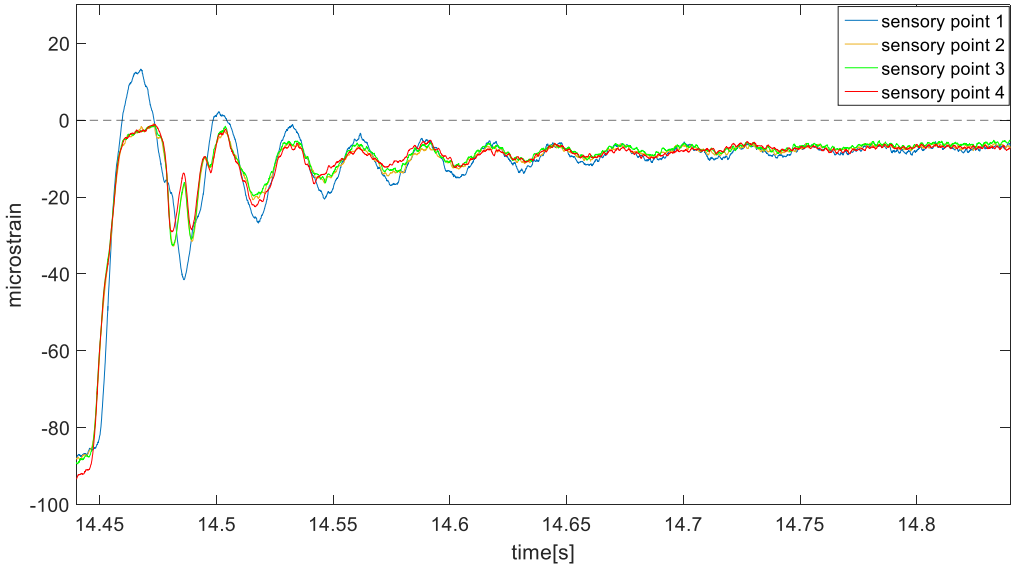


Figure 5.11 Dynamic strain for all sensory points for 10kg mass release for 2.865m drillstring model

The results from the extended drillstring model shows how the apparent frequency of the signal increased, whilst overall damping in the system remained unaltered. Since the placement of top sensory was over 2m from the others, meant that there was a significant variation between the other measurement points. The amplitude remained more or less for the bottom 3 sensory points compared to 0.975m long drillstring. The only noticeable increase in amplitude as seen was for sensory point 1, which was placed on the 2<sup>nd</sup> segment from the top.

## **6 Analytical model approximation and comparison with dynamic strain measurements**

This chapter will elaborate on how the physical drillstring model(chapter 4)is approximated as a lumped element model(chapter 3). This will be done by showing how appropriate values for stiffness and mass are selected, and how the damping for the analytical model is approximated. The analytical model derived shows how the individual displacement of element  $j$  as a function of time, whilst measured data is shows strain as a function of time. This means that the analytical model needs to be modified to display strain in order to be directly compared to the dynamic strain measurements.

The final section in this chapter is dedicated to individually recreate the previous dynamic strain experiments using the approximated analytical model, and compare how numerically accurate the model simulates strain from the measured data. This comparison can then be used to determine whether the damping can be expressed linearly or not, by looking at the degree of variation between the analytical simulation and measured dynamic strain.

### **6.1 How the analytical model is used to represent the DS model as lumped element model**

As with all analytical models the more complex the physical specimen that it is supposed to represent, the more difficult it is to determine appropriate values. The physical drillstring model used for dynamic strain measurements is relatively complex, having interlocking segments of steel and plexiglas, with plexiglas segments overlapping steel segments. This means that finding suitable values for stiffness (spring constant) and mass distribution requires more thought than if the model were a continuous steel/plexiglas pipe.

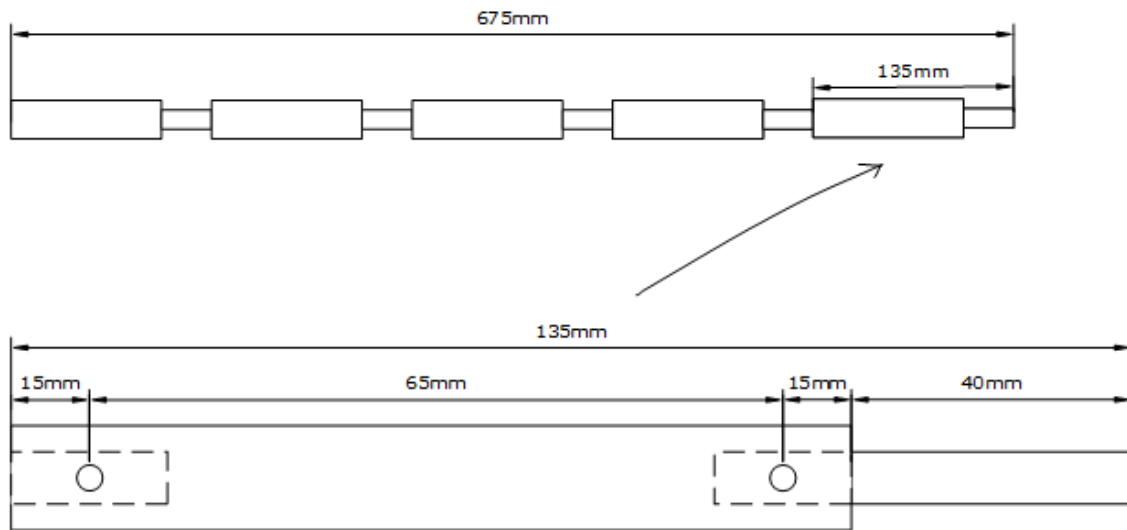


**Figure 6.1** Diagram of DP-section of the physical model showing how it is constructed.

The diagram illustrates the drillpipe section of the physical drillstring model, which is made out of five 135 mm sections with plexiglas and steel segments. It shows the length for each plexiglas and steel segments, and also the position of each bolt connecting the segments

Sub Segment	Outer diameter[mm] $d_{outer}$	Inner diameter[mm] $d_{inner}$	Total Length[mm] $L$	Effective length[mm]	Young's modulus[GPa] $E$
Plexiglas	30	22	95	65	3.1
Steel	18	12	100	70	200

**Table 6.1** Dimensions for DP section of the physical drillstring model highlighting difference between total and effective lengths for plexiglas and steel segments

The analytical interpretation of the model is as a set of massless springs with point masses. There is therefore multiple variations on how the physical drillstring model can be represented as a lumped element model. This is important when comparing analytical and physical data, because poorly approximated parameters (e.g. spring constant, mass) will reduce the analytical models ability give a good numerical representation of experimental data

It is therefore important that the drillstring is given the best approximation as a set of massless springs and point masses. The bolts that connect the plexiglas segments to the steel segments have overlapping sections, with only one material carrying the weight of the drillstring.

This is why the drillstring model needs to be approximated using effective segment length, which highlights only the length of each respective material that is subjected to strain.

These lengths can be determined by looking at 135 mm section shown in figure 6.1. The material overlap is 30mm at each end with exactly 15mm at each side of the bolt. When subjected to tensile stress it is clear what portion of the 135mm section experiences the stress. Only 65mm of the 95 mm long plexiglas segment experiences this tensile force, and only 70 mm of the 100mm long steel segment. The effective segment length for plexiglas is therefore 65mm whilst steel is 70mm. These values are important for reducing the uncertainty associated with approximating the stiffness of physical model to spring constants used in the analytical model.

Depending on how accurately the drillstring model is represented as a lumped element model, there will either be a large difference in spring constant or a small one. The spring constant  $k$  depends on the elastic property of the material  $E$ , cross sectional area and the segment length  $L$  as shown in equation 16 (S.Hovda, 2015).

$$k = \frac{E\pi\left(\frac{d_{outer}^2}{4} - \frac{d_{inner}^2}{4}\right)}{L} \quad (16)$$

The most logical method of evaluating the drillstring as a lumped element model, is by using effective lengths mentioned for plexiglas and steel. The other possibility is to ignore the elastic contribution from steel due to the large difference in stiffness, and only evaluate stiffness based on the total effective length of plexiglas. These two methods for estimating the spring constant will therefore be evaluated, and the difference in accuracy compared.

First method is the use the effective lengths plexiglas and steel calculate an approximated spring constant for the entire length of the model. Since the drillstring model consists of plexiglas and steel segments connected in series, the equation for equivalent spring constant  $k_{eq}$  is the best method for approximating stiffness (Keith.R.Symon, 1971).

$$\frac{1}{k_{eq}} = \sum_{i=1}^n \frac{1}{k_i} \quad (17)$$

The equivalent spring constant equation emphasizes that the larger the value of the spring constant the smaller the contribution to the equivalent spring constant. The equivalent spring constant is determined for the physical drillstring model using the effective lengths of plexiglas and steel as shown

$$k_p = \frac{3.1 \cdot 10^9 \cdot 3.26 \cdot 10^{-4}}{65 \cdot 10^{-3}} = 1.56 \cdot 10^7 \text{ N/m}$$

$$k_s = \frac{200 \cdot 10^9 \cdot 1.41 \cdot 10^{-4}}{70 \cdot 10^{-3}} = 40.3 \cdot 10^7 \text{ N/m}$$

$$k_{eq} = \frac{1}{\frac{5}{1.56 \cdot 10^7} + \frac{5}{40.3 \cdot 10^7}} = 0.30 \cdot 10^7 \text{ N/m}$$

The second method is by assuming that the steel segments are completely rigid and the only noticeable strain occurs in the plexiglas segments. This is done by calculating the spring constant using only the total effective length of plexiglas. The spring constant can then be estimated using equation 16

$$k = \frac{3.1 \cdot 10^9 \cdot 3.26 \cdot 10^{-4}}{5 \cdot 65 \cdot 10^{-3}} = 0,31 \cdot 10^7 \text{ N/m}$$

The results show that there is almost no difference between the spring constant calculation using equation 17 in the first method and equation 16 for the second. Looking the equivalent spring constant demonstrates that contribution to spring constant from steel is minimal because the Young's modulus is roughly 60 times larger. This is despite the fact that the effective segment length is greater per steel segment as well as a smaller cross section, with both of these factors reducing the spring constant.

It is therefore possible to ignore the stiffness contribution of the steel segments by assuming that all significant displacement occurs in the plexiglas segments. However, the method used to approximate the spring constant for the analytical model was still selected to be by using equation 17. This is because this method gives the most accurate representation of the spring constant for the entire length of the drillstring model.

The effective length is important not only for accurately approximating the stiffness of the model. It is also necessary in order to translate the model as a mass-spring system, which is composed of components connected only in series and not in parallel. Using the effective lengths for the analytical model, one can accurately represent the drillstring model as a series of Plexiglas and steel pipes. Where the actual plexiglas and steel segment lengths are 65mm and 70mm instead of 95mm and 40mm.

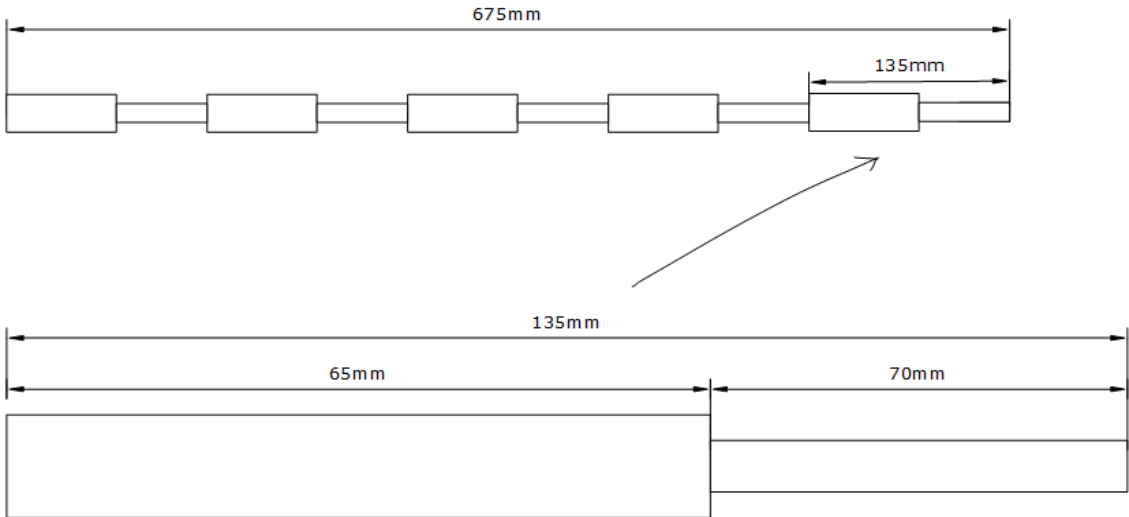


**Figure 6.2** DP-section represented using the effective lengths of plexiglas and steel, which are values used for the analytical model

There are problems with this approximation however, as this modeling method completely discards the overlapping material. This means that the total mass and mass distribution are affected in such a way that it no longer represents the model shown in figure 6.1. The linear density therefore needs to be adjusted in order to offset the deviation in mass caused by the approximation using effective lengths. This can only be done by looking at the specific deviation in mass for each segment of plexiglas and steel. The specific linear density which is defined as the mass per unit length can be expressed by the equation

$$\lambda_m = \rho A \tag{18}$$

Where  $\lambda_m$  is the specific linear density,  $\rho$  is the density of the material and  $A$  is the cross sectional area of the segments. Using this equation the linear density for plexiglas and steel are

$$\lambda_{m,plexiglas} = 1.2 * 10^3 * 3.26 * 10^{-4} = 0.39 \text{ g / mm}$$

$$\lambda_{m,steel} = 7.84 * 10^3 * 1.41 * 10^{-4} = 1.11 \text{ g / mm}$$

The total mass for the first 65mm of the 135mm plexiglas and steel segments then becomes

$$m_{65mm} = \lambda_{m,plexiglas} L_{plexiglas} + \lambda_{m,steel} L_{steel}$$

$$m_{65mm} = 25.4 \text{ g} + 33.3 \text{ g} = 58.7 \text{ g}$$

The total mass for the remaining 70mm of the steel segment then becomes

$$m_{70mm} = \lambda_{m,plexiglas} L_{plexiglas} + \lambda_{m,steel} L_{steel}$$

$$m_{70mm} = 11.7 \text{ g} + 77.7 \text{ g} = 89.4 \text{ g}$$

This shows that the 30mm steel overlaps accounts for more than 50% of the weight in the plexiglas segment, whilst the 30mm plexiglas overlap accounts for only 13%. In order to make the model more accurately represent the mass distribution is to then use the average linear density. This can then be calculated using the equation below where  $\bar{\lambda}_m$  is the average linear density,  $m$  is the segment mass and  $L$  is the segment length

$$\bar{\lambda}_m = m / L \quad (19)$$

The results is that the linear density for the 65mm plexiglas segment and 70mm steel segment becomes

$$\bar{\lambda}_{m,plexiglas} = 58.7 / 65 = 0.9 \text{ g / mm}$$

$$\bar{\lambda}_{m,steel} = 89.4 / 70 = 1.28 \text{ g / mm}$$

Using these values for average linear density gives accurate values of the total mass. The only downside is that the mass distribution is simplified as linear. This is a very rough approximation for plexiglas segments, where in actuality about 77% of the mass is concentrated at the 30 mm end because of the steel overlaps. It is therefore difficult to conclude whether or not using the average linear density are beneficial to numerical accuracy of the analytical model

The BHA also needs an approximate linear density as large parts is hollowed out like a cylinder. The calculated linear density becomes

$$\bar{\lambda}_{m, \text{plexiglas}} = 1574 / 300 = 5.25 \text{ g / mm}$$

This again neglects the fact that most of the mass is concentrated in the bottom half of the BHA, but is a reasonable approximation for mass distribution that is simple to apply to the analytical model.

The final part about approximating the physical drillstring as an analytical model, is the number of discrete points used to recreate mechanical behavior.

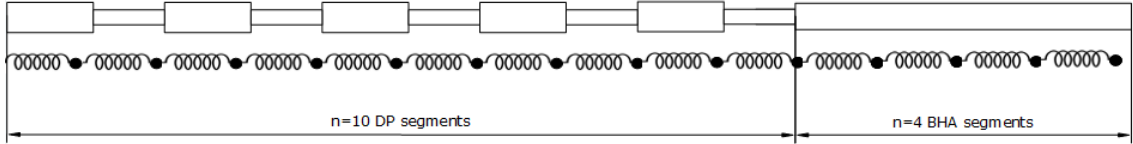


**Figure 6.3** Analytical view of the drillstring model represented by the “smallest” number of elements.

The analytical model being represented as a lumped element model, means that any number of n elements can be used to represent the physical drillstring model. The important fact is that the number of n elements in the model should still represent the physical model as a whole, which is the 675mm long drillpipe section with and without the 300mm long BHA section in the case of figure 6.3. This variation of the model is made out of 5 segments of plexiglas and steel with effective lengths of 65mm 70mm, with the a single BHA segment at 300mm which is represented by n=4 elements. The reasoning behind this to keep the segment lengths for all elements relatively equal in length, which is not necessary. The number of total n elements will then correspond to dividing this fixed total length of the physical drill string model into smaller n element lengths. This means if the total number of elements used to represent the drillpipe is n=50 then this means that each individual plexiglas and steel element length will be 13mm and 14mm respectively.

The analytical model should still be representing the physical model, which means that the first steel segment is now found at  $j=6$  instead of  $j=2$  previously when  $n=10$ . This ensures that the only major difference is the mass distribution in the model, which is enhanced with number of  $n$  elements.

### 6.1.1 Displacement $y_j(t)$ to strain $\varepsilon_j(t)$

In order to compare the analytical model with the measured axial strain from the physical drillstring, the analytical model needs to be adjusted to display axial strain instead of displacement. Strain is defined as the ratio between the change in length and the total length.

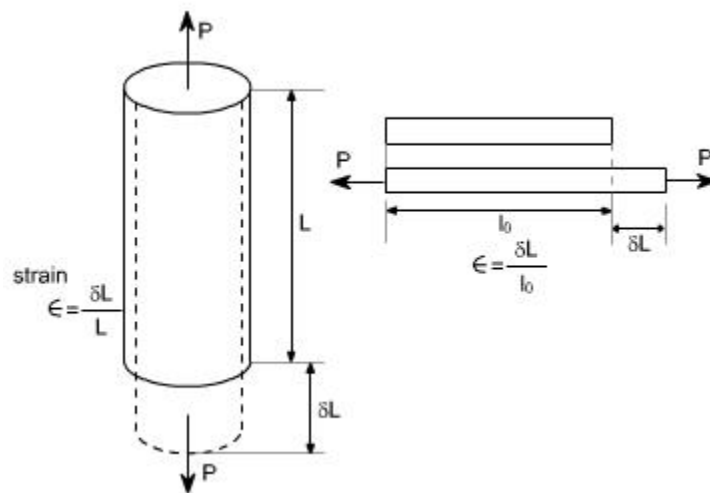


**Figure 6.4** Diagram illustrating the basic principles of strain (NPTEL, 2011)

In order to translate displacement to strain, the correct ratio of length needs to be displayed for every element  $j$ . The adjustment is simple and straightforward as shown in the equation 20 below, which is the same for all the damped scenarios expressed as  $x_i(t)$

$$\varepsilon_j(t) = \frac{\sum_{i=1}^n V_{ji} (\mathbf{V}^{-1} \mathbf{K}^{-1} \mathbf{w})_i x_i(t)}{\sum_{i=1}^j L} \quad (20)$$

This means that when displaying strain for all the elements in the drillstring, each element will have the initial conditions displayed as the relative strain measured at for the respective length at that position. The total axial strain in the drillstring model should abide by the relationship shown in equation 21.

$$\varepsilon_{tot} = \sum_{i=1}^n \varepsilon_i \quad (21)$$

In the situation where the model is a continuous pipe of a single material (e.g steel, plexiglas etc)  $\varepsilon_j(t)$  will measure the same amount of static strain regardless of which element j is evaluated. This is because the displacement  $y_j$  increases proportionally with the total length L at evaluated length.

In the case for the physical drillstring model which is composed of alternating plexiglas and steel segments the initial condition for static strain will be larger at the bottom elements compared to the ones at the top. This essentially means that the initial conditions for the strain at element j will be different, and will not give the same values of strain as one would see with a continuous material. The value of strain from subjecting the drillstring according to the analytical model is shown in figure 6.5, which illustrates the initial strain before the mass is released, which is based on the 0.975m drillstring using a 10kg mass. As there are four sensory point placed sequentially on the plexiglas segments in the physical drillstring model, with the top sensory point being denoted as number 1 and the bottom being number 4. For the analytical model the corresponding position for the top sensory point is element j=3 and the bottom is j=9, when the DP-section is evaluated as n=10 elements.

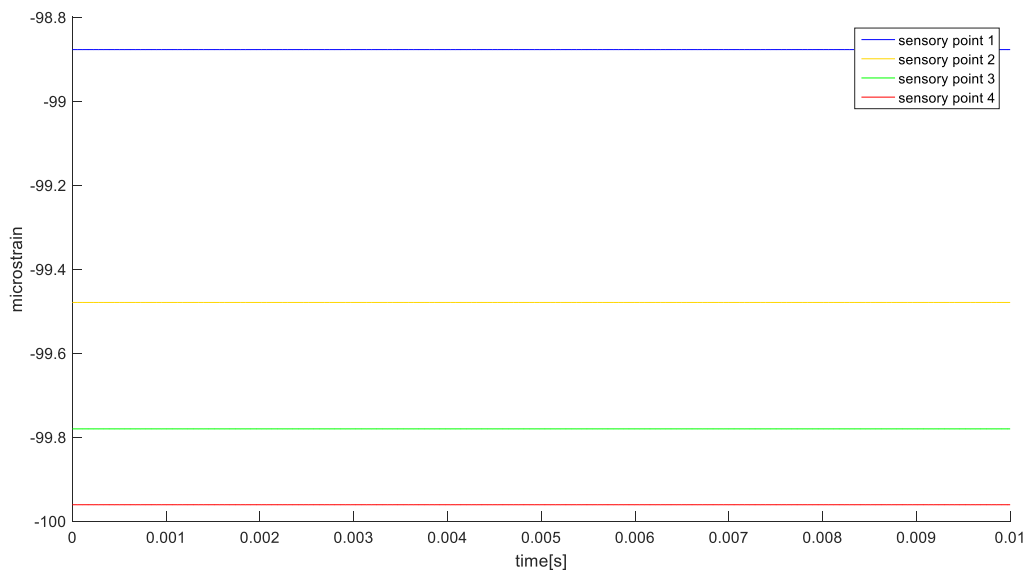


**Figure 6.5** Initial condition for 10kg static strain from the analytical model(equation 20) modelled as a 0.975m drillstring

The results show that static strain for the analytical model when subjected to a 10kg end mass, has roughly 1 microstrain variation between the top(j=3) and bottom segment(j=9).

The result from the analytical model was compared to strain measurement using a static load of 10kg. This was to investigate if there was any glaring variation between theoretical initial conditions and the measured initial conditions. The measured data below illustrates the value of each individual sensory point before 10kg mass is released

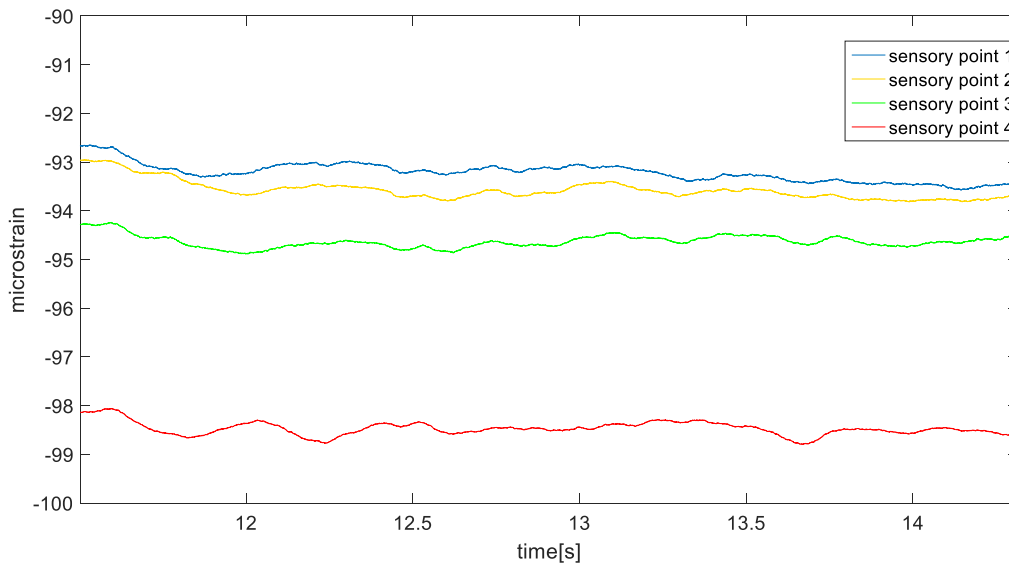


**Figure 6.6** Measured static strain for all four sensory when subjected to 10kg end mass

These results show different initial conditions for each individual sensory point for analytical and measured data. The variation between the maximum and minimum strain was also much larger than the analytical model where the strain was roughly 2.5 microstrain compared to the 1 microstrain. The individual separation between the each sensory point were also different as the values for intital conditions for the lower elements should have been clustered together, assuming that the analytical model is correct. The figure shows uncalibrated data which means that the strain gauges does not coincide with Hooke's law, and is the reason all strain gauges measured notably smaller values of microstrain. This is discussed in further detail in chapter 7.3.

The measured result may indicate that the measured data in figure 6.6 perfectly matches the strain distribution seen in figure 6.5, where strain increases sequentially from sensory point 1 to sensory point 4. However because of the uncertainty in the measurement, this distribution was non consistent as demonstrated with the results in chapter 5(e.g figure 5.8). This therefore meant that the measured data could not be used verify the accuracy the initial conditions from the analytical model

### **6.1.2 Analytical model damping approximation**

In addition to approximating the stiffness and the linear density, the analytical model is also approximated with regards to damping. The two different methods that are shown vary between having the damping constant equal for all the elements, and damping coefficient being equal for all the elements with an alternating damping constant for every element.

Depending on the type of damping mechanism modeled and the dimension and properties of the model itself, the distribution of values for the damping constant might vary greatly. This has therefore direct implication on accuracy of the damping from the analytical model. This is because the linear damping for the analytical model is a non-specific damping mechanism.

The damping constant  $c$  in this thesis refers to the ratio between the damping coefficient  $c_i$  and mass  $m_i$ . For the first method the damping constant  $c$  is the same for all the for all elements in the drillstring. For the second approach the individual damping coefficients  $c_i$  is the same for all elements but the damping constant  $c$  is not. If the model was a continuous plexiglas/steel pipe then method one and method two would be equal as the both would have a constant damping constant  $c$  for all elements  $j$ . The case with the physical chain-model differs from that of a continuous pipe, as it consist of interlocking plexiglas and steel cylinders, which means that  $m_i$  is not constant . This means that one will have alternating damping constant as shown in figure 6.7.

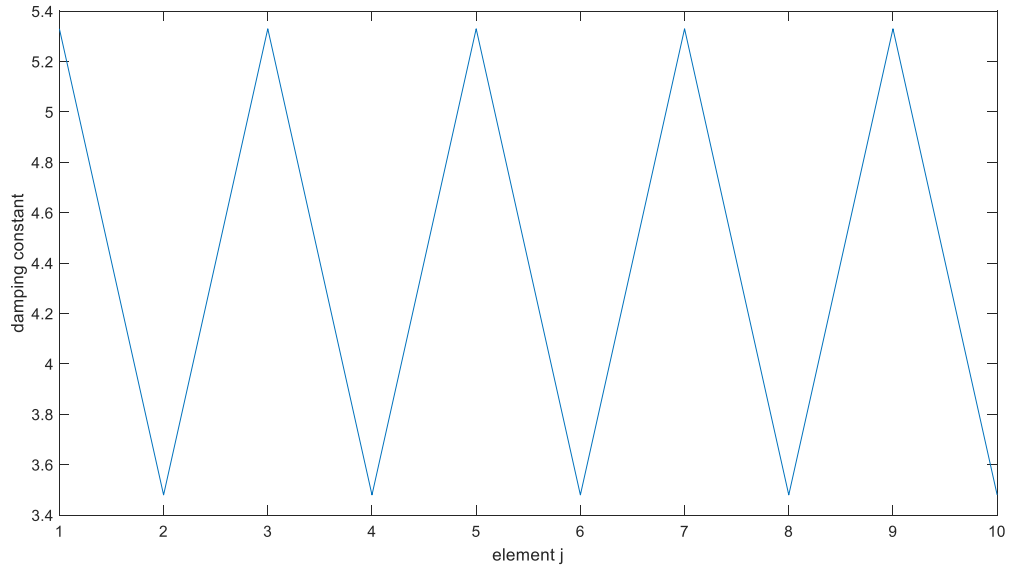


**Figure 6.7** The variation of damping constant expressed by using constant damping coefficient for all elements(2<sup>nd</sup> method)

The overall effect these two methods have on the transient response simulated, is therefore also different. This variation between these two damping approximation are shown in the figure below.

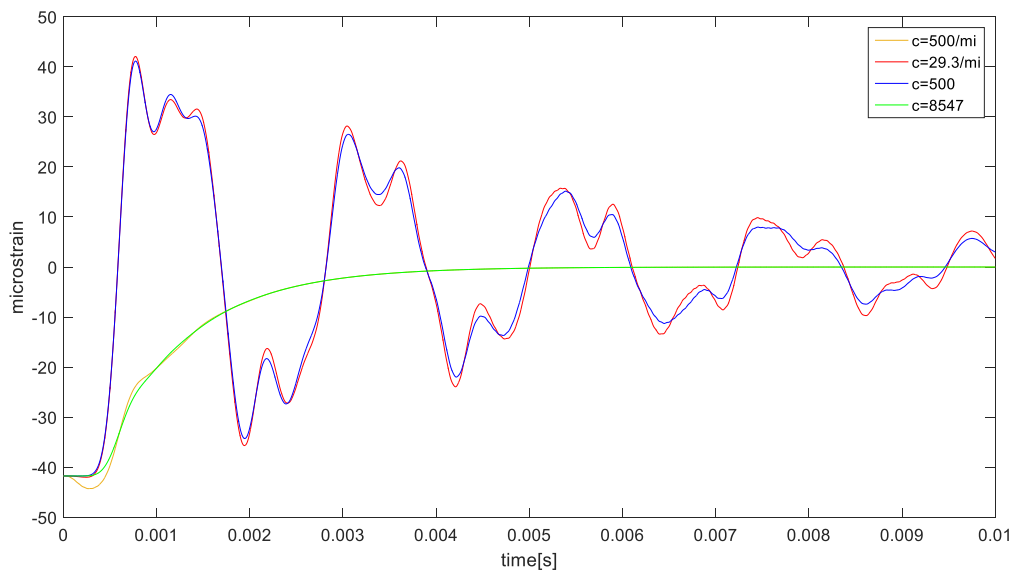


**Figure 6.8** Difference between the two methods of approximating damping for the analytical model shown for the top element  $j=1$

The results show little variation between the first and second approximation when the damping constant is relatively low at  $c \approx 500 \approx 29.3/m_i$ . It does however illustrate an unnatural dip in the trend when applying the same damping coefficient for all the, as seen when the damping coefficient is large  $c = 500/m_i$ . This is the reason why the damping constant was assumed equal for all the elements, for all the results from the analytical model in this thesis. This were done to avoid the same unrealistic dip shown in figure 6.8, where damping coefficient was set equal for all the elements.

## **6.2 Comparison between simulation from the analytical model and the measured dynamic strain**

In this section, the results from chapter 5 are compared with the approximated analytical model. This servers to illustrate the numerical difference, but also the analytical models ability to represent overall mechanical behavior. This will be achieved by using the approximate parameters of stiffness(spring constant), linear density, and approximate values of damping constant to give the most comparable transient response to in the measured dynamic strain.

The simulated scenarios that are presented is such that lab stand setup highlights the difference between inherent mass in the system. With the ceiling hook setup highlighting the variation in length.

In order to keep the comparisons as clean as possible, the analytical model is only compared to a single sensory point from the measured data. The transient response is therefore only compared to the measured data from sensory point 3.

### **6.2.1 Analytical model and dynamic strain measurement for 4.3 kg mass release with BHA(lab stand setup)**

The first simulation to be evaluated is the 4.3kg mass release without the BHA section. The element selected is compared directly to correspond sensory point 3 on the physical drillstring model which in this case is the second lowest plexiglas segment which corresponds to  $j=7$  for drillstring modeled as  $n=10$  elements and  $n=4$  BHA elements.

The damping constants are arbitrarily chosen to show variation between the analytical models behavior and the measured data. whether the system is considered critically damped or underdamped as individual segments have different damping ratios.

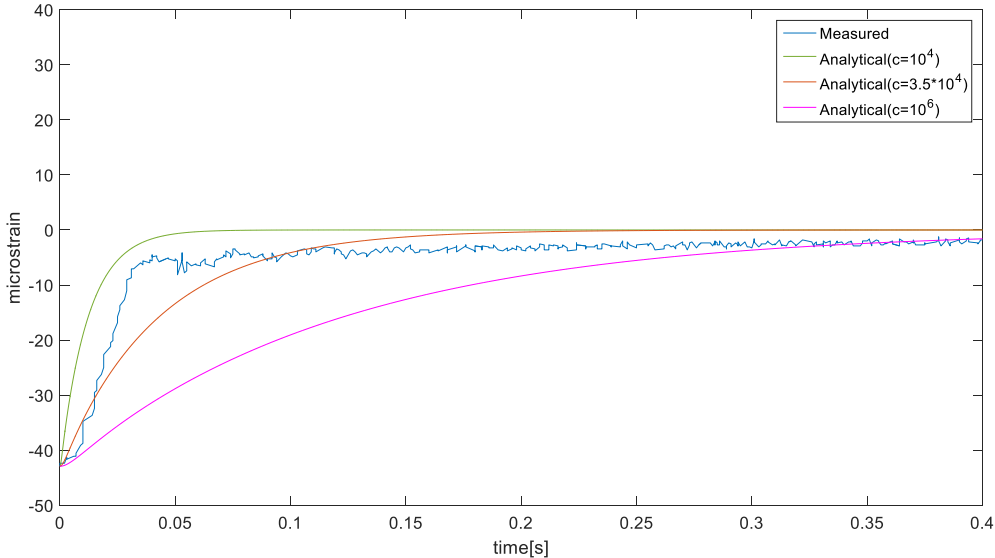


**Figure 6.9** comparison between measured data (sensory point 3) and analytical model for a 4.3kg mass release of the drillstring without BHA section over a 0.4 second interval

The comparison between the measured data and the analytical data as shown in figure 6.9 indicate the significant numerical variation. The analytical result from damping constant  $c = 10^4$  has the most similar shape to the measured data. The difference is also that the measured data seems to have a shifted equilibrium of 2-7 microstrain, because the signal plateaus much earlier than the analytical model. The analytical result when damping constant is  $c = 10^6$  approaches equilibrium at the same speed as the measured data, but have also the largest numerical difference in the first 300 milliseconds.

**6.2.2 Analytical model for 4.3 kg mass release with BHA(lab stand setup)**

The second scenario is when the analytical model simulates the 4.3kg mass release with the BHA. Damping constants are again selected to show variation between the behavior observed in the measured data.

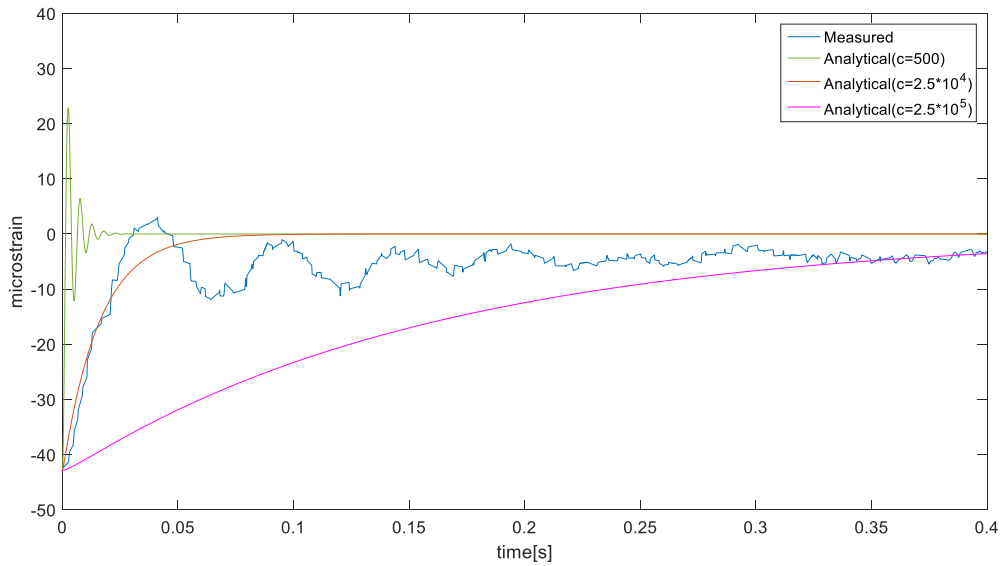


**Figure 6.10** underdamped behavior comparison between measured data (sensory point 3) and analytical model for a 4.3kg mass release of the drillstring with BHA section over a 0.4 second interval

Numerical variation between the measured data and the analytical model is more obvious for this result in figure 6.10. This is because the analytical model struggles to mimic the vibrations (underdamped), simultaneously with the slow asymptotic behavior from an overdamped response, which is shown to give the best overall approximation to the measured data. The underdamped behavior shown for analytical model with  $c = 500$  decays quickly to give an accurate representation of the measured data, whilst the ones with larger damping constant that follow the general trend have no discernible vibration. There is also a persisting variation in the general trend between the analytical simulation and measured data. This is where the vibrations do not occur about equilibrium, but instead around 5-7 microstrain below. It is also difficult to explain exactly why the measured data show clear signs of vibrations when the system is approaching zero at a significantly lower velocity, as there are a multitude of possible explanations.

The change in response between BHA and no BHA is however similar between the analytical model and the measured response. Increasing the mass of the system without altering stiffness (spring constant) will reduce the amount of damping in the system. This is illustrated by the criteria of that determines the type of damping as shown by the set of equations below

- Overdamped  $c^2 - 4mk > 0$
- Critically damped  $c^2 - 4mk = 0$
- Underdamped  $c^2 - 4mk < 0$

Looking at the ODE for an oscillating mass-spring system, one can see that the damping effect is proportional to the damping coefficient and inversely proportional to the mass of the system. If mass is just added to the end however, which is the case for model with and without the BHA. This will instead only increase the apparent frequency in the system. This is because the existing drillpipe section is unaltered, and the only variation is by adding the BHA. This will therefore have a fundamentally different effect compared to altering parameters of mass and stiffness of existing elements.

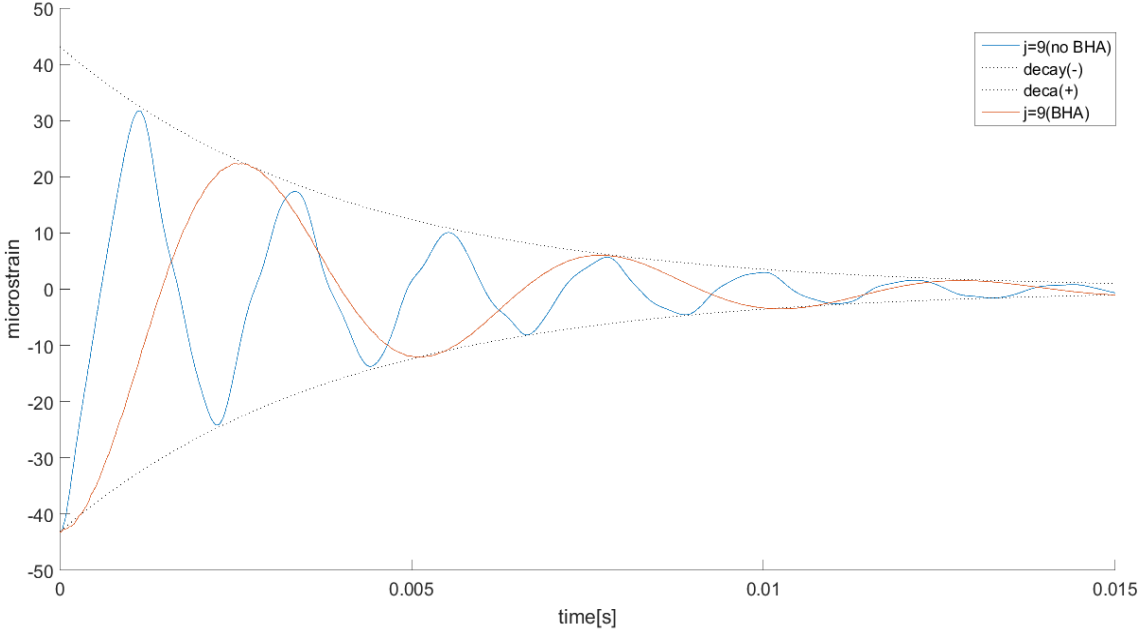


**Figure 6.11** Variation between BHA and no BHA for a 4.3kg mass release from the analytical model evaluated at j=7

The difference between BHA and no BHA section for 4.3kg mass release is shown in figure 6.11, which shows that the simulated signal has a lower frequency than the one without BHA. Decay remains the same, meaning that both signal approaches equilibrium at the same speed. The only major variation compared with the measured results is that the apparent amplitude of the oscillation increased from 6.9 and 6.10. This is because the increased inherent mass should have had a different effect, as it should have theoretically remained the same, which might be a result of an unidentified disturbance in the measurement.

**6.2.3 Analytical model for 10kg mass release with 0.975m drillstring(ceiling hook setup)**

Similar to the 4.3kg mass release for the BHA variation the 10kg mass release is compared to the analytical model evaluated as n=10 DP elements. Where measured data from sensory point 3 is compared to 10kg mass release for 0.975m drillstring.

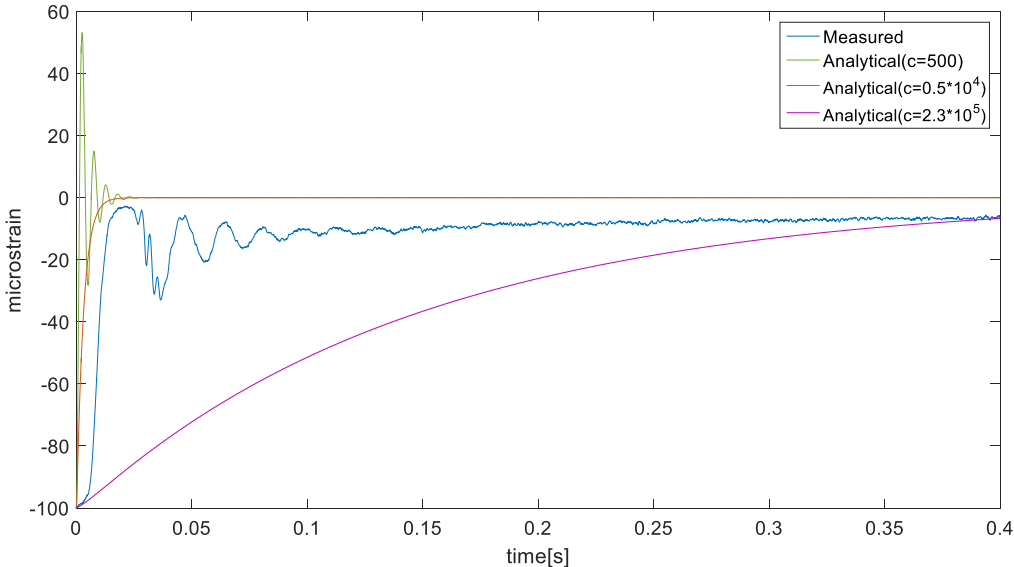


**Figure 6.12** Comparison between measured data (sensory point 3) compared to analytical model transient response for 10kg mass release by varying values of damping constant

Despite the measurement from the ceiling hook setup giving better quality data, the analytical model still varies significantly as shown in figure 6.12. The interesting variation between the two results from 4.3kg mass release and 10kg mass release is that the speed at which the system approaches equilibrium is much greater than expected. This is highlighted by the fact that the initial portion of the response is comparable to the analytical model with a much lower damping constant than previously ( $c = 0.5 \cdot 10^4$  now compared to  $c = 2.5 \cdot 10^4$  before).

This is illustrated by the response from the analytical model with variation between 10kg and 4.3kg mass release with same value of damping constant.

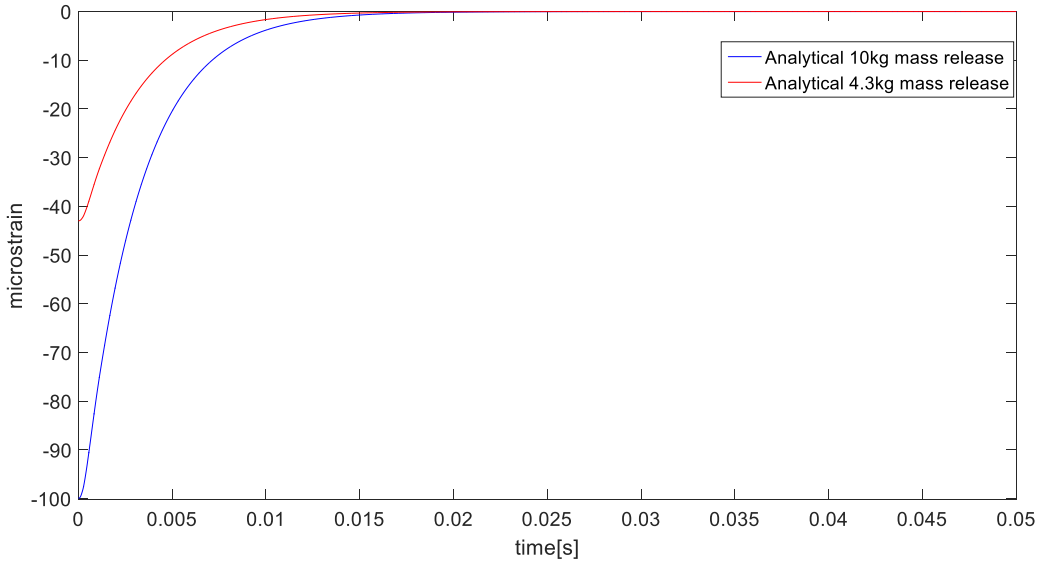


**Figure 6.13** Comparison of how strain rate is the same for 10kg and 4.3kg mass release, from -30 microstrain to zero Analytical model shows that the strain rate is approximately equal at strain above the initial conditions as shown for strain 30 and above where the strain rate has the same behavior for 4.3kg and 10kg mass release.

**6.2.4 Analytical model for 10kg mass release with 2.865m drillstring(ceiling hook setup)**

The final comparison between the analytical and measured data was with the 2.865m drillstring model for 10kg mass release. The analytical model in this comparison was evaluated as n=38 DP segments and n=15 BHA elements.

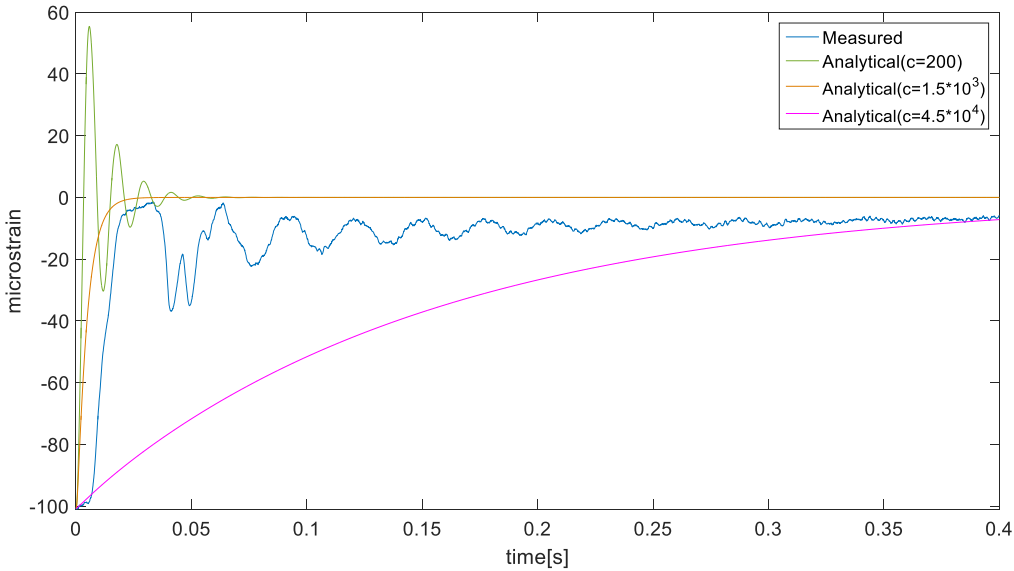


**Figure 6.14** Comparison between measured data (sensory point 3) compared to analytical model transient response for 10kg mass release by varying values of damping constant

It was initially believed that one would achieve better approximation with a longer drillstring with an overall reduced stiffness. However, the overall variation between the analytical model and the measured data remained unaltered. The analytical model is shown again as not being able to accurately model the dynamic strain behavior from the measured data.

The theoretical behavior however is shown to replicate the behavior seen in the measured data, where frequency of the signal increased from figure 6.14 compared to 6.12. This is replicated using the analytical model as shown in figure 6.15

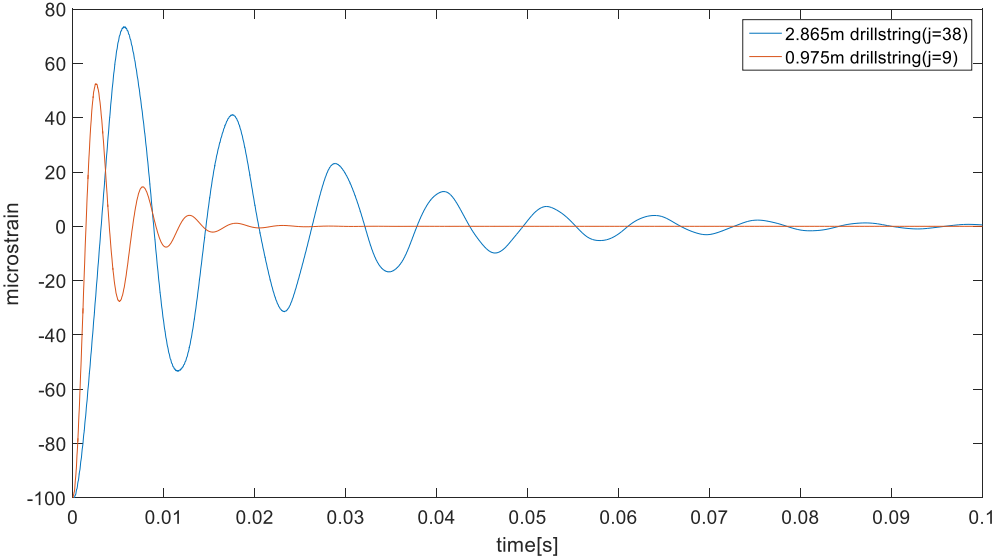


**Figure 6.15** frequency comparison as shown from the bottom elements of a 0.975m and 2.875m long drillstring

This can be said for many aspects of the analytical model as it shows appropriate response similar to that seen in the measured data. In the case of frequency for example, the analytical model had a more notable change than that seen in the measured data.

### 6.3 Fourier analysis

In order to further highlight the difference between measured dynamic strain and the analytical, a Fourier analysis of the results was conducted. This done in order to show one of the reasons why the analytical model fails to numerically model the dynamic strain seen from the measured data.

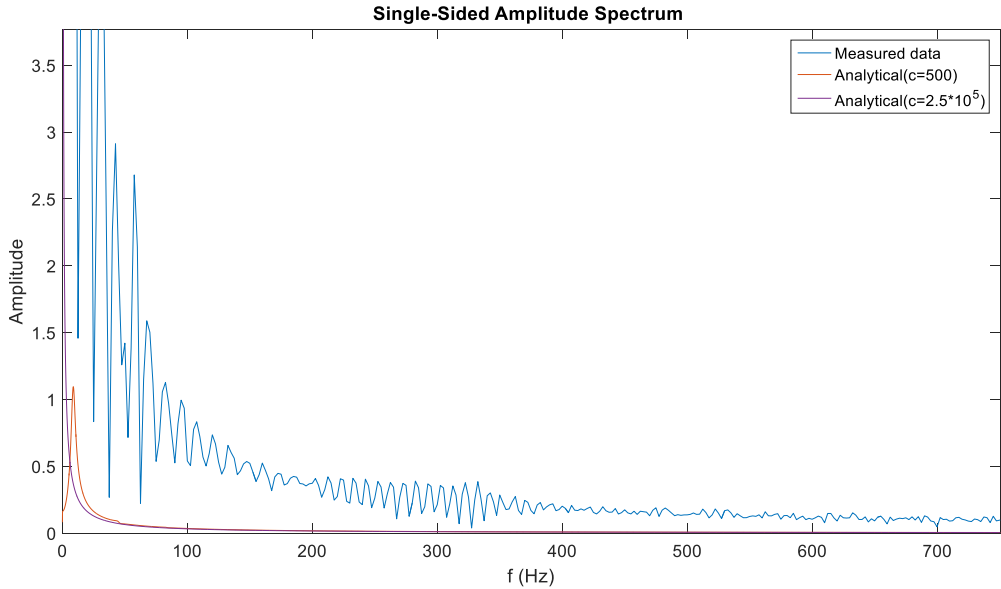


Figure 6.16 Fourier analysis comparison between analytical and measured data

Similar to the comparisons for dynamic strain behavior there is a very large variation between analytical model and the measured values of strain. There was little to no discernable variation between the Fourier analysis for the other measured data, which is the reason why only one was necessary.

## **7 Discussion: Causes for variation between measured strain and the analytical model**

This chapter will discuss and evaluate the different causes behind why the analytical model struggles to accurately simulate the dynamic strain behavior in the measured data from the physical drillstring model. This will be done in three main sections

Section 7.1 will elaborate on what type of damping mechanism most accurately describes the degree of damping observed in the measured results, where the damping mechanism are evaluated individually. In addition to investigating the effect the experimental setup had on the measured dynamic strain.

In section 7.2 the limitation of the analytical model itself will be evaluated in further detail. The uncertainty related to experimental process will also be discussed, and how it may have affected the results.

Lastly, section 7.3 tackles the problems related to general uncertainty of the measurement associated with the use of strain gauges, signal amplifier and ADC.

### **7.1 Damping mechanisms and approximating measured data**

The results shown in the chapter 6 indicate underdamped behavior for most the measured axial vibrations, with only the results from figure 6.9 showing a response similar to a critical or over damped behavior. Depending on the different assumptions used for calculating whether the system is underdamped, critically damped or overdamped, these results can seem reasonable or unreasonable. It is important to note that a system may not always have a visible damping coefficient, but it is always present (Haym & Mark, 2009). This is because no system exists without some degree of damping, and is why the undamped scenario is never realistic.

The results from the conducted tests indicates that the system is significantly damped because of the limited signal duration. It is therefore important to look at the different damping mechanisms that contribute to overall damping in the system, and try to determine what causes the degree of damping seen in the measured data. The problem with determining the main damping mechanism of the system is that there are multiple different damping mechanism that simultaneously contribute to the damping coefficient, which needs to be determined and evaluated.

These damping mechanisms vary in both the degree of which they affect the damping in the system, and also the difficulty at which they can be quantified and approximated. The damping mechanisms will therefore be individually evaluated in order to correctly determine the effect they had on the measurements. This is also done to avoid the added complexity of simultaneously acting damping mechanisms.

### 7.1.1 Viscous Damping

The damping caused by viscous drag is the damping mechanism that is easiest to quantify. This is because the damping force may be correlated as  $F_i = c\dot{x}$  where  $F_i$  is the viscous drag force. It is one of the few damping mechanism that can be modeled as linear without significant inaccuracy.

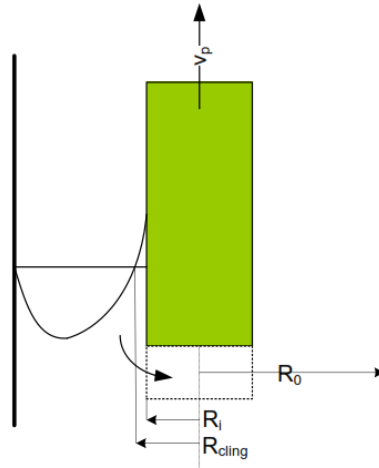


**Figure 7.1** Surge and Swab due to pipe movement that shows the velocity profile in the well (Skalle, 2014)

Using the principle of surge and swab an expression for the damping coefficient can be determined (S.Hovda, 2015). This is phenomenon occurs when the lateral movement of the drillstring causes displacement of the fluid due to the no-slip condition at the physical boundaries.

$$c_i = \frac{F_i}{\dot{x}_i} = -2\pi L_i \mu \left( \frac{2(1 - \alpha_i^2) + (\alpha_i^2 - \alpha_n^2)^2 - (1 - \alpha_n^2)^2 - 4\alpha_i^2 (\alpha_i^2 - \alpha_n^2) \ln(\alpha_i)}{(1 - \alpha_i^4) \ln(\alpha_i) + (1 - \alpha_i^2)^2} \right) \quad (22)$$

Equation 22 illustrates how the damping coefficient  $c_i$  can be calculated. The length  $L_i$  is the individual segment lengths and  $\mu$  is the absolute viscosity of the fluid medium.

The value  $\alpha$  is defined as the ratio between the distance between the center of the drillpipe/BHA to the inner wall of the casing/borehole wall and the radius of the drillpipe/BHA.

There is of course one problem using this principle, which is the fact that the drillstring model used in the measurements was not enclosed by another pipe, like casing would a real drillpipe. This means that one need an approximation for  $\alpha$ . The values of alpha will therefore be arbitrarily selected as there is no distinct physical boundary, which allows it to be easily calculated.

Assuming that viscous drag is the only significant damping factor, then the damping constant  $c$  can be determined with equation 22. Using the viscous damping equation, the damping ratio and damping constant for the drillstring with and without BHA can be determined as shown in the table below.

Drillstring	Without BHA section		With BHA section	
	Damping ratio	Damping constant	Damping ratio	Damping constant
Alpha $\alpha$	$\zeta_1$	$c$	$\zeta_1$	$c$
0.03	$0.9 \cdot 10^{-8}$	$5 \cdot 10^{-5}$	$0.2 \cdot 10^{-7}$	$5 \cdot 10^{-5}$
0.99	$1.6 \cdot 10^{-3}$	9	$3.6 \cdot 10^{-3}$	9

**Table 7.1** show the respective damping parameters for top element  $j=1$  for different values of alpha(evaluated as  $n=10$  and  $n=14$  elements)

Computed values in table 7.1 show the results from the analytical model using only the viscous drag as a source of damping. The computed values are shown for two values of alpha, with  $\alpha = 0.03$  selected as a realistic representation, whilst  $\alpha = 0.99$  a more hypothetical representation to show the range that of damping constant produced using equation 22 with the analytical model. The viscosity of air that was used was  $\mu = 1.86 \cdot 10^{-5} \text{ Pas}$  which is the standard air viscosity at  $25^\circ \text{C}$  for standard atmospheric pressure. Damping constant is also the same for both the models with and without the BHA regardless of the value of alpha, which is because it is the same element that is evaluated in both cases.

The calculated values can be evaluated using settling time for each of these results to give an indication of how big the contribution from air resistance is. This is because the settling time from the measurements can be used to verify the extent at which viscous damping affected the results. The results indicate that with a realistic value of alpha  $\alpha = 0.03$  the system is severely underdamped and the settling time which can be estimated using settling time equation from (S.Hovda, 2015)

$$t_{set} = -\frac{2}{c} \ln\left(\frac{p}{100}\right) \tag{23}$$

Where  $c$  is the damping constant and  $p$  is the value that approximation to zero that defines when the vibration from the measured signal has settled. If the settling time is evaluated at  $p = 10$  then settling time for  $\alpha = 0.03$  is  $t_{set} = 92100\text{sec}$  being approximately 26 hours. This does not coincide with the measured data where the settling time was approximately 1 second when using the same tolerance for  $p$ . If value for alpha is changed to the unrealistic value of  $\alpha = 0.99$ , then this results in a much higher damping constant of  $c = 9$ . The clearance from alpha is reduced by a factor of 33, resulting in an increase in damping constant by a factor of 180 000. This scenario means that the clearing starts becoming so small that the drillstring becomes like a piston in a pump, which results in drastic increase in resistance.

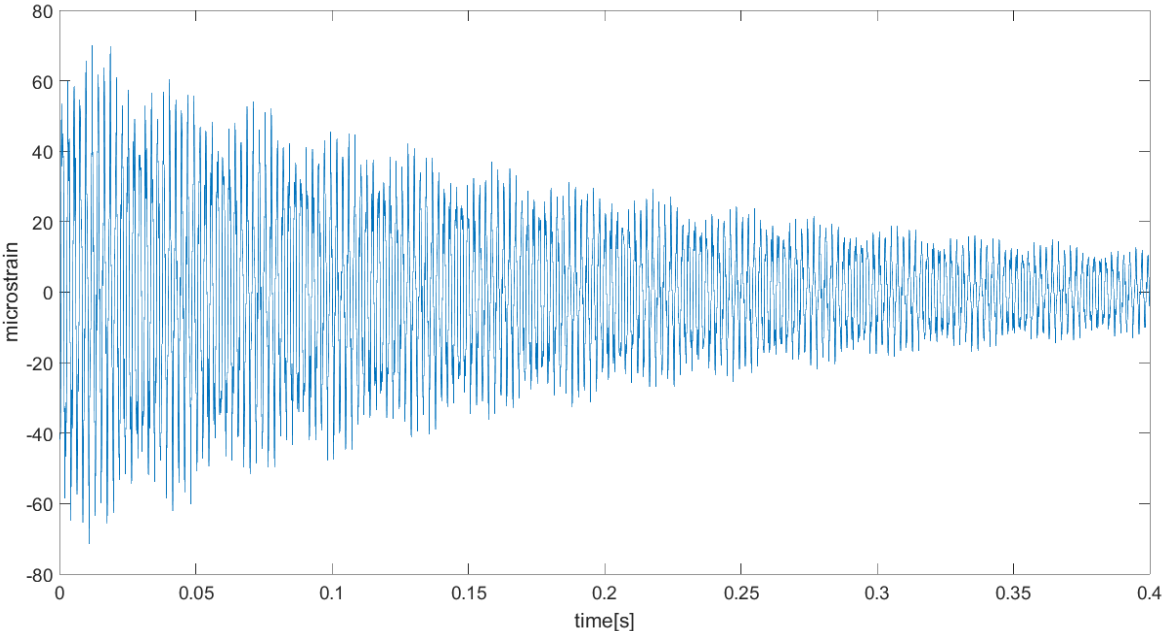


**Figure 7.2** Damping of element  $j=1$  in drillstring without BHA with  $\alpha = 0.99$  shows visible damping in interval of 0.4 seconds

The results can be seen in figure 7.2, which shows a much more similar signal decay to the measured data when compared over the same 0.4 sec interval. This however, is only achieved by using a hypothetical value for alpha.

In addition to this the result in figure 7.2 is achieved by using the damping constant from the top element  $j=1$  which has the highest damping constant according to the analytical model. This means that the results shown are the maximum amount of damping achievable from viscous damping.

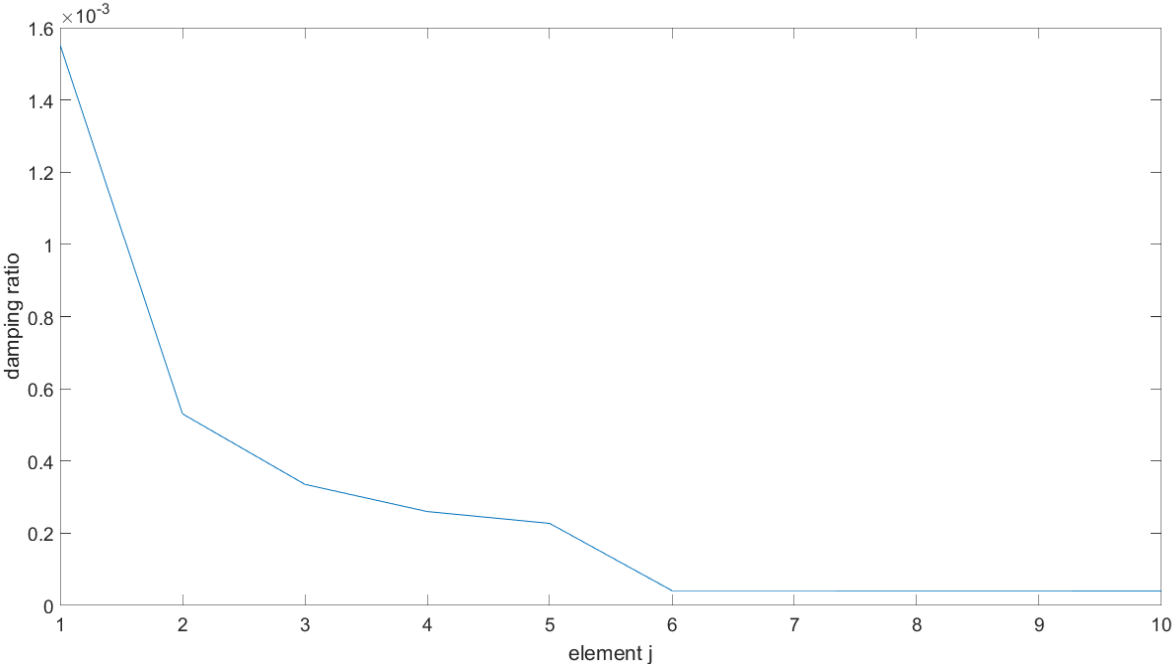


**Figure 7.3** Variation in damping ratios from top element  $j=1$  to bottom  $j=10$  for  $n=10$  element drillstring model without BHA when  $\alpha = 0.99$

The figure illustrates the variation in damping ratios. It is important to note that the damping constant and damping ratio for all scenarios is always greatest at the top element. This is because the model is evaluated as a set of  $n$ -coupled mass-spring where the top element is the one that supports the weight and is restricted by the largest amount of mass, which evidently results in the largest damping ratio.

Using these results it can be concluded that the physical drillstring model which is hanged freely and not enclosed in a cylinder, will be subjected to minimal amounts of viscous drag from air at room temperature. This is because of the small viscosity of air in combination with a realistic small value of alpha, which results very small values for the damping constant.

The effect of viscous damping by itself does therefore not explain the degree of damping observed in the measured data. The reason for this is that the model is made out of two different materials, which have significantly different mechanical properties. The physical drillstring model is also a chain of cylindrical pipe that are bolted together that also contributes to transmission loss of vibration energy. This means that the major contributor to damping must be caused by different damping mechanism than viscous drag.

**7.1.2 Hysteretic/Structural damping**

Structural damping is a damping mechanism that is caused by internal friction in the material, which results in energy being dissipated when being subjected to deformations. The parameters related to structural damping for energy loss are known as the damping quantities. Hysteretic damping occurs because the elastic behavior as described by Hooke’s law does not take into account the time dependence of a resultant deformation from applied load (J. ZHANG, 1993). The assumption therefore only holds true when the loading rate is slow enough for strain rate to be considered instantaneous.

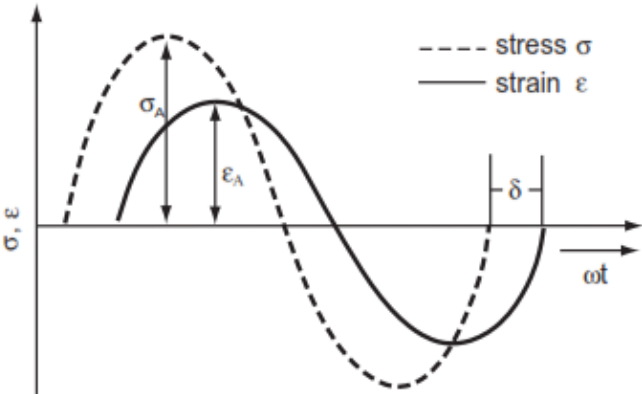


**Figure 7.4** stress-strain curve for linear-viscoelastic material (J. ZHANG, 1993)

The result is that the overall strain  $\mathcal{E}$  is the sum of two parts. The first being instantaneous elastic strain  $\mathcal{E}_e$ , which is independent of time, but also a time dependent strain which lags behind the applied load. Another way to describe this time dependent strain would be as anelastic strain  $\mathcal{E}_a$ .

$$\mathcal{E} = \mathcal{E}_e + \mathcal{E}_a$$

$$\mathcal{E}_a = \mathcal{E}_i \left( 1 - \exp\left(-\frac{t}{\tau}\right) \right) \text{ for loading}$$

$$\mathcal{E}_a = \mathcal{E}_i \exp\left(-\frac{t}{\tau}\right) \text{ for unloading}$$

In the equations from (J. ZHANG, 1993) as shown above, the anelastic strain  $\tau$  is the characteristic relaxation constant with  $t$  being time. This relaxation constant encapsulates the materials behavior when subjected to loading and unloading. These properties are known as the materials retardation and relaxation time, and these parameters are highly dependent on the elastic behavior of the material. The result of these two properties is what causes hysteretic damping.

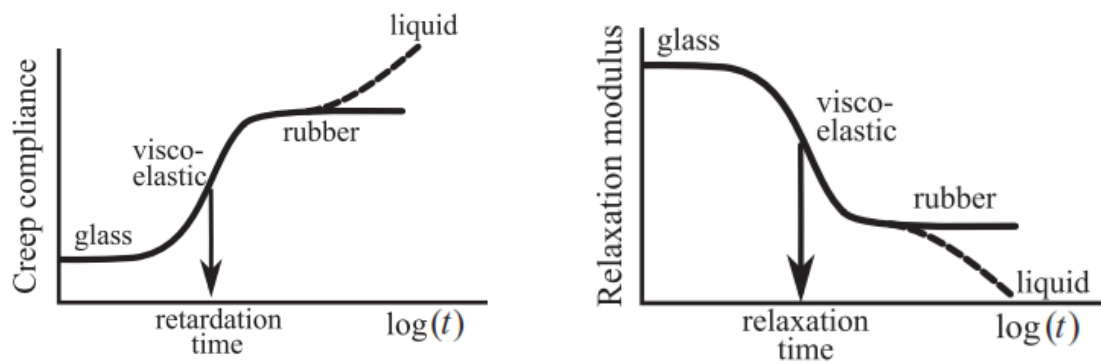


**Figure 7.5** Graph showing relationship between creep compliance and relaxation modulus and time for different materials (Princeton, 2010)

Thermoplastics are known for their viscoelastic behavior, which results in significantly different behavior from linear elastic materials as seen with metals. This is the reason why structural damping is much larger for thermoplastics than metals.

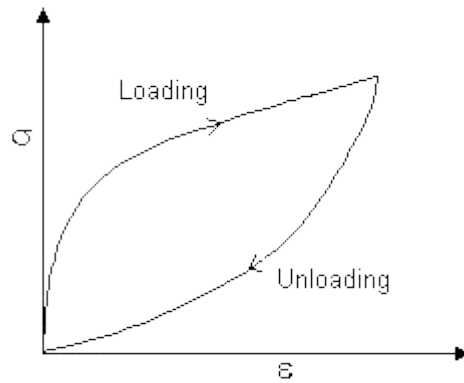


**Figure 7.6** Stress strain curve for a viscoelastic material subjected to hysteresis (University of Cambridge, 2016)

When there is cyclic variation in stress, a lag in strain is produced because of the characteristic relaxation of the material. This then creates a hysteresis loop during cyclic loading.

The area enclosed by this loop represents the amount of energy dissipated during one cycle/oscillation. Loading occurs during compression waves and unloading when wave front passes. In figure 7.6 the difference between loading and unloading stress/strain relationship is pronounced to highlight the hysteresis loop. This type of hysteresis loop is mainly found in materials that behave viscoelastic (e.g rubber). The damping effect due to this anelastic behavior is much smaller in materials such as steel and aluminium, which in turn have a much small loss factor.

There are multiple ways of characterizing the properties associated with internal damping, but as mentioned these are not as easily quantified. The three most common parameter used to define the innate damping characterization of materials are, specific damping capacity, loss factor and logarithmic decrement. Starting with the specific damping capacity, which is the ratio between dissipated energy and the energy stored during one cycle. The logarithmic decrement is similar but instead serves to indicate the amount of decay in the amplitude per cycle. Then finally the loss factor, which is perhaps the most common parameter used to compared the difference between materials and their ability to suppress/absorb vibration. It indicates the amount of energy lost, expressed in terms of the recoverable energy. Materials with large loss factor indicates a larger anelastic strain component, which in turn results in greater hysteresis (Ehrenstein, W, Trawiel, & Pia, 2004).

Specific damping capacity

$$\psi = \frac{\Delta W}{W} = \frac{\oint \sigma d\varepsilon}{\int_{\omega t=0}^{\omega t=\pi/2} \sigma d\varepsilon}$$

Complex modulus

$$E^* = \frac{\sigma}{\varepsilon} = \frac{\sigma_0}{\varepsilon_0} (\cos \phi + i \sin \phi) = E' + iE''$$

Loss factor

$$\eta = \frac{E''}{E'} = \tan \phi$$

Logarithmic decrement

$$\delta = \frac{1}{n} \ln \left( \frac{A_i}{A_{i+n}} \right)$$

Using these parameters it becomes possible to demonstrate that metals such as aluminium and steel has generally a much lower loss factor than transparent thermoplastics such as Plexiglas. It is however important to note that thermoplastics are not as easily defined as metals as some polymers can also have significantly lower loss factors (Pritz, 1994).

All these parameters for structural damping are important for approximating the effect of hysteresis to linear damping. Hysteretic damping being a non-linear damping type therefore needs to be expressed in terms of an equivalent damping coefficient as shown in ODE below for a system with single DOF

$$m\ddot{x} + c_{eq}\dot{x} + kx = 0 \quad (24)$$

Where the term  $c_{eq}$  is the equivalent linear damping coefficient The only simple relationship that can be derived for hysteretic damping is

$$c_{eq} = \frac{h}{\omega} \quad (25)$$

Where  $h$  is the hysteretic damping coefficient,  $\omega$  is the angular frequency. This correlation was determined experimentally, where the energy loss per cycle because of internal friction was independent of the frequency. In addition that the energy loss per cycle was proportional to the square of the amplitude as shown (C. Cai, 2012)

$$\Delta W = \pi h A^2 \quad (26)$$

In order to use these equation to get an estimate of the damping contribution from hysteresis. The hysteretic damping coefficient  $h$  needs to be expressed in terms of known structural parameters so that the type of damping can be calculated for steel and plexiglas. This is done by using (F.C.Beards, 1995). The first step is that the ODE from equation 24 needs to altered in order to incorporate the complex modulus  $E^*$ . This gives the expression in terms of complex stiffness  $k^*$  which can be written as

$$k^* = k(1 + i\eta)$$

The value  $k^*$  is the linear stiffness and  $\eta$  is the loss factor. The correct expression for a single DOF system with hysteretic damping becomes

$$m\ddot{x} + k^* x = 0$$

The reason why hysteretic damping is not expressed as individual term like viscous damping is because material stiffness cannot be separated from the hysteretic damping. The energy dissipated per cycle due hysteresis  $W = \oint \sigma d\varepsilon$  which can also be expressed as

$$\Delta W = \oint F dx$$

Since the it is known that harmonic motion for an underdamped system is  $x = A \sin(\omega t)$  with amplitude  $A$  this then equates to  $\sin(\omega t) = x / A$  and  $\cos(\omega t) = \sqrt{A^2 - x^2} / A$  which can be substituted into  $F$  to give

$$F = kx \pm \eta k \sqrt{A^2 - x^2}$$

Integrating  $W = \int_0^x F dx$  then finally gives the expression for energy loss per cycle which is the same as equation 24

$$\Delta W = \pi \eta k A^2$$

This results in the familiar where the relationship between the hysteretic damping coefficient, structural stiffness and loss factor can be expressed as

$$h = \eta k \quad (27)$$

The damping effect of hysteresis can then be expressed in terms of equivalent damping coefficient  $c_{eq} = \eta k / \omega$ . The damping constant for a system subjected to hysteretic damping with n degrees of freedom can therefore be expressed as shown in equation 28

$$c_j = \left( \frac{\eta k}{\omega m} \right)_j \quad (28)$$

The effect of hysteretic damping can then be approximated using this relationship for the damping constant. Where  $c_j$  is the damping constant for each individual element in the analytical model.

It is however important to note that the loss factor for plexiglas needs to be estimated as there is no given value associated to material properties. The loss factor of plexiglas is therefore assumed to be equal to general loss factors for thermoplastics. This group lies within the PET (polyethylene terephthalate), with an approximate loss factor of  $\eta = 10^{-2}$ . The loss factor for steel is usually given  $0.2 \cdot 10^{-3} \leq \eta \leq 3 \cdot 10^{-3}$ , where the arbitrary value of  $\eta = 10^{-3}$  is selected as the loss factor to represent the structural damping from the steel joint segments.

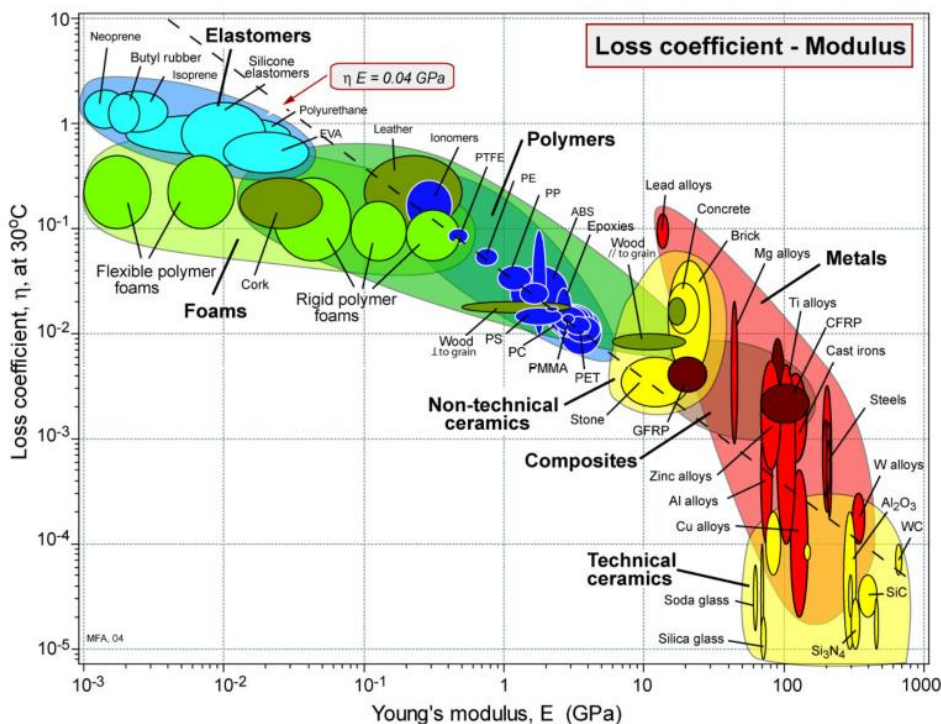
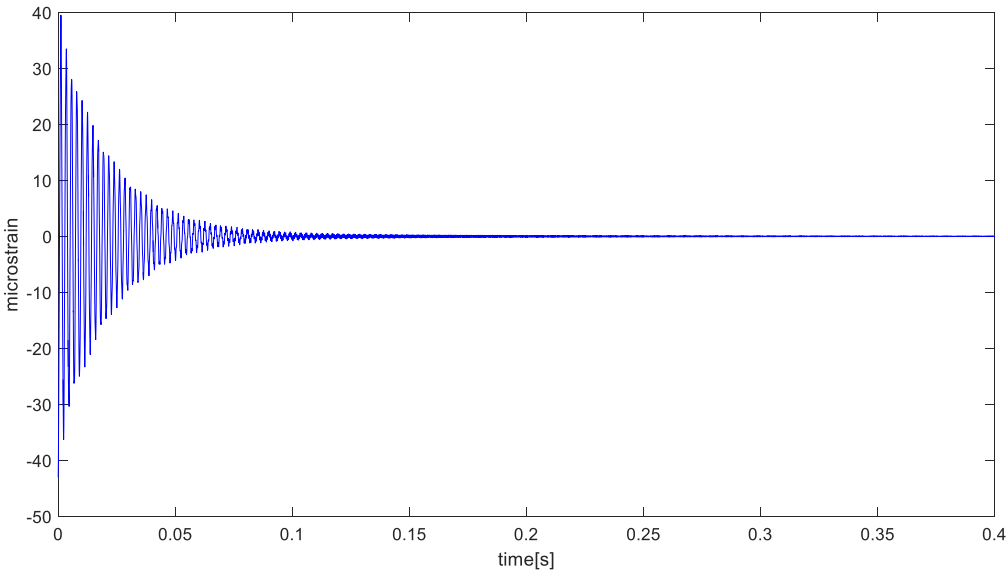


Figure 7.7 Relationship between the loss coefficient and Young's modulus for a large array of different materials (Ashby, 2005)

With the values of loss factor for plexiglas and steel selected the effect damping structural damping can then be computed, with the results shown in the figure below.



**Figure 7.8** damping using equivalent hysteretic damping coefficient showing the results of element j=1

The results in figure 7.8 is from the analytical model approximated as a 0.975m drillstring with DP=10 elements. These results from using hysteretic damping seems to give a much better approximation of the damping that was observed in the measured data. Figure 7.8 however, indicate a higher degree of damping than what observed from the measured data.

The general trend for damping ratio is similar to what experienced from viscous damping where the top five elements are the most damped compared to the bottom five elements

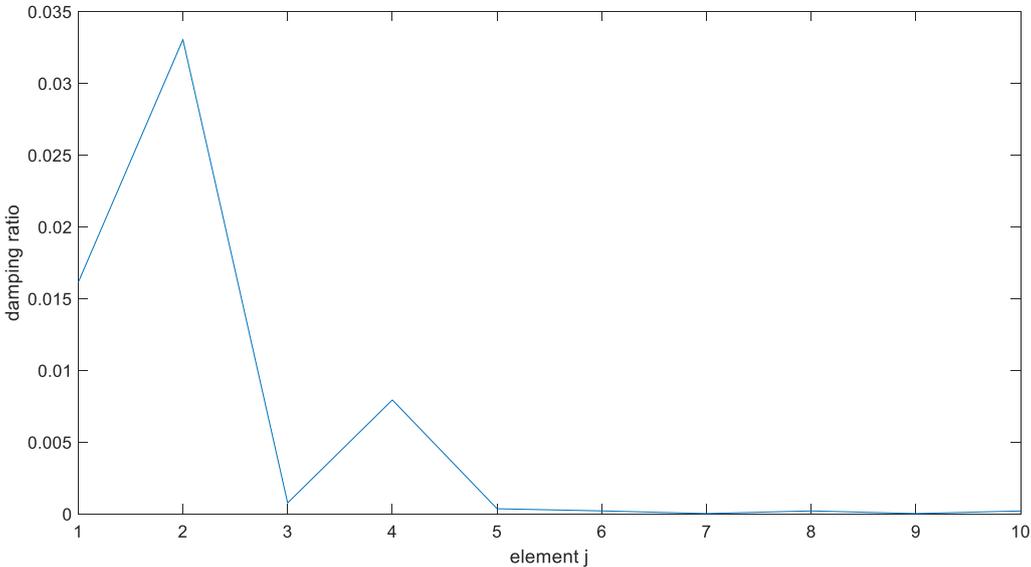


**Figure 7.9** Damping ratio for each element using equivalent damping coefficient from hysteretic/structural damping

The difference as shown is that the damping ratio in the case of hysteric damping ratio is the most prominent in the steel segment as compared to the plexiglas segments.

Overall the results shown in figure 7.8 seem to strongly suggest that hysteretic damping is the damping mechanism that contributes the most to the overall damping in the dynamic strain measurements. It is however important to note that equation 28 is derived based on the relationship from equation 27, which is a behavior that has only been documented to be true for metals and not plastics. Due to the nature of the problem it is difficult to estimate to what extent this affects the numerical approximation.

### **7.1.3 Coloumb friction,kinematic momentum loss and non-axial movement as cause for damping**

The drillstring model is constructed as a chain of plexiglas and steel elements, for which each segment is connected by joints. These joints serve as a source of friction that causes vibrational energy to dissipate.

There are three potential forms of loss at work, affecting the overall damping in the model. The first one being coulomb damping, which is caused by the friction between the joints due to parallel sliding. Even though the contact area is very small and the axial vibrations oscillate at small amplitudes, this will still result in some degree of frictional loss. The major issue is with regards to how much energy loss is caused by the joints between the segments, is that it is very difficult to estimate the actual sliding distance. This is the reason why there is no estimation done for the effects coulomb damping in this thesis, despite estimating the effects of viscous damping and structural damping.

Second form of loss is that the mobile joints are a source of inelastic collisions for which kinetic energy is lost (Young & Freedman, 2011). This effect is unavoidable even if the joints have very small axial freedom, where small “micro” collisions might be affecting the damping in the system

The third form of energy loss is from the non-axial movement, because the joints between the plexiglas and steel segments have a rotational freedom of 14 degrees (7 degrees in both directions). This is therefore also a potential source of energy loss, as some of the potential energy in the drillstring will go into rotation and not into axial movement. The problem with this type of energy loss is that it is impossible for the axial strain gauges to measure. This is because the rotation alleviates the strain that would be recorded if the joint was unable to rotate, and as such does not cause axial strain in the segments. Energy loss of this kind should be minor as the rotation in the joints are not visible, but because magnitude of the strain is in micrometer it cannot be discarded as a possible factor.

The damping caused related to these joints are most likely the smallest contributor to overall damping. However, the only accurate method for determining the degree of frictional loss would be by measuring dynamic strain for a model without joints, such as a continuous plexiglas pipe. The frictional contribution could then be inferred from the difference in the damping coefficient observed in the results.

#### **7.1.4 Damping caused by energy transmission through the creation of external vibrations**

When measuring axial vibration in the drillstring the assumption is that the top segment is attached to a completely rigid body. This is to ensure that the energy from the axial vibrations is contained in the drillstring model, by preventing noticeable energy transfer. The other reason is because the drillstring vibration measurements will be adversely affected by vibrations from external sources. The distinction here is that vibrations originating from the drillstring model is classified as internal, whilst any other mechanical vibration is classified as external. If vibrations are allowed to be transmitted then the vibration in the drillstring would start to produce vibrations in all receptive objects. These external vibrations will then be transmitted back to the drillstring, which are then subsequently recorded by the strain gauges. This distorts the dynamic strain measurement by diluting the data with additional frequencies, as well as an increased damped response. The effect is therefore undesirable, as this causes the comparison between the analytical model and measured data to become less accurate.

The issue regarding having the top segment of the model attached to a fixed point is that this is very difficult to achieve in reality. This is because there is always some degree of movement despite how fixed one assumes it to be. It is the relative scale between the mobility that is important, or more accurately the relative stiffness between the drillstring and the fixed end. As long as drillstring has a significantly lower stiffness than the fixed end, then all of the measured data can be considered to originate from the drillstring model. This would give the best approximation to the analytical model. However, this also means that if the vibrations from the external source is more noticeable than the vibrations in the drillstring, would mean that the model has a much higher stiffness than the “fixed end”. This means that the clamp arms/ceiling hook keeping model suspended cannot be considered fixed/rigid.

This is assuming that it is possible to make the distinction between internal and external vibrations, which can prove to be very difficult. The difficulty with the physical model is that the stiffness (spring constant) is very large, but the sensitivity of the measurements makes it difficult to exclude the possibility that the experimental setup has had an effect on the dynamic strain measurements. If one therefore were to look at a potential source of external vibration in the measurements. Then the clamp arms that the drillstring model is attached to, is the most likely a source.

In order to determine whether the system is influenced by external vibration sources, then measurements needs to be conducted to test sensitivity of the lab stand setup. If this structure is affecting the measured data, then this should be visible if the structural rigidity is adjusted. This was done by decreasing the horizontal separation between the clamp stands and the vertical hanging drillstring. This reduced the bending moment at the center, which directly relates to its vibrational susceptibility, as this change increased the structural rigidity. If the bending moment could be reduced to zero then this would greatly reduce the vibrational amplitude from the clamp arms.

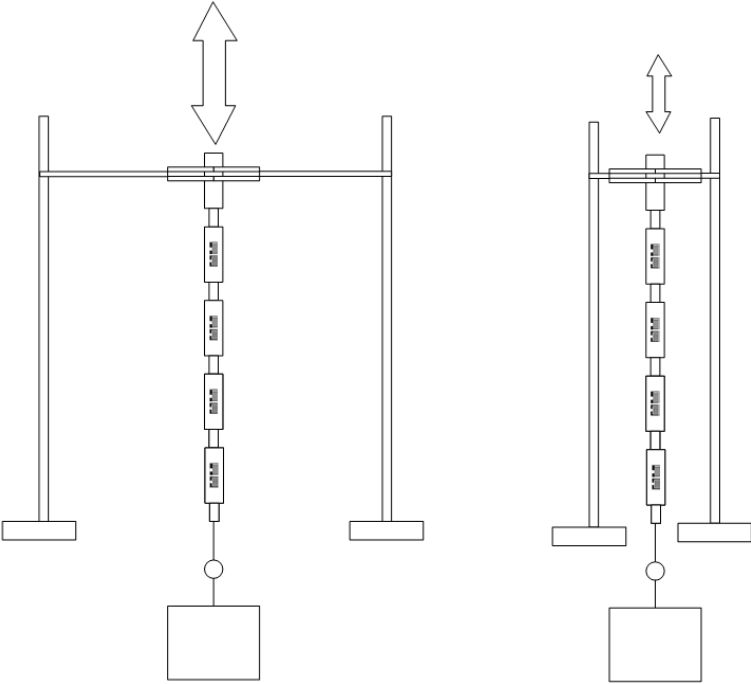


**Figure 7.10** Diagram highlighting the difference between long and short arm lengths for the clamps arms

The stand structure was then altered as shown in figure 7.10 and 10kg mass release test was conducted for both adjustments.

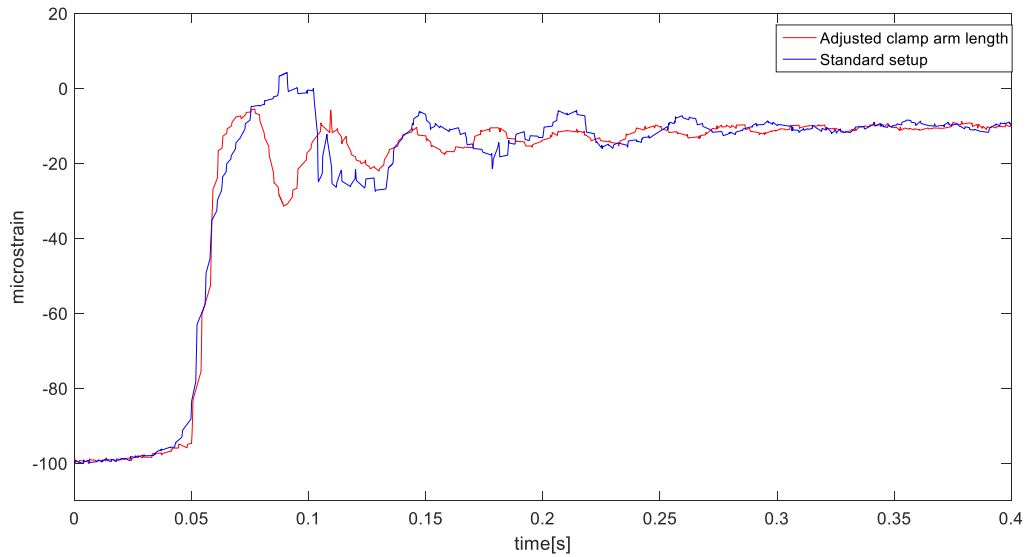


**Figure 7.11** Graph illustrating the results when a 10kg mass is used on the drillstring model(BHA inc) with adjusted arm length for each clamp 0.4 sec interval

The results from altering the clamp arm length to 13cm from 30cm made a slight but noticeable difference. This change seemed to indicate that the stand structure was influencing the measured signal as there was an apparent frequency increase from roughly 20Hz to 50Hz when the stand rigidity was increased. It is important to note that these frequencies are the weighted sum of all frequencies measured by the strain gauges.

A different method for looking at the influence of vibrating from the clamps arms, is by looking at the theoretical vibration of a fixed ended beam system. This is the closest corresponding model to vibration in the clamp arms, and can be expressed as the ODE below (Virginia Tech, 2008).

$$m\ddot{x} + \frac{48EI}{L^4}x = 0$$

Where  $E$  is the Young's modulus for the material,  $I$  is the second moment of area,  $L$  is the total beam length(length of two clamp arms) and  $m$  which is the point mass at the center of the beam. The equation for the second moment of a solid cylinder is shown below

$$I = \frac{\pi}{4}r^4$$

The ODE approximates the oscillation of single element model, with all the downward bending occurring at the center, because of a single point of mass placed at the center. The expression for the natural frequency can then be written as.

$$f = \frac{1}{2\pi} \sqrt{\frac{12E\pi(r_o^4 - r_i^4)}{mL^4}} \quad (29)$$

$r_o$ Outer diameter[mm]	$r_i$ Inner diameter[mm]	$M$ Mass[g]	$E$ Young's modulus[GPa]
30	22	2314	200

**Table 7.2** Dimensions and parameters used to estimate vibration in the clamp arms

The results from using equation 29 shows that  $f = 82Hz$  for clamp arms at length of 60cm and  $f = 440Hz$  when the length is 26cm. This is a rough approximation for the natural frequency of vibration in the clamp arms. The important fact is that the frequency from the clamps increases by a factor of five. If this degree frequency change were visible in the measured data shown in figure 7.9, then this would indicate that the only signal measured originated from the clamp arms. This would mean that the strain measurement would be indirectly measuring the vibration in the clamp arm instead of the drillstring model. There is however instead little to no indication of this degree of frequency increase. This therefore indicates that the strain measurements are only partially affected by external vibrations.

Having looked at the stand clamps as a source of external vibration, there is an additional factor that might also have played a part in affecting the results. This is the vibration due to bending in the vertical arms in the stand itself. The vertical metal rod that is attached to the base of the stand can also cause vibration, as the attached point has a joint mobility similar to a ball joint. All the vibrations that might originate from the lab stand are most likely very minor, but as stated cannot be excluded because of the sensitivity of the dynamic strain measurements.

If the measurements done with the stand setup were indeed influenced by external vibration as demonstrated by figure 7.9. Then this can be accurately verified by directly comparing the results to measured data from the drillstring suspended by the ceiling hooks. Where the measured data from 10kg mass release with the ceiling hook compared to the adjusted clamp arm length is shown in the figure below.

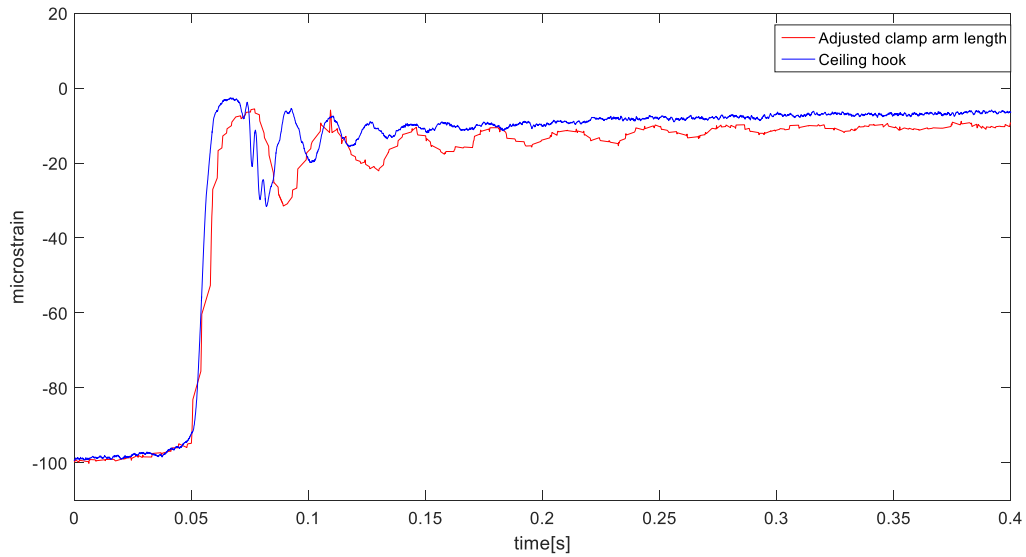


**Figure 7.12** comparison between 10kg mass release with BHA-section for adjusted clamp arm length and ceiling hook with sensory point 3 as reference point

The results show that there is clear variation between the mass release for the adjusted clamp stand and the one from the ceiling hook, with an increase in overall frequency of the signal output. It is therefore possible to conclude that that the entire lab stand setup was sensitive enough to influence the measured vibrations. This verified by the fact that this effect was completely visible in the measured results shown in figure 7.11 and 7.12

External vibration therefore seems to explain some of the variation between the analytical model and the measured data. The reality however is that the influence from external sources are not significant enough to explain the variation between analytical data and the measured data as demonstrated in chapter 6. It was shown that even the best results from the ceiling hook setup, were still not comparable to the analytical model. The overall strain gauge sensitivity means that influence from external vibrations might also have affected the measurements with the ceiling hook setup. This influence will most likely be much smaller than the influence caused by lab stand setup, but could only be verified by using an improved setup. It would however be difficult to find alternatives that would allow better measurements to be conducted than the ones with ceiling hook setup.

## **7.2 Analytical model limitations and difficult experimental process**

It has been shown that the lumped element model developed lack the ability to numerically model the drillstring behavior observed in the dynamic strain measurements. This section deals with the possible causes with regards to limitations of the analytical model as well as limitations as to how it was applied.

In order for any analytical model to accurately depict behavior from a physical measurement, it is very important that entire process involved in the measurement are controlled and understood. Sub-sections 7.2.5 and 7.2.6 deals with the issue that reason why there noticeable variation between the analytical and measured data, is directly related to the issues with the experimental process.

### **7.2.1 Modeling viscoelasticity**

The viscoelastic behavior of thermoplastics is more complex than a fully elastic solid material. The analytical model as shown in chapter 3 is based on the linear elastic behavior of elastics that abide by Hooke's law. Materials that have an approximate behavior to that of Hooke's can therefore be modeled as a single spring element. The actual mechanical behavior of most thermoplastics is a non-linear elastic behavior, especially when subjected to dynamic strain(hysteresis) . This a result of the viscoelastic nature of thermoplastics which is a combination of the mechanical properties of a viscous fluid and a perfectly linear elastic material. When a fluid is subjected to a load, the work applied is not stored as energy in the system, but is instead continuously dissipated. This is a stark contrast to a linear elastic material where all of the work done is stored as retainable energy. The viscoelastic behavior embodies these characteristics, which causes non-linear hysteretic and rate dependent deformation behavior.

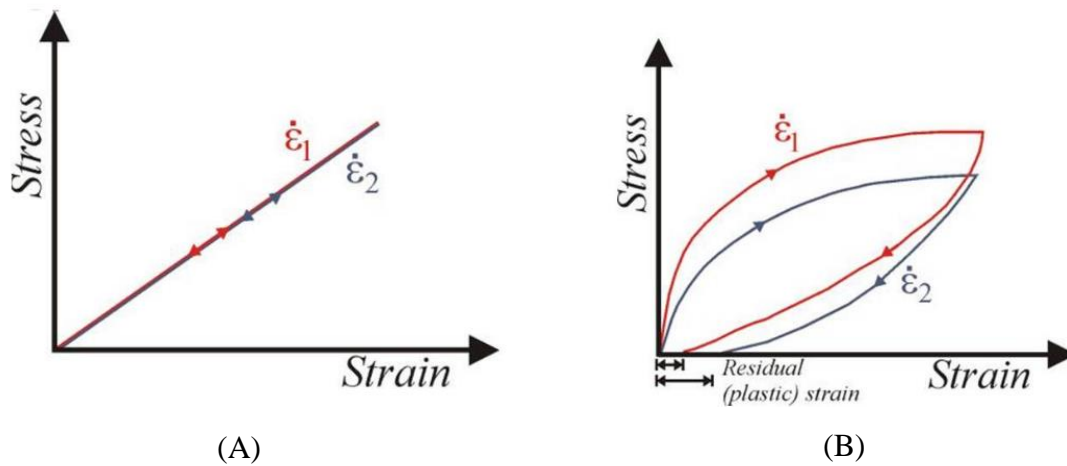


**Figure 7.13** (A) pure linear elastic behavior (spring element), (B) non-linear viscoelastic behavior (Polymod, 2015)

The deformation rate dependence is the effect where faster rate of deformation yields a higher stress-strain curve. This is illustrated in figure 7.13 where the line marked in red shows a higher strain rate than the one marked as blue.

The elastic variation between metals and viscoelastic materials can also be demonstrated using strain vs time curve, for when the system is exposed to constant stress as shown in the figure 7.14

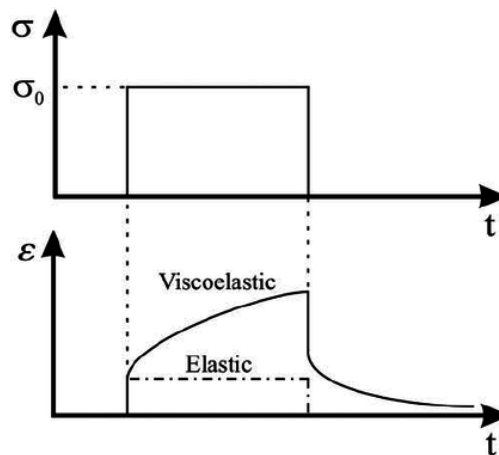


**Figure 7.14** Difference between linear elastic and viscoelastic materials (Misra, Ramesh, & Okamura, 2008)

Metals such as steel, aluminum has a negligible retardation and relaxation time because of their linear elastic behavior, as compared to viscoelastic behavior of plexiglas (thermoplastic)

All these facts indicate that the mechanical behavior of viscoelastic materials can therefore not be accurately approximated as a spring elements, because of the fundamental difference from between thermoplastic and metal. There are however multiple models that are used to represent viscoelastic material. Examples of which include Voigt-Kelvin, Maxwell and standard linear solid also known as Zener. All these models have varying degree of accuracy associated with them, where some are more suitable than others.

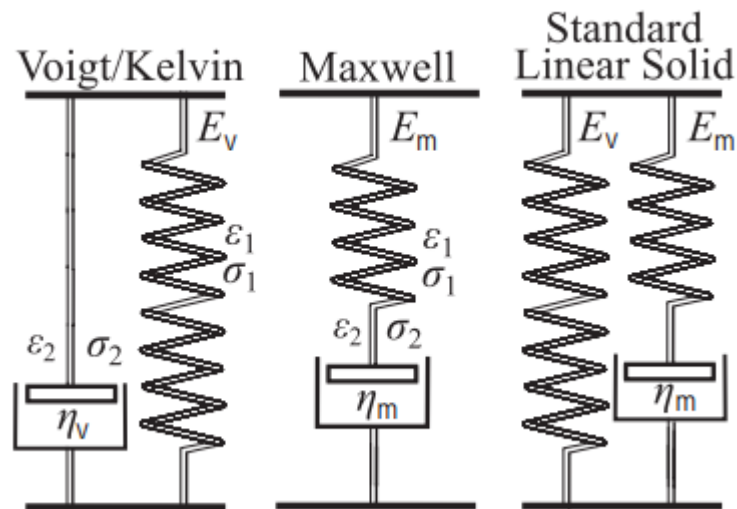


**Figure 7.15** Different modeling approaches used for viscoelastic materials (Princeton, 2010)

The most common model used for viscoelastic materials is the Voigt/Kelvin model. This is where the materials elastic behavior is modeled as a spring and a viscous damper connected in parallel. The problem with Voigt/Kelvin model is that it is unable to recreate stress-relaxation behavior, because the model behaves as an elastic solid under these conditions (Princeton, 2010). The second common modeling method is Maxwell, which is modeled as a spring and a viscous damper connected in series. Maxwell is however unable recreate creep, because when subjected to a constant load the viscous damper keeps the spring in constant tension. This means that the model only recreates the behavior of a Newtonian fluid in the viscous damper. The last model used for viscoelastic materials is Zener, which is more advanced than the simpler Voigt/Kelvin and Maxwell models. It does have the major advantage of being able model the viscoelastic behavior for the stress relaxation and creep. The problem Zener has is that although it can be good at accurately recreating general shape caused by viscoelastic creep, it has difficulties with numerical representation, which is equally important.

If one were to more accurately model the same mechanical behavior observed in the dynamic strain measurements, then the lumped element model would have had to been model more as shown in the figure below.

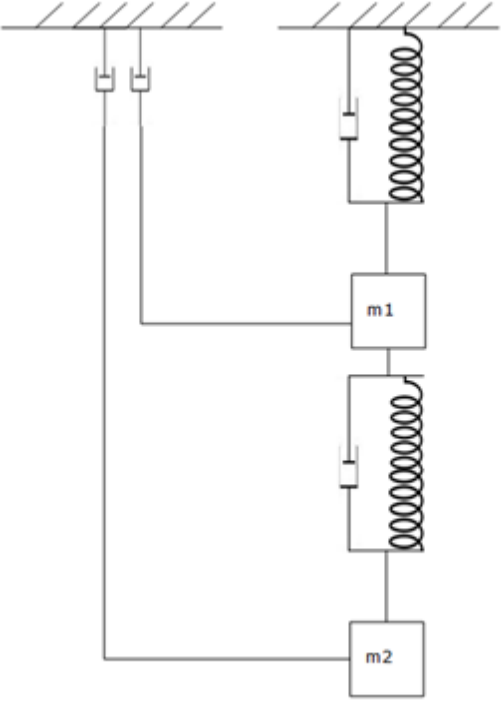


**Figure 7.16** Alternative lumped element model in order to encapsulate viscoelastic behavior using Voigt/Kelvin

The analytical models inability to simulate the viscoelastic behavior of thermoplastic is most likely the major reason why the measured data cannot be expressed numerically using the analytical model. It is therefore possible that altering the analytical model to encompass the more complex behavior of viscoelastic materials, one would see much more comparable results than what observed in chapter 6.

### **7.2.2 Accurately comparing analytical model to the measured data originating from the strain gauges**

When comparing the strain measured from the physical model, it is important to be aware of how to correctly compare these measurements to the analytical model. Making sure that the point(e.g. element j) on the analytical drillstring model is compared to corresponding position from the measurements(e.g. sensory point). This is important because the results vary depending on the point that is evaluated.

The measurements recorded originate from the 20mm long biaxial strain gauges, being the Tee-rosette type. This means that in order to get the most accurate comparison between the analytical and the physical model, the element length in the analytical model should be equal to length of the strain gauges. If the analytical element size is larger, the actual relevant data becomes obscured by additional information, which makes the results less accurate. The same happens if the analytical element length is smaller than the strain gauge length, where the results would then only partially show the correct strain.

The limitations concerning analytical element size is that the most accurate comparison to the real life scenario is when the number of elements(n) is allowed to become as large as possible. This therefore means that degree of accuracy that one can attain becomes more dependent on the length of the physical drillstring model. Where a longer drillstring would allow the model to be evaluated as a larger set of elements than when compared to short drillstring with the same size limit for each element.

In all of the results shown in chapter 6, the element size was evaluated as being equal to the segment size of plexiglas and steel. An example of this is that the DP-section with 10 segments was evaluated as  $n=10$  for the analytical model. The problem with using the same amount elements n for the analytical model as the number of segments in the physical model, is that the ability to accurately portray reality is greatly enhanced with increasing number of elements per unit length. This is because the analytical model more accurately depicts mass distribution with increasing n elements, as it is modeled as a lumped system.

Based on these facts one might assume that because the analytical model was evaluated as element size larger than the strain gauges, in addition to the limited number of elements used, this had then profound effect on the numerical accuracy of the model. In actuality, this increased accuracy translates only to slight variations when evaluating the drillstring at larger number of n elements.

This can be seen in the two figures 7.17 and 7.18 where the DP is evaluated as  $n=10$  compared  $n=100$ , and the underdamped oscillation seen from the top plexiglas segment in the physical model. The basis for both these analytical models is the 675mm DP without the BHA section.

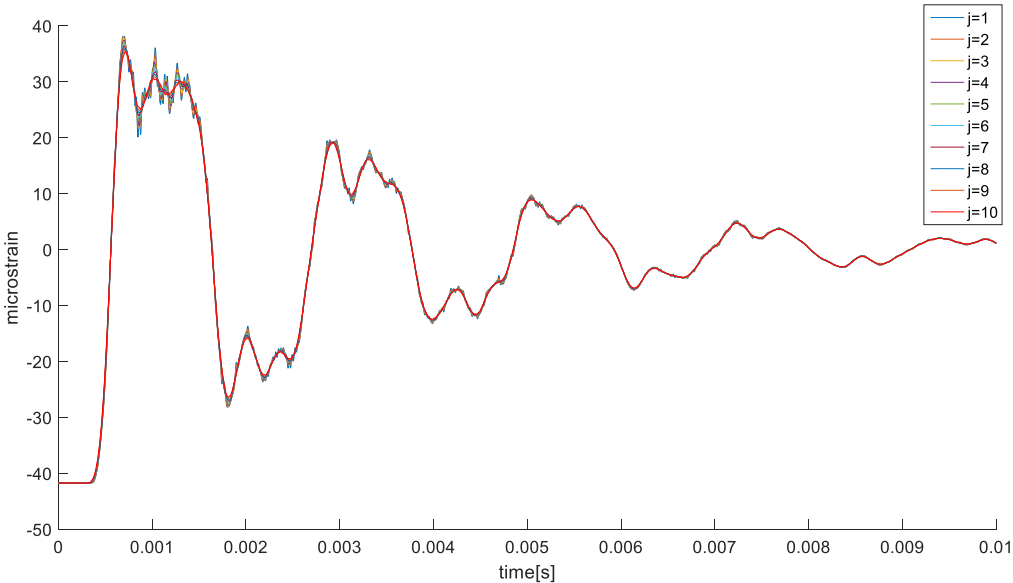


**Figure 7.17** Evaluating the DP as  $n=100$  elements showing the first 10 elements in the top plexiglas segment

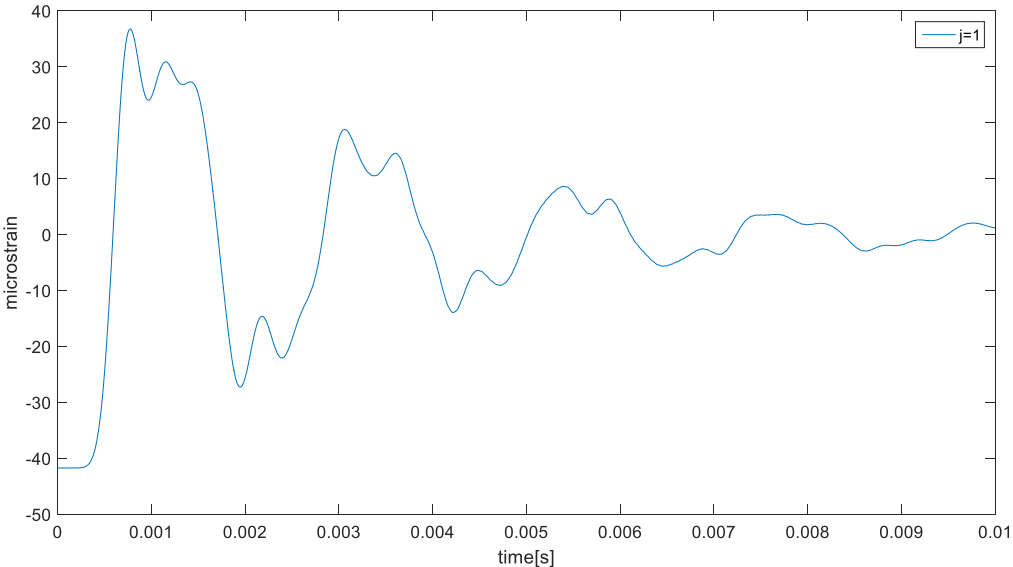


**Figure 7.18** Evaluating the DP as  $n=10$  elements showing the first 1 elements in the top plexiglas segment

The results in figures show that the model with DP section modeled as  $n=10$  elements varies only slightly from the more accurate model with  $n=100$  elements in the DP section, with the overall trend for dynamic strain being the same.

It therefore becomes apparent that the poor approximation of the measured data was not because of the relatively small number elements used to evaluate the drillstring model, as the improvement in accuracy from increasing the number of elements would be marginal.

**7.2.3 Difficulty approximating the analytical model as underdamped, critically damped and overdamped.**

The important thing to highlight about the analytical model is that due to the nature of the coupled system, the values for damping ratios will be different depending on the element that is evaluated. This means that the drillstring can be overdamped in the top section whilst simultaneously being underdamped in the lower section. Determining whether a single mass-spring system is damped or underdamped is simple criterion for a single element model, as the system has a single damping constant, and single frequency that determines the entire vibration. The signal produced from a coupled system on the other hand is the weighted sum of sines, which is why this distinction becomes much more difficult. This means that a seemingly over damped signal can be the result of any number of combination of overdamped, critically damped and under damped elements in the drillstring.

It is possible however to get an approximation of the damping constant that would cause the system to be critically damped or overdamped. Using the analytical model the conditions for these situations can be determined as shown in table 7.3, which is based on 0.675m DP section with and without BHA for a 4.3kg mass release.

Drillstring	Without BHA section	With BHA section
Damping of DP element	Damping constant $c$ value for being underdamped	Damping constant $c$ value for being underdamped
Top element	$c < 5800$	$c < 2500$
Bottom element	$c < 2.23 \cdot 10^5$	$c < 2.0 \cdot 10^5$

**Table 7.3** Values for which different parts of the drillstring is defined as underdamped for 0.675m and 0.975m drillstring

The calculated values from the figure indicates the damping constant for which the element behaves according to an underdamped harmonic oscillator. These values for both drillstring model variations (with/without BHA) indicate the damping constant required for all the elements in the drillpipe section to be underdamped.

These results illustrate an additional reason why it is difficult to confirm or deny the behavior observed by the measured data. This is because the range of combinations that might cause the system to appear overdamped/underdamped, is the sum of the damped behavior of the individual elements in the model.

#### **7.2.4 Lingering weight during mass release**

When the analytical data is compared with the measured data the assumption is that system behaves according to the transient solution. The concern is that because of the relative small margins of error with regards to system behavior, it is possible that the time function associated with the pin release method causes the system to be a function of both the transient solution  $x_t(t)$  and a steady state solution  $x_s(t)$  (Young & Freedman, 2011) as shown below

$$x_i(t) = x_t(t) + x_s(t)$$

This would mean that scenario from for which the dynamic strain was measured, could then not be compared to the analytical model.

This is directly related to the “pin” release mechanism described in chapter 5. The bolt/screwdriver is balanced/supported at the opposite side of the noose in order to prevent the bolt to rotate and slide off. The time it takes for the bolt to do this action was most likely affecting the parameters of the measurements. This is because when the end mass balances the system is at its initial condition and is then released, this action has no time associated function in the analytical model. In reality however, when the mass is released the force applied on the system does not go down to zero instantaneously, instead the force will decrease to some value that is defined by the surface friction between the steel noose and the steel blade of the screwdriver. This force will be very small and brief but there is still a possibility that this force was significant enough to have an effect. If this was the case then it would explain why the analytical model differs from the measured values, as the model was lacking the  $x_t(t)$  term from the overall  $x_i(t)$  expression. This is of course highly speculative as it is very difficult to determine the actual force in order to verify the actual influence on the systems harmonic response.

### 7.2.5 The difficulty of determining the true time stamp for mass release during dynamic strain measurements

Values from the analytical model and the measured data have been consistently compared over an interval of 0.4 seconds. The issue with the measured data, was the absence of being able to determine the start of the transient response. This was because the time at which the mass was released for the measurements conducted were not accurate enough, to verify the time stamp associated with the transient response. Using equipment such as a stopwatch would serve no purpose for these experiments as the human reaction time on average is only 0.2 seconds, which is too slow compared to the transient response of system. The only method for getting a time stamp for the mass release would have been to create a remote release mechanism, where the time could have been recorded for the rapid mass rerelease action.

The absence of this time stamp meant that the data comparison was limited to parameters such as amplitude, frequency and decay, because parameters such as phase shift are completely dependent on having accurate measurement of the starting position with respect to time.

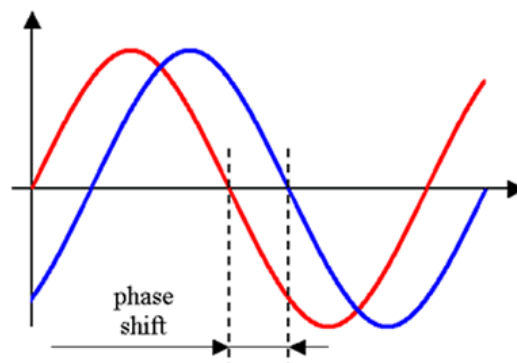


**Figure 7.19** phase shift between two sinusoidal waves (Australian Government:Bureau of Metrology, 2016)

This is illustrated in figure 7.19, which shows that phase shift is directly related to starting position. The starting position for measured was therefore empirically chosen for each set of dynamic strain measurements, which was the best method available. However, the overall variation between the measured data and the analytical model was not because of the offset between the starting positions. This would have been much more relevant if the analytical model were more similar to the transient response observed from the measured strain data.

### **7.3 Uncertainty when measuring the axial vibrations produced in the drillstring model**

For any type of measurement, it is important to limit the number of sources of uncertainty in order to avoid adverse effects on accuracy. The fact of the matter is that most uncertainties in the measurements are difficult to remove, where most of the uncertainties can only be partially suppressed. This section will present the potential causes of uncertainty related to the dynamic strain measurements. It is therefore important to discuss the general effect the strain gauges, signal amplifier and ADC had on the uncertainty. In addition to the general effect of noise, and the importance of selecting appropriate sampling rate for the ADC.

#### **7.3.1 Strain gauge as a source of error in strain measurements**

Strain gauge measurements are very sensitive, and is the reason why it is difficult to control uncertainty related to the experiments conducted to measure dynamic strain. This is the reason why modifications were done to the drillstring model in order to reduce the overall uncertainty. Example being that steel joint segments were wrapped in an insulating tape. This was to prevent interference with the copper tape attached on the inside of the plexiglas segments. In order to prevent the metal on metal connection from causing a short circuit, which would cause additional uncertainty in the voltage.

These sub-sections will present the major effects that temperature, gauge mounting and creep had on the strain gauge measurements, and also how calibration factors are necessary because of the deviation from Hooke's law.

##### **7.3.1.1 Temperature**

Temperature changes can have a major impact on the strain gauges. Where a small change in temperature can have a significant effect on the output voltage. These temperature changes might generate a measurement error of several microstrains on their own. Some strain gauges are made to compensate for the thermal expansion of the specimen, which will reduce the overall thermal sensitivity, but the effects are never completely nullified.

This effect of temperature is observed when the strain gauges are initially subjected to a current of electricity, this causes temperature to increase in the metal threads. Where this increase in temperature causes resistance to gradually increase as time goes on (Coates, 2016). The temperature causes zero drift in the measurements as the voltage in the bridge circuit is continuously increasing. It is therefore important that measurements were not done until this drifts stopped, which occurred when thermal equilibrium is achieved. This is effect had therefore no influence on the measured data.

The bridge circuits used for every sensory point is set up with temperature compensation, in order to offset variation due to thermal strain. The limitations with the setup is that the strain gauges must be exposed to the same temperature in order to completely nullify this effect. The measurements done on thermoplastic segments might have suffered because of non-uniform temperature distribution, because of the poor thermal conductivity of plastic compared to metals.

### **7.3.1.2 Gauge mounting**

The reason why the different strain gauge sensory points measures different values of voltages when the offset is not nullified (figure 5.6), is because the strain gauges are not completely balanced. The high sensitivity of the gauges causes this variation to persist even after offset nulling calibrations. How the strain gauges are mounted on the plexiglas segments are therefore most likely the reason for the slight variations in strain between individual sensory point, because of how every individual sensory point have different value of non-zero voltage.

The strain gauges are attached by hand, which means that the strain gauges will never be completely parallel to axial direction of the plexiglas segment. This will then create an angle with segment axis. Additionally the strain gauge placement might also not be fully centered.

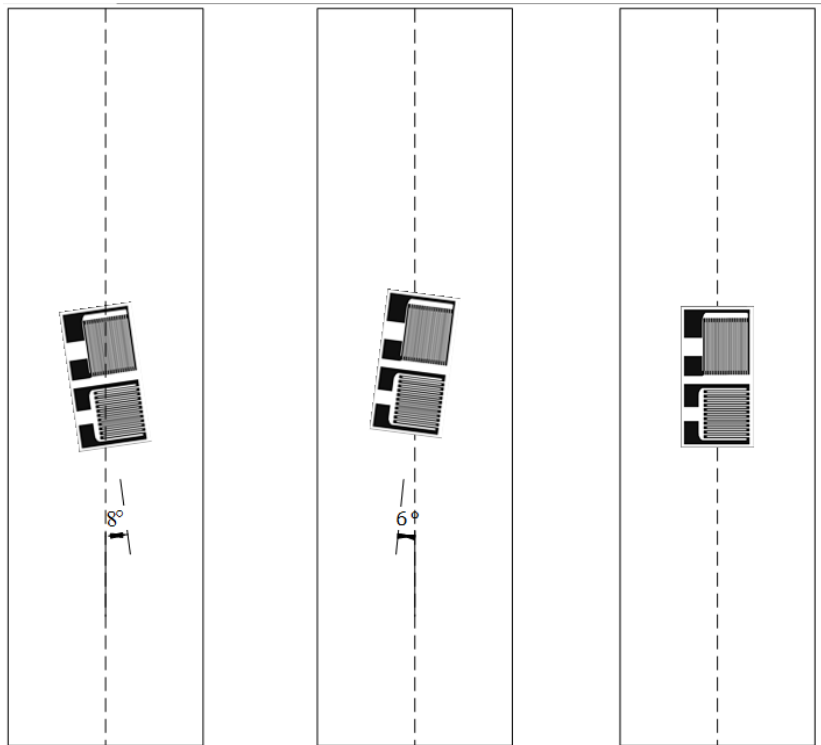


**Figure 7.20** illustrates combination of mounting variations possible with strain gauges on one side of a plexiglas segment (angles are exaggerated for illustration purposes)

The number of strain gauges per sensory point(bridge circuit) used for the strain measurements is two, which means that total error from gauge mounting is a combination their alignment and placement. The combination of placement and misalignment is therefore one of the cause for bridge circuits not balancing out, because this causes individual sensory point to have different sensitivity towards axial strain. This error caused by gauge alignment is mostly minimal in most cases, because angles are usually very small, much more so than illustrated in figure 7.20.

### 7.3.1.3 Creep/zero-drift strain

Creep is a phenomenon that can have profound effects on strain gauge measurements under the right circumstances. It is uncertain whether or not creep is actually affecting the strain readings, but there is evidence to suggest as much.

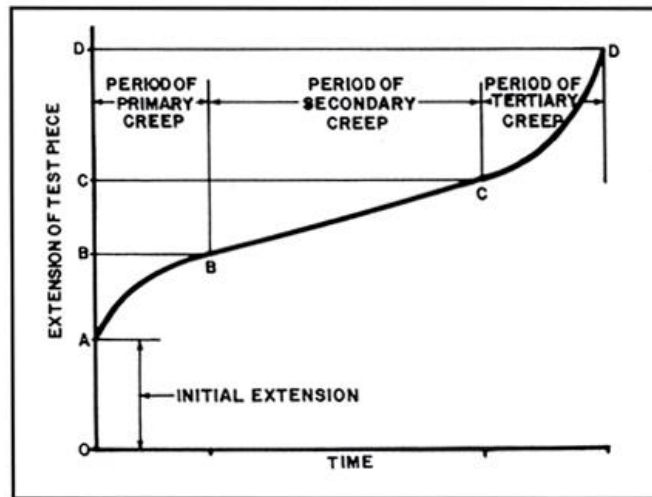


**Figure 7.21** strain as function of time for a viscoelastic material subjected to constant stress (French, 1991)

Creep can be caused by a wide variety of factors, where generally the rate of deformation is affected by the temperature of the material, the size of the applied load, the time of duration the material is subjected to the applied load and elastic properties of the material (French, 1991). This effect normally occurs at high temperatures (30 -50% of melting point) and high loads, or a combination of both. It is however still possible for creep to occur at room temperature, which is often the case with metals with low melting temperature and plastics (e.g. thermoplastic). The effect of creep is therefore normally highly prevalent in thermoplastics owing to the materials a high creep compliance

When conducting the measurements, the applied static load is released which produces the signal for systems transient response. The nature of this damping is seen as a the signal(strain) asymptotically approaching zero. This trend can however also indicate creep as this effect is known to cause zero drift and would also be displayed as strain slowly decreasing asymptotically back towards zero when static load has been relieved (Vaughan, 1975). Test were conducted to infer whether or not this was true by hanging a 10kg mass to drillstring model for an extended period of time.

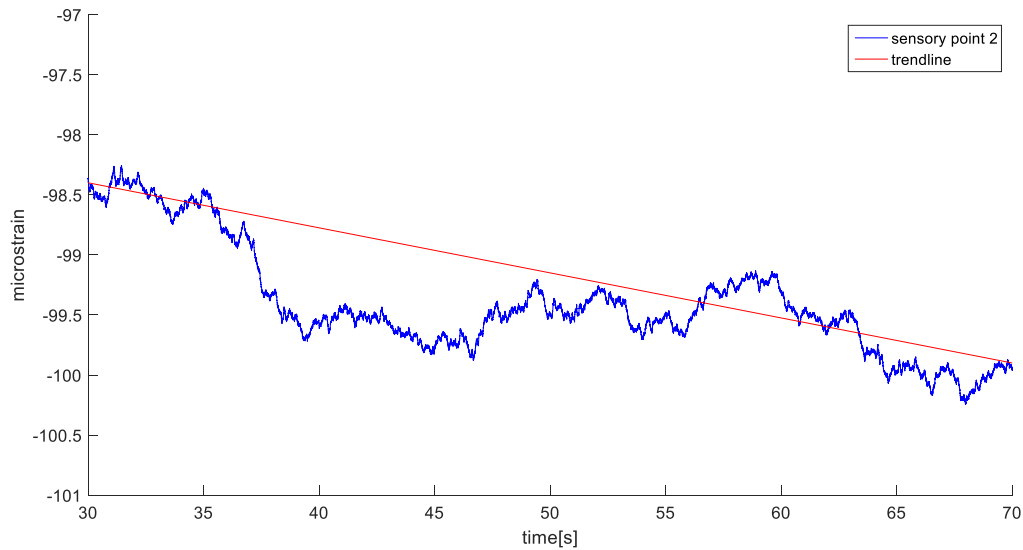


**Figure 7.22** Strain reduction with time when subjected to static load of 10kg

The measured data shown in figure 7.22 shows that the static strain measurement has in fact a downward sloping curve, which means that strain is increasing with time whilst subjected to a constant load. It is difficult to determine what the type of creep witnessed due to small variation with time relative to the uncertainty in the strain measurements. The type of creep is however most likely secondary creep because of the steady reduction of strain with time.

The effect of creep can also be seen in figure 5.8 and 5.9, where the end mass is increased from 4.3kg to 10kg. These results show that the horizontal drift increased when the end mass was increased, which shows that rate dependence of plexiglas. Creep therefore provides a plausible explanation why all the results from the physical model had a downward shifted equilibrium.

#### **7.3.1.4 Strain gauge calibration**

The measurements done showed that there was noticeable deviation between static strain expected by Hooke's law and the measured static strain for any given load.

The strain gauges were therefore calibrated in order to ensure that the measured values matched with Hooke's law. This variation is caused by multiple factors with one possibility being that the strain gauges are not mounted perfectly symmetrical, which is something that cannot be removed when the gauges are mounted manually.

The calibration is done by measuring static strain for a given mass, since the cross sectional area is known, the normal stress can then be calculated. The Young's modulus  $E$  can be

calculated from the ration between normal stress  $\sigma$  and strain  $\varepsilon$  . The calibration factor is then determined from the ratio between the calculated Young’s modulus and the actual Young’s modulus for plexiglas  $E = 3.1GPa$  . The example below shows how the calibration factor is calculated using sensory point 2, with static loads of 4.3kg

$$\sigma = \frac{F}{A} = \frac{42}{3.26 * 10^{-4}} = 1.28 * 10^5 Pa$$

$$\varepsilon = 35 * 10^{-6}$$

$$E = \frac{\sigma}{\varepsilon} = 3.66GPa$$

$$factor = \frac{3.66}{3.1} = 1.18$$

The calibrated values illustrate that the strain readings are less than what is expected for the applied static loads. This is due asymmetry in the bridge configuration partially cancelling out the reading. It is however important to note that these calibration factors are non-consistent for the measurements, which indicates the degree of uncertainty involved.

Sensory point number	Strain calibration factor
1	1.131
2	1.180
3	1.101
4	1.049

**Table 7.4** Calibration values for measured voltage that causes measured data to coincide with Hooke’s law

When comparing the measured and analytical data, the initial condition for the measured data is forced to the same initial condition as the analytical model using the calibration factor for the sensory point evaluated. This was done for all the measured data in chapter 6, that was compared to the analytical model. It was done to improve the numerical comparison, but the calibration factors might have had an opposite effect. Applying these factors might have distorted the measured values, by assuming that this calibration factor remains constant for a dynamic strain measurement. This is because the calibration factors were calculated from strain variation caused by a static load, and not variation during the entire dynamic strain measurement. It is therefore difficult to say whether or not applying these factors was more beneficial to the overall comparison with analytical model, compared to just using the uncalibrated data.

### 7.3.2 SNR/Background noise

Background noise or simply referred to as noise is undesirable fluctuations that interfere with the accuracy of the dynamic strain measurements, and can be especially problematic when measuring small voltage levels, as is the case with measurements performed. Noise originate from many different sources, but the most common is the measurement device itself. There are also many different types of noise like white, Brownian, Gaussian, thermal noise etc. Types of noise range from being constant to others who vary in amplitude. Noise in measurements are unavoidable, and is the reason why Signal-to-noise ratio is so widely used in signal processing (National Instruments, 2012).

Signal-to-noise ratio(SNR) is the ratio of amplitude between the signal and the noise (ncalculators, 2016). The SNR for dynamic strain measurement can be calculated using equation 30

$$SNR = \frac{\mu}{\sigma} \quad (30)$$

Where  $\mu$  is the mean the expected value(or mean value) and  $\sigma$  is the standard deviation.

The SNR for the static measurement is therefore close to zero when no load is applied, because  $\mu = 0$ . This relationship between expected value and the standard deviation means that SNR is estimated over a specific interval of time. The value of SNR is therefore dynamic and constantly changing by definition. The largest SNR is seen momentarily after the mass is released, where SNR ranges between 3 and 1.5, indicating that that desired signal is 1.5/3 times stronger than the noise

The issue with the dynamic strain measurements is that the background noise has a fairly constant amplitude whilst the desired signal does not. When the weight was released in the measurements and the voltage/strain measurement moves towards equilibrium, the signal decreases continuously whilst noise interference remains constant. This effectively means that the SNR is decreasing as strain is approaching equilibrium, until SNR becomes less than one and the signal can no longer be distinguished from noise. This problem is a result of the variation between the expected value  $\mu$  becoming increasingly smaller relative to the standard deviation  $\sigma$ , which is synonymous with background noise.

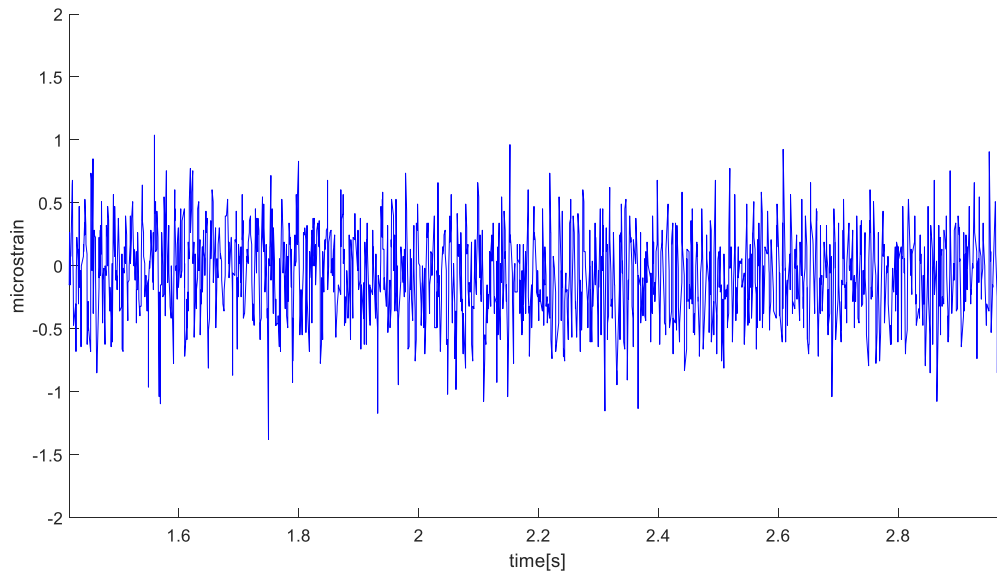


**Figure 7.23** Background noise recorded during static measurement, where no load is applied

Figure 7.23 shows the recorded background noise during the static measurement. The recorded amplitude for noise in the interval can be approximated to be around 2 millistrain with the applied filter of SMA. During the 0.4 sec interval used to evaluate the measured data the SNR can be calculated to be approximately 0.2-0.4, which illustrates the dynamic nature of SNR.

The final issue regarding noise in measurements is that it can be very difficult to remove if not impossible. The most basic method for removing or reducing noise is by applying a filter, such as simple moving average(SMA), which is one out many different types of data filters for improving SNR. These filters vary from being applied using weighted,unweighted averages to convolution, with some filters being better at improving SNR than other without distorting the signal. The limitations with all filters is that they can only improve the SNR so far until it starts filtering out too much of the desired signal. This is seen with SMA, which takes the average over given intervals for a set of data, where the intervals is defined as the sample size for each set of data points (MathWorks, 2016). The larger the sample size the more likely it is that the signal becomes distorted, until reaching a point where all valuable information from the signal is filtered out with the noise. Example of this effect can be seen in figure 7.24, where a large sample size has profound effect on signal.

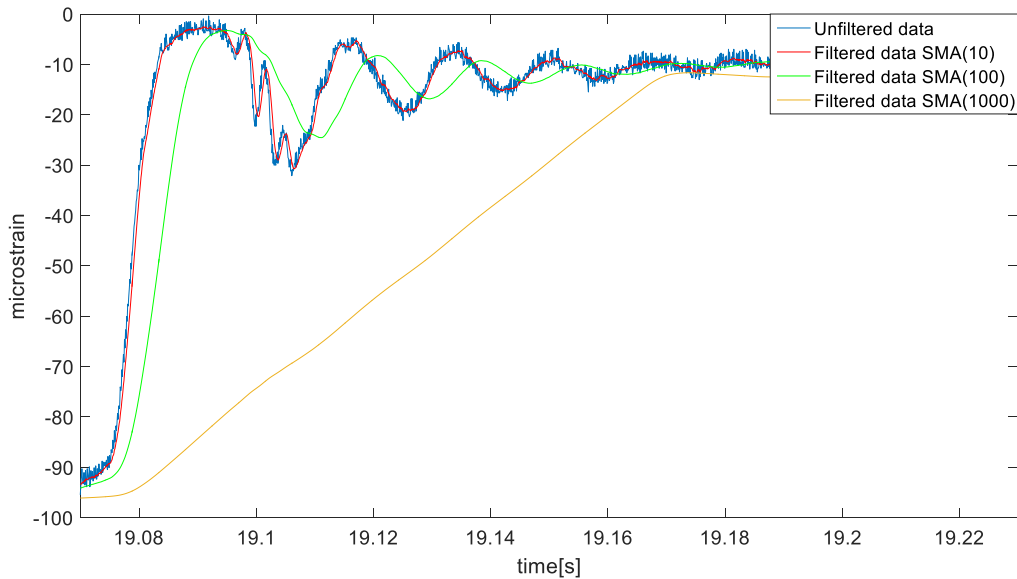


**Figure 7.24** Comparison between different degrees of filters using simple moving average with different sample sizes ranging from 10-1000

The filter and sample size used for smoothing the measured data in this thesis was SMA(10), which retains the general shape without noticeable distortion. This is however not the case for sample size 100 and 1000, as seen with SMA(100) and SMA(1000).

The other alternatives for reducing noise besides filtering is to increase the signal amplitude. This can be done by choosing a more sensitive strain gauge or increasing the amplitude of the excitation voltage. It is easiest however to improve SNR by increasing the excitation voltage. The excitation voltage needs to be carefully adjusted because self-heating errors in the strain gauges might outweigh the benefits of improved SNR (National Instruments, 2012). In addition to this, one could improve the SNR by selecting a material with a lower Young's modulus.

Noise that are produced by external sources are often associated with specific frequencies, and this means that they can be filtered out if the frequencies are known. This is done by so called band-stop filter, but can only be done against noise that is predictable. One good example of predictable interference is from power lines which show up as 50-60 Hz noise in the measurements.

It is important to emphasize that as long as SNR is at acceptable values, being higher than one then the results can be considered useful. For all the dynamic strain measurements conducted, the SNR remained above 1 for the 0.4 sec interval used when comparing the results with the analytical model. This indicates that Noise was at least not a limiting factor for the signal resolution in the dynamic strain measurements, despite it being very noticeable.

### **7.3.3 Signal Amplifier and ADC**

The signal amplifier and ADC are the final components in the signal chain after the strain gauge, with both contributing to the total noise generated. However, documented results show that signal amplifier contribute 50% more to the total noise than the ADC (Jayamohan, 2013). Where testing signal chains with and without signal amplifiers, showed that the signal amplifier had more profound effects on the noise generated on the signal output than that of an ADC.

If possible, one should therefore avoid using signal amplifiers. The problem with the dynamic strain measurements conducted in this thesis is that removing the signal amplifier from the signal chain was not an option. This is because the small forces involved to create axial vibration in the physical model with very large stiffness, produced too small voltage variations to be measured without a signal amplifier. In fact, an amplification factor  $k$  of 1000 was required in order to measure the variation in voltage, which was roughly 0.2-0.4 mV without any amplification. It would therefore have been impossible to measure axial vibrations without the use of a signal amplifier. This is also the major reason why thermoplastic was used in the drillstring model, as steel had too large stiffness to allow strain measurements with a signal amplifier to be conducted.

The total uncertainty however is not related to the amplification factor  $k$ . This is because the signal power increases in tandem with the noise generated. The background noise is increased with the same amplification as the signal, and SNR remains constant since the parameters of the experiment are kept constant.

There was therefore little that could have been improved with regards to noise generation from the signal amplifier and the ADC. The signal amplifier was essential for dynamic strain measurements, and the only way to reduce noise from the ADC would be to change to a different ADC, which produced less noise. Another possibility would be have been to increase the scale of the model and the forces involved to such an extent so that at least the signal amplifier could be removed.

The total reduction in noise from these alterations can however be only determined through actual measurements. In addition to the fact that increasing the length of the drillstring model would make it very cumbersome to use. These are the two reasons that makes the change in length difficult to recommend.

#### **7.3.4 Sampling rate/frequency**

Sampling rate is perhaps the most important factor for being able to measure the axial vibrations in the drillstring. The high frequency of the small-scale drillstring model means that a correspondingly high sampling rate is required. The deformation velocity is the lower limit for being able to measure the axial vibrations, which is equal to the speed of sound in that medium. This is directly related with the natural frequencies in the system. It is therefore important that the sampling frequency exceed the frequency of vibration in the drillstring model.

The primary factors that determine the rate of sampling is the ADC itself. The ADC converts continuous signals in the form of voltage to discrete time values, which allows the signal to be digitally reconstructed (Salomon, 2007). The core principle of converting continuous signals is that the ADC is unable to do instantaneous conversions from analog to digital data. This in turn means that the input value at any given point in time is held constant until the signal is converted. This is the conversion time of the ADC, which uses an input circuit known as sample and hold. The time associated with the sample and hold conversion sets the maximum capacity of sampling rate for the ADC. Where the maximum sampling frequency for the ADC used in the measurements being 44 000Hz. This means that if a single sensory point (bridge circuit) is used. Then this sensory point would have a sample frequency equal to the maximum capacity of the ADC. This however means that increasing the number of strain gauge sensory points would subsequently reduce their individual sampling rate. The ADC capacity is shared equally between the strain gauges, which meant the sampling rate for the 4 sensory points used were equivalent to 11 000 Hz.

The second factor that determines the sampling rate available is the processing speed of the computer. This is because increasing values of sampling rates also increases the processing demand on PC. The Computer used could sustain each individual measurement for approximately a minute, before the buffer reached its maximum capacity, and subsequently stopped the measurement. The only limitation this had was that live filtering had to be disabled, if one wanted to measure the dynamic strain over longer periods.

The most important fact about sampling rate, is that it has to be adequate in order to avoid signal distortions. This is determined by the Nyquist rate, which is the lower limit for which any signal can be sampled without any significant degree of distortions (Kester, 2005). This rate is equal to twice the signal bandwidth that one wish to record. Further increasing the sampling rate beyond this point, would not result in any significant improvement in the reconstruction of the signal resolution. Oversampling however, does improve the measurement by reducing noise, avoiding aliasing and phase distortion (Salomon, 2007)

Due to the significant difference between apparent frequency from the analytical model compared to measured dynamic strain, it is difficult to determine the necessary sampling rate (Nyquist rate) required. Based on the analytical model, the distribution of natural frequency from the 0.975mm and 0.675mm long drillstring model is as shown in figures 7.25 and 7.26

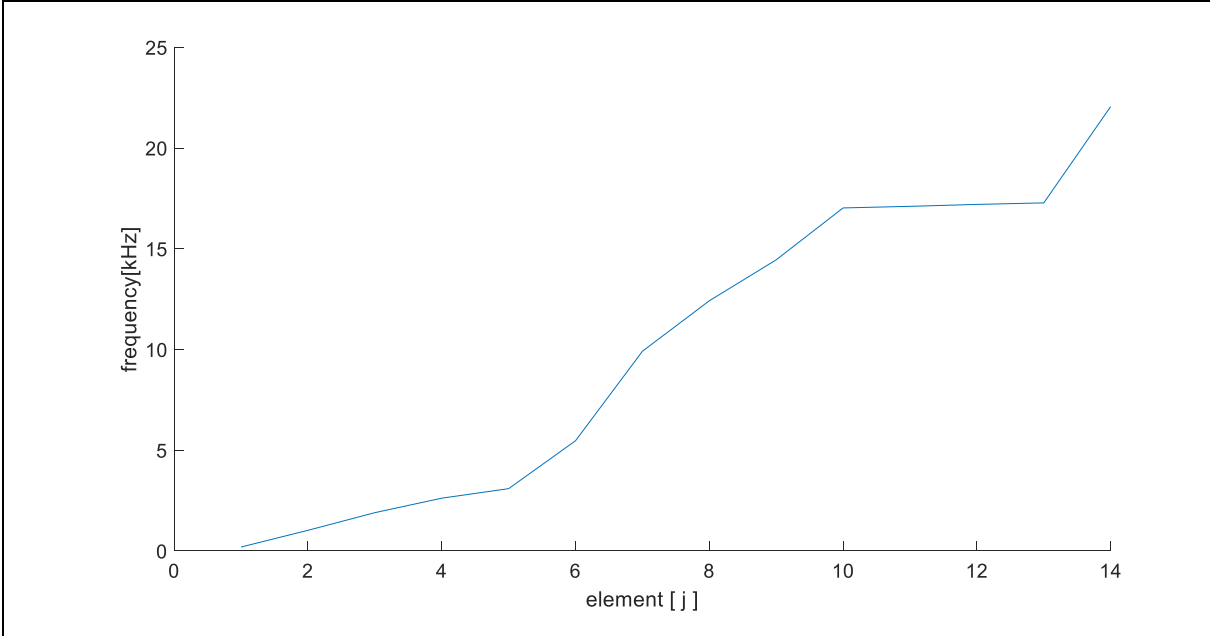


**Figure 7.25** Natural frequency of elements from the analytical model evaluated as n=14 elements with BHA(DP-section with n=10)

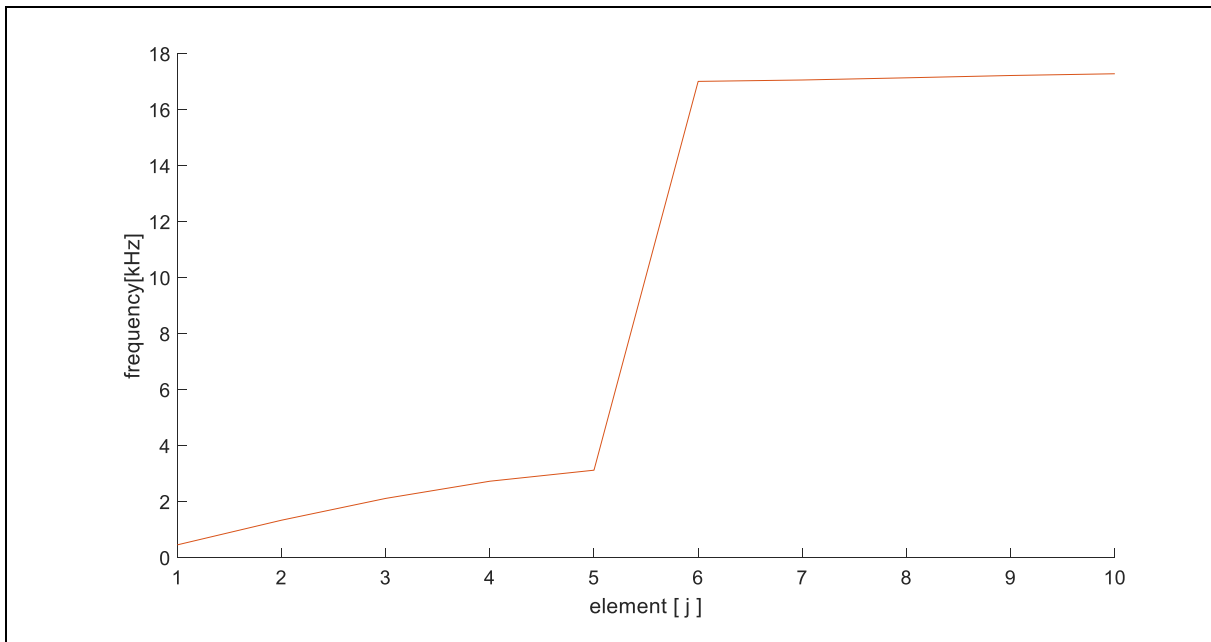


**Figure 7.26** Natural frequency of elements from the analytical model evaluated as n=10 elements without BHA

The maximum frequency based on analytical model results is 18 000Hz and 22 000Hz. According to these results the required sampling rate/Nyquist rate would be 36 000Hz and 44 000Hz. The actual required sampling rate for the measured dynamic strain is most likely much lower, but the possibility that the sampling rate was inadequate cannot be excluded. This is because there is no easy method for numerically determining actual frequency distribution from the physical drillstring model

## 8 Conclusion and Future work

### 8.1 Conclusion

The lumped element model, as with all models have limitations associated with them. This in combination with the sensitivity related to dynamic strain gauge measurements, and the lack of appropriate equipment, meant that numerically modelling axial vibration in a small-scale drillstring model proved to be a grand undertaking.

This was illustrated through the plethora of factors that combined to cause significant variation between the analytical model and the measured axial vibration, as indicated by the comparison between simulated strain and dynamic strain measurements. These factors were individually investigated and discussed, in order to highlight their plausible effects on the overall difference between the analytical and measured data. The two major factors that caused this difference was the limited analytical model, with the second being related to how uncertainty prone the experimental process was.

The first major reason as stated was most likely because of limitations with the analytical model. This was despite showing that the analytical model had the ability to predict general variation in frequency, amplitude and strain rate, when changing the parameters (e.g. increasing mass, length etc.) of the measurements. The analytical model struggled to simulate dynamic strain behavior from the measurements, with numerical accuracy. The only part of the lumped element model that showed to give good approximation to the measured results was the signal decay associated with hysteretic/structural damping. The analytical model's overall inability to numerically compare with the measured strain, originated most likely from how the elastic behavior modeled by the analytical model, was not representative of the viscoelastic behavior of thermoplastic.

The second major reason for the overall variation, being that the measurements conducted were far too complex compared to the tools and processes used, which resulted in uncertainty prone measurements. This was highlighted by showing how the strain gauges were sensitive enough to be affected by the small vibrations from the experimental setup, which were not visible to the naked eye. In addition to this, there was a large amount of experimental variation between each individual measurement. This like most of the uncertainties was a combination of multiple factors, but is believed to be primarily caused by pin release

mechanism used for the mass release. The crude process of releasing the mass most likely was what caused a great deal of variation in the measured data.

The overall combination of the analytical models limitations, and the crudeness of the measurement process as compared to the sensitivity of the measurements. Is therefore the most probable causes for the lumped element models failure to numerically recreate the measured dynamic strain.

## **8.2 Future work**

If one were to implement the knowledge from this thesis, then one out of two possible options are available, in order to improve the numerical comparison between the analytical model and the measured strain.

The first option is that one need to increase the complexity of the lumped element model by using viscoelastic models such as Voigt/Kelvin, Maxwell or Zener. Selecting this option means that one can continue conducting experiments with the small-scale drillstring model(chapter 4). The problem with this approach would be that it is difficult to get these type of models numerically correct.

The second option is that the entire physical model needs to be changed, so that strain measured originate from metal segments instead of plexiglas. The SNR from the measured dynamic strain, indicate that conducting the same measurements with metals might be impossible. This is because even aluminium, which is softest metal that is cheap to acquire, has a Young's modulus that is roughly 23 times that of thermoplastic. It might therefore be impossible to conduct the same small-scale measurements shown in this thesis, because of the reduced strain gauge sensitivity.

## 9 Bibliography

- Analog devices. (2016). *Analog to Digital Converters*. Retrieved from <http://www.analog.com/en/products/analog-to-digital-converters.html>
- Ashby, M. (2005). *Materials and Process Selection Charts*. Retrieved from [http://www.mie.uth.gr/ekp\\_yliko/2\\_materials-charts-2009.pdf](http://www.mie.uth.gr/ekp_yliko/2_materials-charts-2009.pdf)
- Australian Government:Bureau of Metrology. (2016). *Phase Changes and Velocity Measurement*. Retrieved from [http://www.bom.gov.au/australia/radar/about/phase\\_changes.shtml](http://www.bom.gov.au/australia/radar/about/phase_changes.shtml)
- Benaroya, H. (2004). *Mechanical Vibration:Analysis,Uncertainties,and Control* . Marcel Dekker.
- Buck Bernat, H. B. (1997, March 11). *Mechanical oscillator frees stuck pipe strings using resonance technology*. Retrieved from <http://www.ogj.com/articles/print/volume-95/issue-44/in-this-issue/drilling/mechanical-oscillator-frees-stuck-pipe-strings-using-resonance-technology.html>
- C. Cai, H. Z. (2012). *Modeling of Material Damping Properties in ANSYS* . Retrieved from <http://easc.ansys.com/staticassets/ANSYS/staticassets/resourcelibrary/confpaper/2002-Int-ANSYS-Conf-197.PDF>
- Coates, E. (2016, March 31). *Temperature Effects on Resistance*. Retrieved from [http://www.learnabout-electronics.org/Resistors/resistors\\_01a.php](http://www.learnabout-electronics.org/Resistors/resistors_01a.php)
- Dupriest, F. (2010). *Borehole Quality Design and Practices to Maximize Drill Rate Performance*. Retrieved from <https://www.onepetro.org/download/conference-paper/SPE-134580-MS?id=conference-paper%2FSPE-134580-MS>
- Ehrenstein, W, G., Trawiel, G., & Pia. (2004). *Thermal Analysis of Plastics*. Carl Hanser Verlag GmbH & Co. KG. Retrieved from [http://files.hanser.de/hanser/docs/20041012\\_2411215439-82\\_3-446-22673-7.pdf](http://files.hanser.de/hanser/docs/20041012_2411215439-82_3-446-22673-7.pdf)
- Electronic Tutorials. (2016). *The Differential Amplifier*. Retrieved from [http://www.electronics-tutorials.ws/opamp/opamp\\_5.html](http://www.electronics-tutorials.ws/opamp/opamp_5.html)
- Engineering 360. (2011). *Analog-to-Digital Converters Information* . Retrieved from [http://www.globalspec.com/learnmore/data\\_acquisition\\_signal\\_conditioning/signal\\_conversion/analog\\_to\\_digital\\_converters](http://www.globalspec.com/learnmore/data_acquisition_signal_conditioning/signal_conversion/analog_to_digital_converters)
- F.C.Beards. (1995). *Engineering Vibration*. Edward Arnold.
- French, D. N. (1991). *Creep and Creep Failures* . Retrieved from <http://www.nationalboard.org/Index.aspx?pageID=181>
- Hartenberg, R. S., & Denavit, J. (1964). *Kinematic synthesis of linkages*. New York: McGraw-Hill.

- Haym, B., & Mark, L. (2009). *Mechanical Vibration*. CRC Press Inc.
- J. ZHANG, R. J. (1993). *Documentation of damping capacity of metallic, ceramic and metal-matrix composite materials*. Retrieved from [https://faculty.engr.utexas.edu/sites/default/files/jmatersci\\_v28n9y1993p2395.pdf](https://faculty.engr.utexas.edu/sites/default/files/jmatersci_v28n9y1993p2395.pdf)
- Jayamohan, U. (2013, February). *Understanding How Amplifier Noise Contributes to Total Noise in ADC Signal Chains*. Retrieved from [http://www.analog.com/library/analogDialogue/archives/47-02/VGA\\_noise.html](http://www.analog.com/library/analogDialogue/archives/47-02/VGA_noise.html)
- Keith.R.Symon. (1971). *Mechanics*. Wesley.
- Kester, W. (2005). *The Data Conversion Handbook*. Newnes.
- Layne. (2015). *VIBRATION TECHNOLOGY*. Retrieved from <http://www.layne.com/en/solutions/drilling/vibration-technology.aspx?mid=600>
- MathWorks. (2016). *Filtering and Smoothing Data*. Retrieved from <http://se.mathworks.com/help/curvefit/smoothing-data.html>
- Misra, S., Ramesh, K. T., & Okamura, A. M. (2008, october). *Modeling of Tool-Tissue Interactions for Computer-Based Surgical Simulation: A Literature Review*. Retrieved from [https://www.researchgate.net/figure/41192564\\_fig3\\_Figure-3-Examples-of-characteristic-properties-of-viscoelastic-materials-a-creep-and](https://www.researchgate.net/figure/41192564_fig3_Figure-3-Examples-of-characteristic-properties-of-viscoelastic-materials-a-creep-and)
- National Instruments. (2009, May 15). *Using the NI USB-8451 SPI Interface to Evaluate a Texas Instruments Analog to Digital Converter*. Retrieved from <http://www.ni.com/tutorial/4692/en/>
- National Instruments. (2012, November 15). *Making Accurate Strain Measurements*. Retrieved from <http://www.ni.com/white-paper/6186/en/#toc2>
- National Instruments. (2016, May 25). *Measuring Strain with Strain Gages*. Retrieved August 2, 2016, from <http://www.ni.com/white-paper/3642/en/>
- National Instruments. (2016, August 16). *What is LabVIEW?* Retrieved from <http://www.ni.com/newsletter/51141/en/>
- nvalidators. (2016). *Signal to Noise Ratio Calculator*. Retrieved from <http://nvalidators.com/statistics/signal-noise-ratio-calculation.htm>
- NPTEL. (2011). *Analysis of Strain*. Retrieved from <http://www.nptel.ac.in/courses/Webcourse-contents/IIT-ROORKEE/strength%20of%20materials/lects%20&%20pics/image/lect7/lecture7.htm>
- Polymod. (2015). *Viscoelastic Materials:Introduction*. Retrieved from [http://polymodmw.csi.muohio.edu/?page\\_id=276](http://polymodmw.csi.muohio.edu/?page_id=276)

- Princeton. (2010). *Basic Elasticity and Viscoelasticity*. Retrieved from <http://press.princeton.edu/chapters/s9774.pdf>
- Pritz, T. (1994). *Dynamic Young's Modulus And Loss Factor Of Plastic Foams For Impact Sound Isolation*. Retrieved from <http://www.sciencedirect.com/science/article/pii/S0022460X8471488X>
- S.Hovda. (2015). *Drill String Models*.
- Salomon, D. (2007). *Data Compression*. Springer.
- Schlumberger. (2010). *Drillstring Vibrations and Vibration Modeling*. Retrieved from [https://www.slb.com/~media/Files/drilling/brochures/drilling\\_opt/drillstring\\_vib\\_br.pdf](https://www.slb.com/~media/Files/drilling/brochures/drilling_opt/drillstring_vib_br.pdf)
- Schlumberger. (2016). *Drillstring Dynamics Analysis: Shock & Vibration*. Retrieved from [http://www.slb.com/services/drilling/engineering\\_modeling/optimization/drilling\\_optimization\\_real\\_time/shock\\_vib.aspx](http://www.slb.com/services/drilling/engineering_modeling/optimization/drilling_optimization_real_time/shock_vib.aspx)
- Skalle, P. (2014). *Drilling Fluid Engineering*. bookboon.com.
- tradeKorea. (2016). *Physical Measuring Instruments*. Retrieved from [http://www.tradekorea.com/product/detail/P476902/Single-Linear-type-\(S\)120%CE%A9-Cas-Strain-Gauge.html](http://www.tradekorea.com/product/detail/P476902/Single-Linear-type-(S)120%CE%A9-Cas-Strain-Gauge.html)
- University of Aberdeen. (2014). *Drill-String Dynamics*. Retrieved from <http://www.abdn.ac.uk/engineering/research/drillstring-dynamics-154.php>
- University of Cambridge. (2016). *Viscoelasticity and hysteresis*. Retrieved from <http://www.doitpoms.ac.uk/tlplib/bioelasticity/viscoelasticity-hysteresis.php>
- Vaughan, J. (1975). *Application of B&K Equipment to Strain Measurements*. Brüel & Kjær.
- Virginia Tech. (2008). *Beam Vibrations*. Retrieved from <http://www.dept.aoe.vt.edu/~mpatil/courses/BeamVibrations.pdf>
- Young, & Freedman. (2011). *University Physics with modern physics*. Pearson Custom Publishing.

## Appendix A: Non-conventional recovery method using axial vibrations

Resonant vibration technologies is alternative to method for stuck freeing stuck pipe, liner and tubing. The recovery method is based on the principles of resonance and utilizes resonant vibrations to deliver large amounts of sustained energy to the stuck point.

There are two types of equipment used in this method, which surface based and sub-surface based tools, such as downhole impulse tool (cannot be used with regular drilling fluid) and fishing agitator tool (part of BHA).

The equipment needed for the method is mechanical oscillator, which uses two counter rotating weights to create axial vibration that travel down the drillstring. The hydraulic power unit is what delivers the energy to mechanical oscillator. These hydraulic power units are capable of delivering tremendous amount of force, which in turn are used to power the hydraulic motor inside the mechanical oscillator.

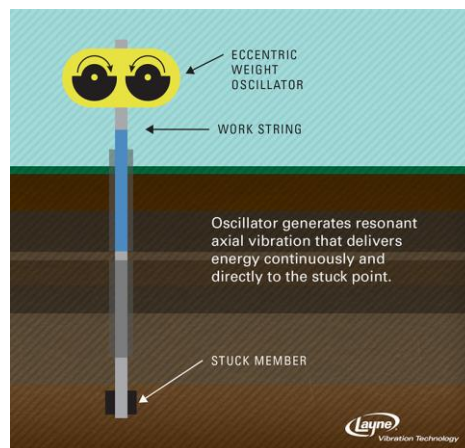


**Figure A.1** Overview of surface based recovery method using resonant vibration technology (Layne, 2015)

Process for pipe recovery is then to adjust the axial vibration to the resonant frequency of the drillstring. The vibrations then delivers a continues amount of energy to the stuck point whilst overpull is gradually increased. The overpull is also sometimes alternately increased and decreased during the recovery operation. This process of varying overpull whilst vibrating the drillstring at its resonant frequency is continued until the drillstring is freed. Where the average time for a freeing a stuck member is approximately 4 to 6 hours.

The major difference between using this recovery method and the conventional ones is that there is no downhole equipment required. This in essence means that it is entirely surface based. This results in little to no rig up time, with a current average for rig-up at two hours.

For successful recovery operations there is a major difference in recovery time as shown in figure A.2. The conventional methods also suffer from the fact that the energy is not delivered directly and continuously to the stuck point and is therefore the major cause for the large difference in time required to successfully free stuck pipe



**Figure A.2** Charts highlighting the benefits of resonant vibration for releasing stuck pipe compared to conventional method with regards to recovery time and actual energy transferred to the stuck point (Layne, 2015).

Resonant vibration technologies remains to this day a predominantly unexplored area with regards to its full potential as an alternative recovery method. In spite of its limited use there are documented results for which resonant vibration recovery methods are vastly superior to the conventional recovery methods, as mentioned previously.

The purpose of further understanding drillstring vibration can be greatly beneficial this type of recovery method. The ability to determine the resonant frequencies of the drillstring, makes it possible to determine what resonant frequency will result in the largest resonant amplitude at the stuck point. This will enable the operator to maximize the amount of energy delivered in order to free the stuck member. In addition it can determine the resonant amplitude on any given point in the drillstring. This information is essential with regards to avoiding unnecessary stress and fatigue in areas that are not in close proximity to stuck point.

